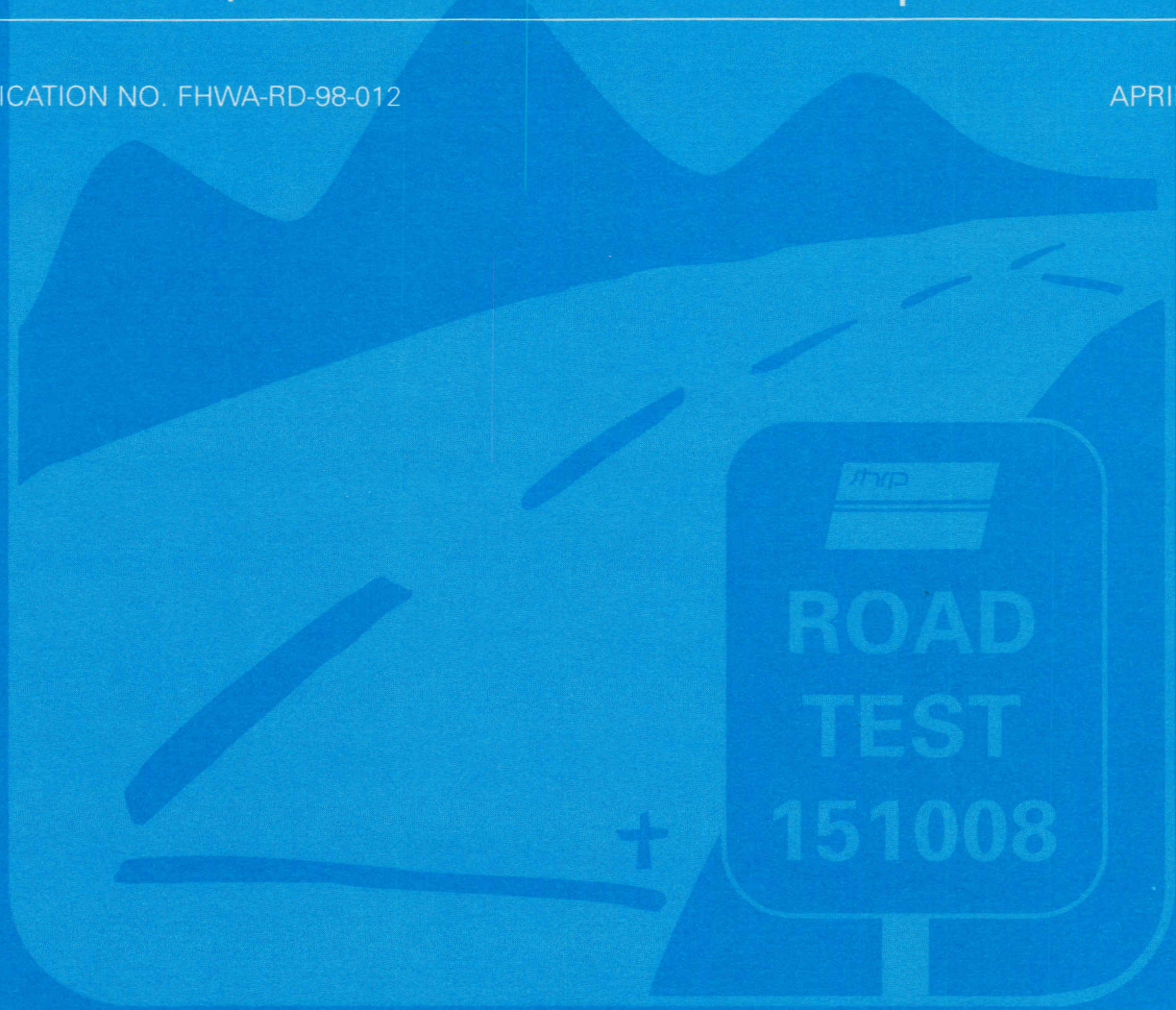

Mechanistic Evaluation of Test Data From LTPP Flexible Pavement Test Sections, Volume I: Final Report

PUBLICATION NO. FHWA-RD-98-012

APRIL 1998



U.S. Department of Transportation
Federal Highway Administration

Research and Development
Turner-Fairbank Highway Research Center
6300 Georgetown Pike
McLean, VA 22101-2296

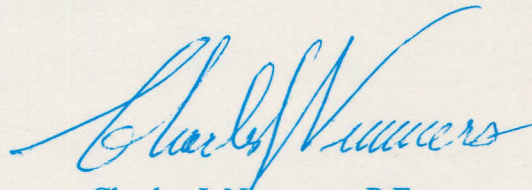


FOREWORD

The days in which we can significantly advance the science of pavement engineering through purely empirical approaches are over. Instead, we must turn to mechanistically based analyses, which seek to explain the mechanisms associated with pavement deterioration. This fact is reflected in the requirement that the *2002 Guide for Design of New and Rehabilitated Pavement Structures* (2002 Guide), currently under development through the National Cooperative Highway Research Program, be based on mechanistic concepts.

This report is the first of a two-volume series documenting the first-ever application of Long Term Pavement Performance (LTPP) data to the evaluation of mechanistically based performance prediction procedures for flexible pavements. Volume II: Final Report—Appendices is available only through the National Technical Information Service (NTIS).

This report will be of benefit to those interested in the development of mechanistically based performance prediction and design procedures for flexible pavements. It will be of particular interest to those involved in the development of the 2002 Guide.



Charles J. Nemmers, P.E.
Director
Office of Engineering
Research and Development

NOTICE

This document is disseminated under the sponsorship of the Department of Transportation in the interest of information exchange. The United States Government assumes no liability for its contents or use thereof. This report does not constitute a standard, specification, or regulation.

The United States Government does not endorse products or manufacturers. Trademarks or manufacturers' names appear herein only because they are considered essential to the object of this document.

1. Report No. FHWA-RD-98-012	2. Government Accession No.	3. Recipient's Catalog No.	
4. Title and Subtitle MECHANISTIC EVALUATION OF TEST DATA FROM LTPP FLEXIBLE PAVEMENT TEST SECTIONS, Volume I: Final Report		5. Report Date April 1998	6. Performing Organization Code
		7. Author(s) Hesham A. Ali and Shiraz D. Tayabji	8. Performing Organization Report No.
9. Performing Organization Name and Address ERES Consultants, Inc. 9030 Red Branch Road, Suite 210 Columbia, Maryland 21045		10. Work Unit No. (TRAVIS)	
		11. Contract or Grant No. DTFH61-95-C-00028	
12. Sponsoring Agency Name and Address Office of Engineering Research and Development Federal Highway Administration 6300 Georgetown Pike McLean, Virginia 22101-2296		13. Type of Report and Period Covered Final Report Feb. 1995 to Dec. 1997	
		14. Sponsoring Agency Code	
15. Supplementary Notes Contracting Officer's Technical Representative (COTR): Cheryl Allen Richter, HNR-30			
16. Abstract <p>The study reported here was conducted to assess how well some of the existing asphalt pavement mechanistic-empirical distress prediction models performed when used in conjunction with the data being collected as part of the national Long Term Pavement Performance (LTPP) program. As part of the study, appropriate data were obtained from the National Information Management System (NIMS) for the GPS-1 and GPS-2 experiments. The first phase of the data analysis involved using the deflection test data to backcalculate pavement layer moduli values. Using representative values of the layer moduli, structural analyses were performed for up to 140 axle-load configurations for the selected test sections. Then, the Asphalt Institute and the Shell procedures were used to predict fatigue cracking and rutting damage. The computed results were compared with observed values. Based on the results, new forms of the fatigue cracking models have been proposed. Also, a new approach to predicting rutting has been developed. This new procedure would account for rutting in each pavement layer and would consider rate-hardening typically observed in the development of rutting.</p> <p>This study has shown that, even given the many current limitations in the LTPP database, the LTPP data can be used successfully to develop a better insight into pavement behavior and to improve pavement performance.</p> <p>This volume is the second in a series. The other volume in the series is: FHWA-RD-98-020 Volume II: Final Report—Appendices</p>			
17. Key Words Asphalt pavement, backcalculation, fatigue cracking, LTPP, NIMS, pavement performance, pavement testing, rutting.		18. Distribution Statement No restrictions. This document is available to the public through the National Technical Information Service, Springfield, VA 22161.	
19. Security Classification (of this report) Unclassified	20. Security Classification (of this page) Unclassified	21. No. of Pages 108	22. Price

SI* (MODERN METRIC) CONVERSION FACTORS

APPROXIMATE CONVERSIONS TO SI UNITS					APPROXIMATE CONVERSIONS FROM SI UNITS				
Symbol	When You Know	Multiply By	To Find	Symbol	Symbol	When You Know	Multiply By	To Find	Symbol
LENGTH					LENGTH				
in	inches	25.4	millimeters	mm	mm	millimeters	0.039	inches	in
ft	feet	0.305	meters	m	m	meters	3.28	feet	ft
yd	yards	0.914	meters	m	m	meters	1.09	yards	yd
mi	miles	1.61	kilometers	km	km	kilometers	0.621	miles	mi
AREA					AREA				
in ²	square inches	645.2	square millimeters	mm ²	mm ²	square millimeters	0.0016	square inches	in ²
ft ²	square feet	0.093	square meters	m ²	m ²	square meters	10.764	square feet	ft ²
yd ²	square yards	0.836	square meters	m ²	m ²	square meters	1.195	square yards	yd ²
ac	acres	0.405	hectares	ha	ha	hectares	2.47	acres	ac
mi ²	square miles	2.59	square kilometers	km ²	km ²	square kilometers	0.386	square miles	mi ²
VOLUME					VOLUME				
fl oz	fluid ounces	29.57	milliliters	mL	mL	milliliters	0.034	fluid ounces	fl oz
gal	gallons	3.785	liters	L	L	liters	0.264	gallons	gal
ft ³	cubic feet	0.028	cubic meters	m ³	m ³	cubic meters	35.71	cubic feet	ft ³
yd ³	cubic yards	0.765	cubic meters	m ³	m ³	cubic meters	1.307	cubic yards	yd ³
MASS					MASS				
oz	ounces	28.35	grams	g	g	grams	0.035	ounces	oz
lb	pounds	0.454	kilograms	kg	kg	kilograms	2.202	pounds	lb
T	short tons (2000 lb)	0.907	megagrams (or "metric ton")	Mg (or "t")	Mg (or "t")	megagrams (or "metric ton")	1.103	short tons (2000 lb)	T
TEMPERATURE (exact)					TEMPERATURE (exact)				
°F	Fahrenheit temperature	5(F-32)/9 or (F-32)/1.8	Celcius temperature	°C	°C	Celcius temperature	1.8C + 32	Fahrenheit temperature	°F
ILLUMINATION					ILLUMINATION				
fc	foot-candles	10.76	lux	lx	lx	lux	0.0929	foot-candles	fc
fl	foot-Lamberts	3.426	candela/m ²	cd/m ²	cd/m ²	candela/m ²	0.2919	foot-Lamberts	fl
FORCE and PRESSURE or STRESS					FORCE and PRESSURE or STRESS				
lbf	poundforce	4.45	newtons	N	N	newtons	0.225	poundforce	lbf
lbf/in ²	poundforce per square inch	6.89	kilopascals	kPa	kPa	kilopascals	0.145	poundforce per square inch	lbf/in ²

* SI is the symbol for the International System of Units. Appropriate rounding should be made to comply with Section 4 of ASTM E380.

TABLE OF CONTENTS

	Page
CHAPTER 1. INTRODUCTION	1
The LTPP Program	2
M-E Distress Modeling Fundamentals	3
Scope of Work	6
Report Organization	7
CHAPTER 2. DATA ACQUISITION	9
Monitoring Data	9
Inventory Data	12
Cross-Section Data	12
Climatic Data	12
Materials Data	12
Traffic Data	12
Seasonal Data	13
Data Variability	13
Missing Data	13
Test Sections	13
Experimental Cell Design	16
CHAPTER 3. PAVEMENT LAYER MODULI BACKCALCULATION	19
PADAL Program and Results	19
WESDEF Program and Results	19
MODULUS Program and Results	21
Deflection Basin Fit Criteria	21
AC Layer Modulus Temperature Adjustment	22
Mean Annual Pavement Temperature Calculation	22
Temperature Adjustment Algorithm	27
CHAPTER 4. PAVEMENT STRUCTURAL ANALYSIS	29
Introduction	29
Consideration of Spatial and Seasonal Variations in Pavement Layer Properties	29
Consideration of Traffic Loading	31
Calculation of Cumulative Traffic Application	33
Calculation of Critical Strains	36
CHAPTER 5. FATIGUE DAMAGE ANALYSIS	39
Introduction	39
Observed Fatigue Cracking	39
Asphalt Institute Fatigue Cracking Model	39
Comparison: Predicted Versus Observed Performance, GPS-1 Sections	43
New Fatigue Cracking Model	43
Model Calibration	45

TABLE OF CONTENTS (Continued)

	Page
Linear Model	45
Exponential Growth Model	49
Fatigue Modeling Discussion	49
Fatigue Cracking Analysis, GPS-2 Sections	49
Summary	52
CHAPTER 6. RUTTING ANALYSIS	55
Introduction	55
Observed Rutting	55
Asphalt Institute Rutting Model	55
Comparison: Predicted Versus Observed Rutting	58
Summary	61
CHAPTER 7. THE SHELL MODELS	63
Introduction	63
Shell Fatigue Cracking Model Evaluation	63
Shell Rutting Model Evaluation	66
Summary	69
CHAPTER 8. CASE STUDY: COMPARING METHODS OF ASSESSING THE EFFECTS OF SEASONAL VARIATIONS ON DAMAGE ANALYSIS	71
Case Study: LTPP Section 311030	71
Comparison: Approach 1 Versus Approach 2	75
CHAPTER 9. NEW RUTTING MODEL	77
Introduction	77
Model Formulation	77
Model Calibration	83
Model Calibration Results	83
Goodness of Fit	85
Model Validation	85
Summary	90
CHAPTER 10. SUMMARY AND RECOMMENDATIONS	91
General Observations	91
Fatigue Cracking: Mechanistic Prediction Procedures	91
Rutting: Mechanistic Prediction Procedures	93
LTPP Data Issues	94
Materials Data	94
Traffic Data	95
Deflection Test Data	95
Distress Data	96

TABLE OF CONTENTS (Continued)

	Page
Sensitivity Data	96
Summary	96
REFERENCES	99

LIST OF FIGURES

Figure		Page
1	Typical transverse profiles	11
2	Flow chart of data analysis steps	14
3	Pavement layer models used in backcalculation analysis	20
4	Response points	32
5	Cumulative traffic consideration	34
6	Layer model used in the structural analysis	37
7	Plot of fatigue cracking versus damage ratio for GPS-1	44
8	Constrained growth model	46
9	Modified constrained growth model	47
10	Linear model	48
11	Exponential growth model	50
12	Fatigue damage versus fatigue cracking for GPS-2	51
13	Fatigue cracking, GPS-1 versus GPS-2	53
14	Rutting for GPS-1	59
15	Rutting for GPS-2	60
16	The Shell fatigue model, GPS-1 sections	64
17	The AI versus the Shell fatigue models, GPS-1 sections	65
18	Shell rutting model, GPS-1 sections	67
19	Comparison between the AI and the Shell rutting models	68
20	Seasonal variation effects on fatigue damage ratio	73
21	Seasonal variation effects on rutting damage ratio	74
22	Three-dimensional strain model	78
23	Histogram of residuals	86
24	Observed versus predicted rut depth	87
25	Observed versus predicted rut depth, based on validation data set	88
26	Rutting development for section 091047 (GPS-1)	89

LIST OF TABLES

Table		Page
1	Data elements and their source tables	10
2	Fatigue cracking in sections with traffic data	15
3	Fatigue cracking in sections missing traffic data	15
4	GPS-1 sections in the analysis	17
5	GPS-2 sections in the analysis	18
6	PADAL versus WESDEF backcalculation results	22
7	Pavement layer thicknesses for GPS-1 sections	23
8	Pavement layer thicknesses for GPS-2 sections	24
9	Layer moduli for GPS-1 sections	25
10	Layer moduli for GPS-2 sections	26
11	Observed fatigue cracking in GPS-1 sections	40
12	Observed fatigue cracking in GPS-2 sections	41
13	Observed rutting in GPS-1 sections	56
14	Observed rutting in GPS-2 sections	57
15	T-test for the difference between the AI and the Shell fatigue models	66
16	T-test for the difference between the AI and the Shell rutting models	66
17	Effects of seasonal variations on damage analyses	72
18	Uncertainty factors and their expected effects on pavement performance	92

CHAPTER 1. INTRODUCTION

Over the years, pavement engineers have been attempting to develop “rational” design procedures for both flexible and rigid pavements. These rational procedures have focused on using mechanistic considerations to explain the behavior of pavements under traffic and environmental loadings. The basic assumption of these rational procedures is that the primary pavement distresses are a result of damage induced by stresses, strains, or deformations that in turn result from traffic and environmental loadings. Under normal operating conditions, damage to the pavement occurs from a large number of repetitive traffic and environmental loadings over a period of time. Thus, each incremental loading results in some damage to the pavement, and the cumulative effect of the damage over a period of time results in the manifestation of specific distress, such as fatigue cracking in asphalt concrete (AC) and portland cement concrete (PCC) pavements, rutting in AC pavements, and faulting in PCC pavements. A pavement is considered to have failed when the distress level (severity and extent or magnitude) reaches or exceeds a predefined acceptable level for that distress, for a given category of highway.

Since the 1950s, as the techniques for analyzing pavement response to loading began to be available, there have been many attempts to develop rational design procedures, now commonly referred to as mechanistic-empirical (M-E) procedures, to define/describe the development of specific distresses in pavements. Also, the proposed revision of the *AASHTO Guide for Design of Pavements*, to be completed by the year 2002, will be based on M-E procedures. The M-E procedures typically involve the following steps:

1. Establishment of a hypothesis for the mechanism involved in the development of the specific distress. For example, the development of fatigue cracking in AC pavements is considered by many to be due to the repeated application of bottom tensile strain in the AC layer. This is the most critical step, as all the subsequent steps depend on the correctness of the hypothesis. The hypothesis determines the type of analysis needed to compute the critical response(s), as well as the material and traffic characterizations needed for the analysis.
2. Comprehensive material characterization, incorporating: changes in material properties as a function of the state of stress (stress dependency), environmental conditions (temperature and moisture), aging, and continual deterioration under traffic loading.
3. For each set of conditions, determination of critical responses (stresses, strains, deformations) within the pavement layers when subjected to traffic and environmental loadings.
4. Estimation of damage due to each set of conditions of traffic and environmental loading. This is typically done using distress prediction models or transfer functions that relate a critical structural response to specific distress damage. A different model is used for each distress and pavement type.

5. Evaluation of the damage accumulation over a period of time. Miner's fatigue damage hypothesis [1] is generally used to account for this cumulative damage. Based on predefined relationships between accumulated damage and distress development, the amount of distress that may develop at the end of the selected service life is estimated. The selected pavement may then be redesigned, if the estimated amount of distress exceeds the acceptable level, or is significantly less than that level.
6. Selection of the pavement design that results in acceptable levels of distresses at the end of the target service/design life.

Similar steps are followed to evaluate the performance of existing pavements. If the previous traffic loading, material properties, and environmental conditions are known (or can be estimated), the six steps may be followed to estimate accumulated distress-specific damages in the pavement and predict future pavement performance. Although these six steps may seem simplistic, the actual process is very complex, because of the many still-undefinable factors associated with pavement design and construction, traffic loading, and environmental conditions.

As part of an FHWA-sponsored project, a study was undertaken to use test data from the currently ongoing Long Term Pavement Performance (LTPP) program in conjunction with currently available M-E design procedures, to assess how well those procedures would perform using that data. In essence, the LTPP test data were used to perform a reality check on the validity of several M-E-based distress prediction procedures. Under this study, existing M-E design procedures were used to determine cumulative damage in relation to a specific distress, in each applicable LTPP test section. The estimated distress was then compared to the predicted distress. In addition, an attempt was made to develop calibrated distress models that would relate the accumulated damage to the observed level of distress.

This report presents the study results applicable to AC test sections from the LTPP program. In the subsequent sections, details are presented on the LTPP program, the LTPP data used in the study, and the procedures used to compute the cumulative damage. Additional background information related to this study is given in a companion volume. This companion volume, FHWA Report No. FHWA-RD-98-020 (*Mechanistic Evaluation of Test Data From LTPP Flexible Pavement Test Sections, Volume II: Final Report – Appendices*), contains appendixes A to E.

The LTPP Program

The LTPP program is a 20-year program established under the now-completed Strategic Highway Research Program (SHRP). The first 5 years of the LTPP program (mid-1987 to mid-1992) were funded under the SHRP funding; since mid-1992, the FHWA has assumed the management and funding of the LTPP program. While the LTPP program was conceived to meet many needs of the pavement engineering community, one major objective was to develop a national pavement performance database that could be used to develop and/or validate pavement design procedures. The study reported here was aimed at fulfilling that objective.

The LTPP program is collecting information on the long-term performance of various pavement structures under a range of traffic loadings, climatic factors, and subgrade soils. The LTPP program includes two fundamental classes of studies: the General Pavement Studies (GPS), and the Specific Pavement Studies (SPS). The GPS experiments are a series of selected in-service pavement studies structured to develop a comprehensive, national pavement-performance database. These studies are restricted to pavements that incorporate materials and designs representing good engineering practice and that are in common use across the United States and Canada. Studies included in GPS are:

First Performance Period

- GPS-1 - AC on granular base.
- GPS-2 - AC on bound base.
- GPS-3 - Jointed plain concrete.
- GPS-4 - Jointed reinforced concrete.
- GPS-5 - Continuously reinforced concrete.

Overlays

- GPS-6 - AC overlays on AC.
- GPS-7 - AC overlays on PCC pavements.
- GPS-9 - Unbonded PCC overlays on PCC pavements.

Details on the GPS experiments pertaining specifically to the study reported here are provided in later sections of this report.

The SPS program involves the study of specially constructed, maintained, or rehabilitated pavement sections incorporating a controlled set of experimental design and construction features. Test data from the SPS experiments were not included in this reported study. No additional discussion on the SPS experiments is provided here.

As part of the LTPP program, an extensive data collection effort has been underway since about 1989. These data types are classified within the LTPP program as follows:

1. Inventory.
2. Materials testing.
3. Climatic.
4. Monitoring.
5. Traffic.
6. Seasonal.

In addition, maintenance, rehabilitation, and construction data are also collected, as appropriate.

M-E Distress Modeling Fundamentals

The M-E distress modeling approach involves the following elements:

1. A structural analysis model that can consider the geometry of the pavement (principally, the layered system), the loading condition (multiple wheel loads), and the stress dependency of paving materials. The model must also be capable of reliably determining the critical responses appropriate to the distress being considered. For AC pavements, both linear-elastic and viscoelastic structural analysis models are available. However, most of the M-E distress model work has been done using linear-elastic models.
2. A fairly reliable estimate of traffic loading. Advanced M-E procedures consider the axle loading spectra, while other models are based on the use of equivalent loading (e.g., equivalent single axle load [ESAL]), in which case all loadings are transformed into a single load type using load equivalency concepts. However, the use of such equivalent traffic loading limits the usefulness of many of these models in developing rational design procedures.

The traffic loading data may need to be available on a seasonal basis and, in the case of concrete pavements, on a diurnal basis, as well as by lateral placement along the width of the traffic lane.

3. A fairly reliable estimate of seasonal climatic conditions, to account for changes in material properties and, in the case of concrete pavements, also to account for the effect of internal-concrete temperature differentials on curling stresses.
4. Comprehensive material characterization. The AC material properties need to be characterized in terms of temperature effects and in terms of aging. The granular material properties need to be characterized in terms of stress dependency and in terms of seasonal variation as a result of seasonal moisture and temperature variations within these materials. For example, the spring-thaw characterization for fine-grained materials is very important. For PCC materials, seasonal effects are not considered.
5. Availability of “calibrated” mechanistic distress models, or transfer functions that incorporate mechanistic responses. The general approach has been to develop “absolute” models based on laboratory testing and laboratory failure criteria and then to extrapolate those laboratory models to field conditions, using a shift factor to account for different levels of distress development and other unaccounted for factors. For example, for AC fatigue cracking, a model was developed on the basis of laboratory testing and the first crack-initiation as the failure criterion. This model was then expanded to account for different levels of fatigue cracking, as observed at the pavement surface. For example, the Asphalt Institute version of the model uses 20 percent fatigue cracking.
6. Acceptance of Miner’s fatigue damage hypothesis. Miner’s hypothesis suggests a method for combining various levels of damage done by a combination of traffic and environmental loadings. Miner’s hypothesis states that the structural fatigue damage is cumulative, and that a structure’s fatigue life, defined by the allowable

number of load applications prior to failure, is finite. Each load application consumes a small amount of fatigue life. When the actual number of load applications equal the number of allowable load applications, the fatigue damage is 1.0, or 100 percent, and failure occurs. Miner's hypothesis is typically stated as follows:

$$\text{Fatigue Damage, } D_f = \sum \frac{n_i}{N_i} \quad (1)$$

where: D_f = Cumulative fatigue damage.
 n_i = Actual number of load applications for a given set of conditions i .
 N_i = Allowable number of load applications to failure for a given set of conditions i .

In an ideal M-E procedure, damage (in relation to a specific distress) should be determined as follows:

$$\begin{aligned} \text{Damage}_{ijkl} &= f(e_{ijkl}) \\ \text{and} \\ e_{ijkl} &= f(E_{jkl}) \end{aligned} \quad (2)$$

where: e_{ijkl} = Critical pavement structural response that is considered to be a predictor of the distress under consideration for the i th axle group at the j th time period of the k th month of the l th year.
 E_{jkl} = Modulus of elasticity of each layer of the pavement system at the j th time period of the k th month of the l th year.

Thus, a major consideration in developing and using M-E procedures is the appropriate characterization of E_{jkl} for each pavement layer.

Our capability for realistically modeling pavement behavior has seen much progress in the last few decades. However, the capability to consider realistically the material characterization (e.g., E_{jkl}) for the pavement layers remains less than desired, because of a lack of knowledge of realistically accounting for seasonality effects, spatial variability, and deterioration effects due to traffic loading and environment.

It should be noted that the steps described here are applicable to the use of the M-E distress models for the design of new or rehabilitated pavements, or for checking such designs. The application of the M-E distress models to existing pavements to validate/calibrate the models further requires very reliable data on material properties, pavement section layering, past traffic loading history, past environmental conditions, and distress manifestation.

The validation/calibration process involves predicting the cumulative damage or distress and comparing the predicted distress to the observed distress. Because a large number of AC pavement distress prediction models have been developed, the study reported here was aimed at validating or calibrating some of these models.

Scope of Work

The overall objective of this study was to assess the performance of several existing M-E-based distress prediction procedures when used in conjunction with LTPP data.

The scope of work included the following for GPS-1 and GPS-2 experiments:

- Use deflection data to backcalculate the pavement layer moduli — an important input to structural evaluation. The nonlinear behavior of the subgrade was modeled by dividing it into five layers, to allow for different moduli at various depths.
- Use a linear elastic program to calculate the critical strains. The horizontal tensile strain at the bottom of the AC layer was used as a predictor of fatigue cracking, and the vertical compressive strain at the top of the subgrade was used as a predictor of rutting. Pavement response was calculated for each load level and axle category.
- Although viscoelastic models may be the best for modeling the mechanical behavior of AC mixtures, such models could not be used in this study, because the viscoelastic analysis requires several parameters, such as the creep compliance of the AC mix, that are not available in the LTPP database.
- Use existing transfer functions (i.e., those developed by the Asphalt Institute and Shell Oil Company) to predict the damage associated with each load level. The damage was summed over all load groups and over the entire service life of the pavement. The resulting total damage was then compared to the observed pavement distresses to ascertain if there was a reasonable agreement between the observed and the predicted distress levels. Also, since the current distress prediction procedures only allow a “one-point” comparison (e.g., 20 percent fatigue cracking when the fatigue damage approaches 100 percent), an attempt was made to develop a continuous distress prediction function/model that would relate the accumulated distress to the computed cumulative fatigue damage.
- The lack of fit between observed and predicted rutting prompted the development of a theoretical rutting model, which was calibrated using the LTPP data. The model was formulated such that traffic could be characterized by axle load/type counts, rather than the commonly used ESALs.

Report Organization

As discussed, the study reported here was aimed at using LTPP data to assess the applicability of several existing M-E analysis procedures, specifically, the Asphalt Institute and Shell Oil Company procedures for predicting the development of fatigue cracking and rutting in AC pavements. Chapter 2 details the process used to develop the necessary data needed for the study, using the LTPP database. Chapter 3 describes the backcalculation procedure used to establish representative layer moduli values for each LTPP test section used in the study. Chapter 4 describes the structural analysis techniques used to compute the critical structural responses in the LTPP sections due to traffic loading.

In chapter 5, analysis results are presented for an assessment of the Asphalt Institute fatigue cracking prediction procedure. In addition, new continuous-function models are presented that predict the amount of fatigue cracking as a function of computed fatigue damage. In chapter 6, analysis results are presented for an assessment of the Asphalt Institute rutting prediction procedure.

In chapter 7, the Shell fatigue cracking and rutting models are evaluated. Chapter 8 presents a case study of the different methods available to account for the seasonal variations in damage analysis. The development, calibration, and validation of a new rutting model is presented in chapter 9. This new model accounts for rutting in each pavement layer and considers the “rate-hardening” typically observed in the progressive development of rutting. Finally, chapter 10 presents a summary of the findings and includes a discussion of improvements needed to advance the reliability of M-E procedures using LTPP data.

The final report also incorporates appendices A through E. These appendices are contained in Volume II: Final Report – Appendices. The following appendices are included in Volume II:

- Appendix A – Test Sections With Missing Data
- Appendix B – Sample of Backcalculation Output
- Appendix C – Analysis of GPS-2 Sections With Other Base Treatment Than Asphaltic
- Appendix D – Sample of WESLEA Output
- Appendix E – Summary of Damage Ratio Values

CHAPTER 2. DATA ACQUISITION

The LTPP data used in this analysis were obtained from NIMS during February 1996 (Release 6.0 data). It was the most recent version of the data release, as of the date of this study. The NIMS data is categorized into seven modules: inventory, environment, materials testing, monitoring, maintenance, rehabilitation, and traffic. In each module, the data are stored in tables; each table is given a name and contains a group of variables. This section briefly discusses the data elements used in the analysis, the specific tables from which the data were obtained, the manipulation performed on the data, and the test sections that were excluded from the analysis because of the lack of data. More details are presented in chapters 3, 4, and 5, as relevant.

Monitoring Data

The monitoring module contains data from various performance monitoring activities. The falling weight deflectometer (FWD) deflection data, fatigue cracking data (from distress surveys), and rutting data were obtained from the tables listed in table 1.

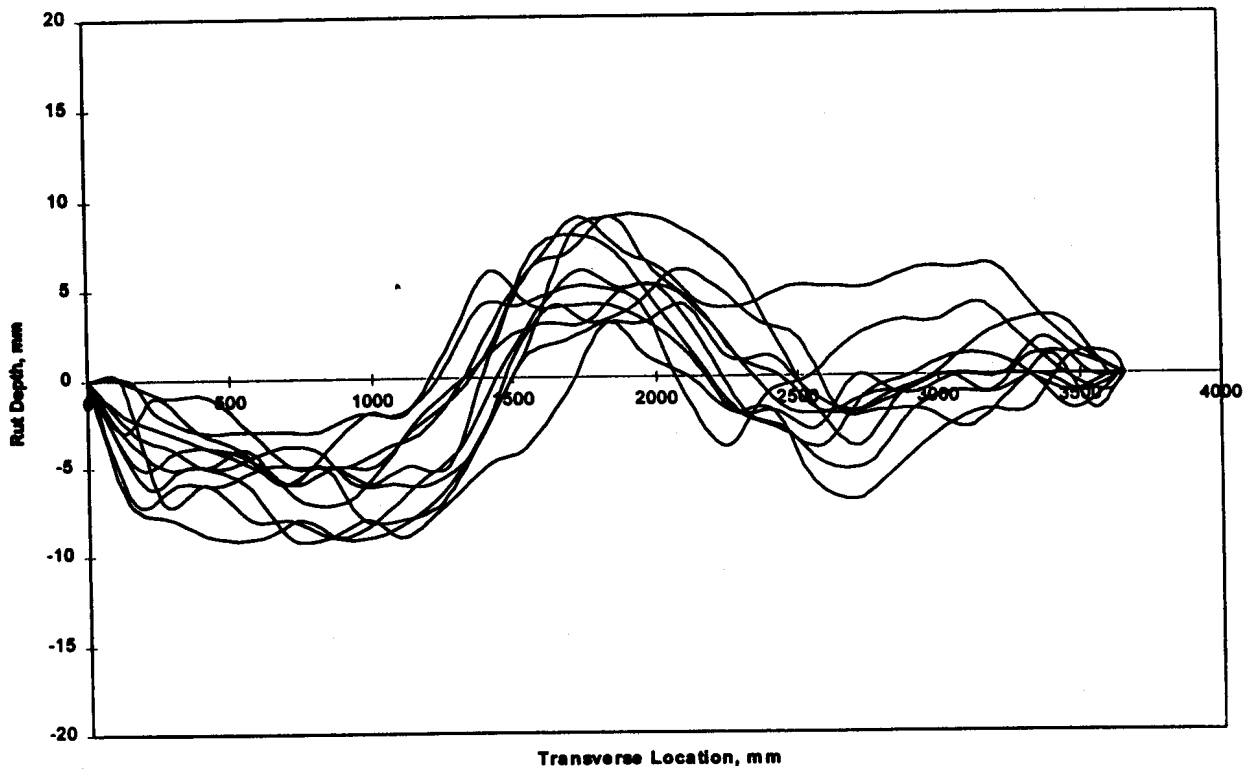
The pavement temperature during FWD testing was necessary to adjust the AC layer backcalculated modulus to the mean annual pavement temperature. Pavement mid-depth temperature was manually collected during FWD testing. Pavement temperature was collected at approximately 1-hour time intervals, whereas FWD testing was conducted at approximately 2- to 6-minute intervals. A linear regression process was used to estimate the pavement mid-depth temperature during FWD testing. Pavement layer thicknesses and the mid-depth pavement temperature were combined with the deflection data to perform the backcalculation.

Typical transverse profiles, as measured in the LTPP program, are shown in figure 1. It should be noted that transverse profiles are measured using a photographic technique at a spacing of about 15 m (50 ft). As such, the rut depth used for a given section is the average of the 11 values. The precision of the rut depth measure has been reported to be ± 2 mm (0.079 in). The average rut depth was calculated from the cross profile data and was based on a 1.8-m (6-ft) straightedge. The rut depth data were provided by Brent Rauhut Engineering (BRE), Austin, Texas.

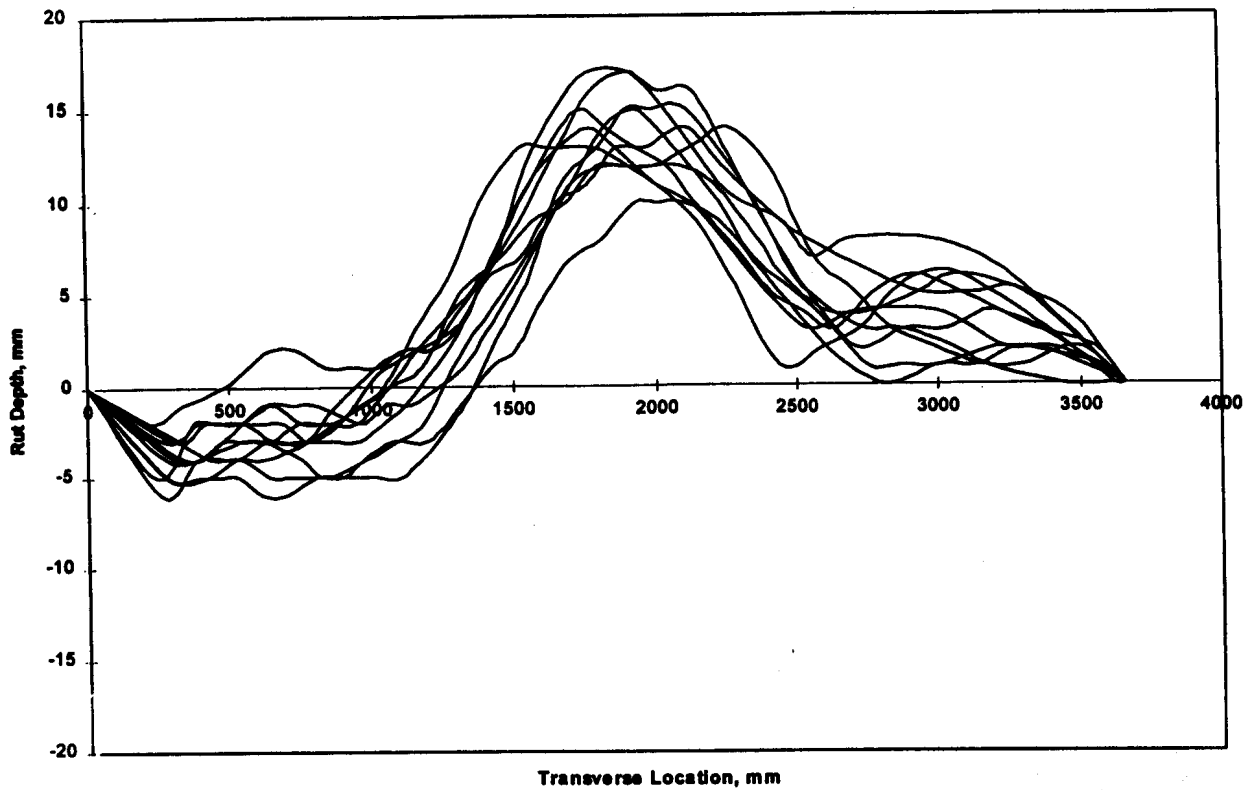
For the fatigue cracking analysis, data for all severity levels were grouped together. Under the LTPP program, fatigue cracking is categorized as low, medium, and high severity. In addition, in the field, fatigue cracking is measured using two procedures — the PASCO photographic procedure, and manual surveys. It should be noted that the results of the two methods have been found not to be consistent. For this study, the manual survey data were the data of choice. For those sections missing manual surveys, the PASCO data were used. The last distress survey for each section was used in the analysis, and the associated date was used in estimating the cumulative traffic counts from the “traffic open” date to the date of the last distress survey.

Table 1. Data elements and their source tables.

Data Element	Table Name	File Extension	Comments
Pavement layers and material description.	TST_LO5B	*.T32	
Deflection testing.	MON_DYNATEST_DROP_DAT	*.M06	
Pavement temperature at various depths.	MON_TEMPERATURE_TEMPS	*.M22	
Temperature depths.	MON_TEMPERATURE_DEPTH	*.M21	
PASCO distress survey.	MON_DIS_PADIAS_AC	*.M15	These two tables were combined and the last survey was used.
Manual distress survey.	MON_DIS_AC	*.M10	
Rutting transverse profile.	MON_RUT_MASTER	*.M23	
Rutting from profilometer data.	MON_RUT_DEPTHS	*.M24	Based on 1.8-m (6-ft) straightedge.



Measurements obtained from test section 48B340 on March 8, 1991.



Measurements obtained from test section 48B340 on March 4, 1993.

Figure 1. Typical transverse profiles.

Inventory Data

The inventory module supplies such data as the date the section was opened to traffic, the construction date, material types, and layer thicknesses. The information regarding the traffic opening date for each section were obtained from tables INV_AGE. For those GPS sections that were recently overlaid, a deflection analysis and the distress survey had to be interpreted accordingly. Major improvements data were obtained from tables INV_MAJOR_IMP.

Cross-Section Data

The cross-section data were obtained from table TST_L05B. These data were based on average values obtained from the test pits at each end of the test section. The data included layer thicknesses and material types. All layers, including the AC layers, were reported separately. The multiple AC layers were combined into one layer and the multiple granular subbase layers were combined into one layer.

Climatic Data

The environment data module contains statistical measures of selected climatic variables for each section. The mean monthly air temperature (MMAT) data were available for a number of years for each section, based on data extrapolated from adjacent weather stations. These values were averaged for each section and were used to derive the mean monthly pavement temperature and the mean annual pavement temperature. Table ENV_MONTHLY_PARAMETER was the source of MMAT.

Materials Data

The descriptions of pavement layers (material types) were obtained from table TST_L05B. Material descriptions were used to classify the treated base layers into cement-, lime-, or asphalt-treated, soil cement, lean concrete, or others. Materials data, as developed through laboratory testing, were not directly used in the study. The primary materials data needed for the mechanistic analysis was the layer moduli data. These data were developed using the deflection test data.

Traffic Data

Traffic data were obtained from tables TRF_MONITOR_AXLE_DISTRIB. The tables give the annual number of counts of a particular load/axle combination. There are 140 axle-load/type categories for each section. The axle categories include single, tandem, tridem, and four-axle assemblies. The axle counts were extrapolated from the days of actual weigh-in-motion (WIM) data. For example, if the counts were based on 350 days of WIM data, then the reliability of the annual figure would be higher than if the counts were based on, say, 14 days. Therefore, in cases where counts were given for more than one year, the year with the maximum number of WIM days was used to calculate the cumulative traffic counts. The number of WIM days was given in tables TRF_MONITOR_BASIC_INFO. The WIM data available were from 1990 to 1992. It should be noted that reliable traffic data are very critical for the development/

calibration/validation of mechanistically based design procedures. Although, there was a concern about the reliability of the then-available monitored traffic data, those data are the best available and a decision was made to use that data. A discussion of backcasting the traffic data to the year each section was opened is given later.

Seasonal Data

The seasonal monitoring data were not available at the time of the study. Therefore, seasonal adjustments to account for changes in material properties were not directly incorporated in the analysis. For the AC layer, the seasonality (temperature dependency) of the moduli values was accounted for by using seasonally adjusted moduli values, as discussed later.

Data Variability

The LTPP data, similar to other pavement related data, incorporates a wide range of variability in the various data elements. For the purpose of this study, only average values of the data were used, as appropriate.

Missing Data

The total number of GPS-1 sections is 233 and the total number of GPS-2 sections is 144. Some sections were missing traffic data, layer thickness data, deflection testing data, rutting data, and/or distress survey data. These sections were not used. Appendix A contains a series of tables that report the sections with missing data, grouped by the missing variables.

Test Sections

The pavement layer elastic moduli were backcalculated for all GPS-1 and GPS-2 sections for which there was deflection and layer thickness data. Structural analysis was carried out on the sections for which backcalculation was performed successfully (i.e., the deflection basin match error was within tolerance, as discussed later in the backcalculation section) and for which traffic and pavement temperature data were available. Figure 2 outlines the analysis steps.

The amount of fatigue cracking is an important variable in this analysis. The availability or lack of fatigue cracking in the analysis sections has a significant influence on the analysis results. Table 2 shows the sections in the analysis, categorized by the amount of fatigue cracking (expressed as the ratio between cracked area to total area). The table shows that there was only one GPS-1 section with fatigue cracking greater than 5 percent and less than 25 percent, and three sections had fatigue cracking greater than 25 percent. Similarly, there was only one GPS-2 section with fatigue cracking greater than 5 percent and less than 25 percent. The small number of sections exhibiting fatigue damage constrained the effort to study the development of such pavement distress. The number of data points in the failing region was less than the number needed to build a reliable model. Further discussion on this matter is provided later.

Table 3 shows the amount of fatigue cracking in sections that were excluded from the analysis for lack of traffic data. The table indicates that there were 13 sections in GPS-1 that

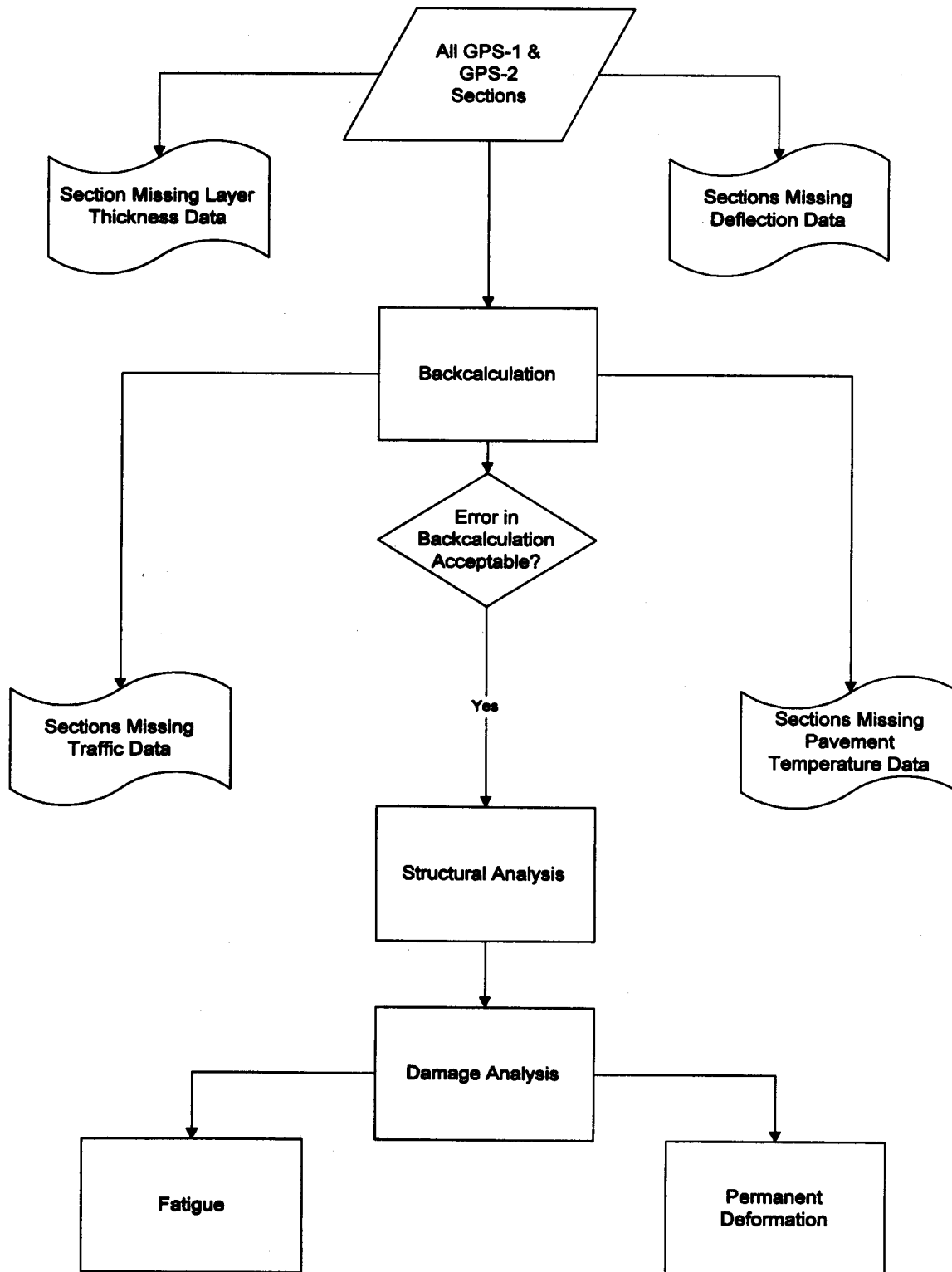


Figure 2. Flow chart of data analysis steps.

Table 2. Fatigue cracking in sections with traffic data.

GPS-1 Sections		GPS-2 Sections	
Less than 25% and greater than 5% of area	Greater than 25% of area	Less than 25% and greater than 5% of area	Greater than 25% of area
261012	123997 271019 341030	014073	

Table 3. Fatigue cracking in sections missing traffic data.

GPS-1 Sections		GPS-2 Sections	
Less than 25% and greater than 5% of area	Greater than 25% of area	Less than 25% and greater than 5% of area	Greater than 25% of area
041007	014127	067491	283090
041018	014155	082008	721003
041037	041021	283085	
068156	124102	482176	
131001	231009		
134111	371802		
307088	451008		
371024	451025		
451011			
481039			
481093			
481116			
481168			

exhibited fatigue cracking greater than 5 percent and less than 25 percent, and 8 sections had fatigue cracking greater than 25 percent. Four of the GPS-2 sections exhibited fatigue cracking greater than 5 percent and less than 25 percent, and two sections had fatigue cracking greater than 25 percent. The large number of sections exhibiting fatigue cracking and missing traffic data stresses the need for obtaining traffic data so that these sections can be utilized in future analysis and can be made productive.

Experimental Cell Design

Tables 4 and 5 show the experimental cell design of the analysis sections for GPS-1 and GPS-2 experiments, respectively. The cell assignment of the sections was based on inventory data. Table 5 shows that many of GPS-1 sections were located in a wet-freeze zone. No sections in the analysis represented the dry/no-freeze zone. There were no sections with fine subgrade in the wet/no-freeze zone. Many sections had a moderate to high AC stiffness. The sections were well distributed over traffic rate, AC stiffness, base thickness and AC layer thickness. Table 5 indicates that many of GPS-2 sections in the analysis were located in a wet/no-freeze zone. The sections were well distributed over traffic rate, AC stiffness, base thickness, subgrade type, and AC layer thickness.

Table 4. GPS-1 sections in the analysis.

MOISTURE			WET								DRY							
TEMPERATURE			FREEZE				NO-FREEZE				FREEZE				NO-FREEZE			
SUBGRADE TYPE			F		C		F		C		F		C		F		C	
TRAFFIC RATE			L	H	L	H	L	H	L	H	L	H	L	H	L	H	L	H
AC Stiff-ness	Base Thick-ness	AC Thick-ness	[REDACTED]															
L	L	L			271016								531006					
		H								123996								
	H	L																
		H				851801				123997	081029							
M	L	L			271019 276251					121030	311030		836451					
		H	261012 291002 511002	871620	211010 261004	261013 341003 871622			473075	011019 124106	321021							
	H	L	501004	891127	881645					124099	081047 081057 831801		836450					
		H	341030 421597		091803 251003	341031								531008				
H	L	L	211034 291008	291010 511464	271023 271029 271085	271028 271087			531801		201005		201010					
		H	171003	171002 181028		511023		014126										
	H	L		421605		331001												
		H	421599 501002	251004		251002 341011												

Table 5. GPS-2 sections in the analysis.

MOISTURE			WET								DRY							
TEMPERATURE			FREEZE				NO-FREEZE				FREEZE				NO-FREEZE			
SUBGRADE TYPE			F		C		F		C		F		C		F		C	
TRAFFIC RATE			L	H	L	H	L	H	L	H	L	H	L	H	L	H	L	H
Binder Type	Base Thickness	Surface Thickness	[REDACTED]															
Bitum- inous	L	L	361644 501683 892011		501681 881647	341033 473109	473110	014073	124108 479025					327000			404165	
		H						471028 473108	479024									321030
	H	L				341034		124097	124096 124100		087781						404163	
		H					361008	053071		053058								
Non- Bitum- inous	L	L																
		H	512021						011021	283082								
	H	L																
		H																

CHAPTER 3. PAVEMENT LAYER MODULI BACKCALCULATION

One of the most important structural parameters used in the M-E analysis is the modulus of elasticity of pavement layers. To predict pavement stresses, strains, and distresses, structural and damage analyses rely on the elasticity (resilient) moduli of the layers. Only a limited amount of data on the laboratory-derived resilient modulus of pavement layers were available in the LTPP database at the time of this study. The reliability of these data has been in question. For instance, a recent study by BRE [2] showed that the laboratory-derived AC layer modulus measured at 5°C appeared to be in error. Also, it is well known that pavement structural properties may exhibit significant seasonal and spatial variations. Unlike laboratory testing, in-situ deflection testing is performed over a longer period of time and at many testing points along the section. The pavement layer moduli backcalculated from deflection testing were therefore used in subsequent analysis, since they were derived using a larger sample size that covered wider ranges of time and space.

Three backcalculation programs were used to analyze deflection data: PADAL [3], WESDEF [4], and MODULUS [5]. It should be noted that the backcalculation results were based on deflection testing at a 40-kN (9,000-lb) load magnitude. The following paragraphs present a brief background and discussion of the assumptions made in the analysis of deflection data.

PADAL Program and Results

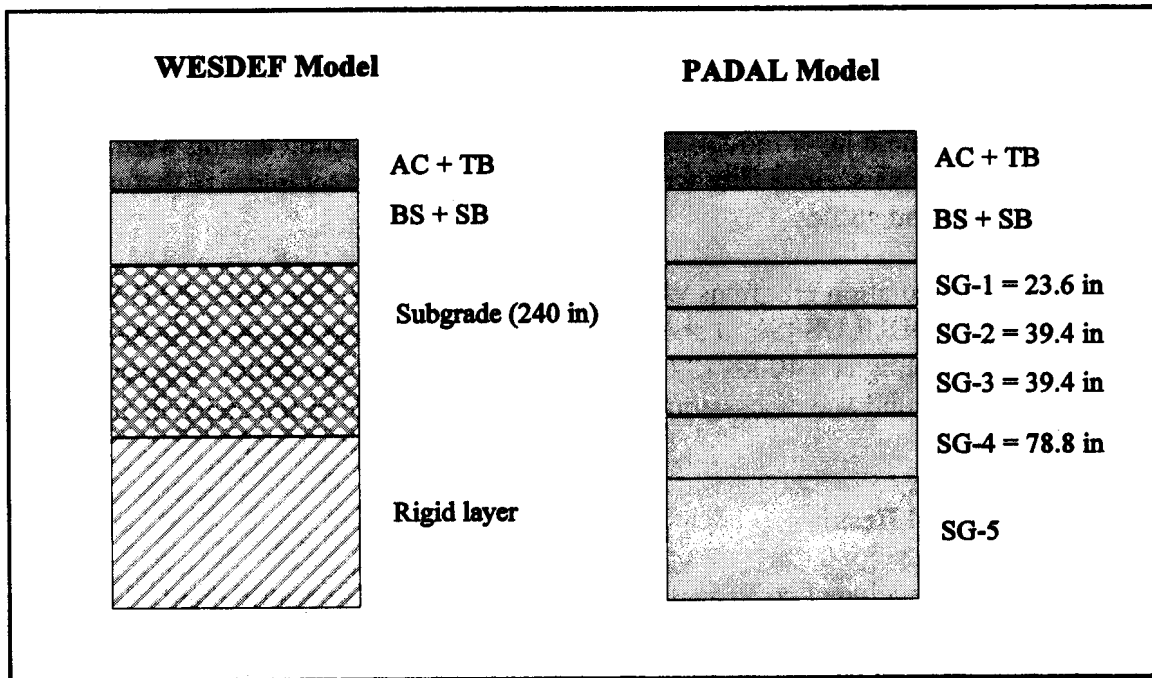
PADAL was developed by Brown, et al., at the University of Nottingham. The program is a linear elastic layer program that accounts for the nonlinearity of the subgrade by dividing it into five layers and assuming that the layer stiffness is a function of the stress state. The program implements an efficient deflection-matching algorithm, which results in fast program execution.

PADAL was used to backcalculate the elastic layer moduli of all available test points. Deflection testing is being performed 12 to 14 times a year, approximately every month, for seasonal sections and once every few years for nonseasonal sections. Deflection testing is conducted at 21 points along the wheelpath and along the lane centerline. Only the wheelpath test data were used for the backcalculation analysis.

In that analysis, the pavement was modeled as a seven-layer structure, as shown in figure 3. The first layer is the surface layer, the second layer is the combined base and subbase layers, and the third through the seventh layers are the subgrade layers, with thickness of 0.6, 1.0, 1.0, 2.0 m (23.6, 39.4, 39.4, 78.8 in), and infinity, respectively. Appendix B shows a sample of the output of PADAL.

WESDEF Program and Results

WESDEF is a linear elastic program that was developed by the Army Corps of Engineers, Waterways Experimental Station. The program uses a program called WESLEA [12] to perform a forward calculation of deflections. WESDEF implements an optimization method using least square fit between the observed and calculated deflections. The program divides the subgrade



1 in = 25.4 mm

Figure 3. Pavement layer models used in backcalculation analysis.

into two layers: an upper layer 6 m (240 in) deep, and a stiff lower layer. The layering arrangement used is shown in figure 3. The optimization procedure stops when the absolute sum of the percent differences between the computed and the measured deflections, or the predicted change in modulus values, becomes less than 10 percent.

WESDEF was used to backcalculate the elastic moduli of pavement layers for the GPS-1 sections. The pavement was modeled as the surface layer, the combined base and subbase (if available), the upper portion of the subgrade [6 m (240 in)], and the lower layer. Appendix B shows a sample of the WESDEF output.

MODULUS Program and Results

MODULUS [5] is a backcalculation program that can be applied to two-, three-, or four-layer systems with or without a rigid bedrock layer. A linear elastic program is used to generate a database of deflection bowls by assuming different modulus ratios. A pattern search routine is used to fit the measured and calculated bowls. The solution is defined as the optimum set of modulus ratios that minimizes the weighted sum of the difference between the observed and calculated deflections.

MODULUS was used to backcalculate the pavement layer moduli for the GPS-2 sections with a base layer treatment other than asphaltic. For these sections, the backcalculation error that resulted from using WESDEF was too large to consider using the results in the subsequent analysis. MODULUS was found to produce less error for these sections.

Deflection Basin Fit Criteria

It is generally recommended that the error for each FWD sensor location be calculated as the percent difference between the field deflection, and theoretical deflection, and runs with an absolute error per sensor of more than 2 percent be considered unacceptable [6]. Hence, such runs were excluded from further analysis. It was found that PADAL, in general, produced less error than WESDEF. Therefore, it was decided to use the PADAL backcalculation results in the pavement structural analysis.

Table 6 presents a comparison between the PADAL and WESDEF results for Section 11019. The table shows that the AC layer modulus derived by the two programs is similar. The granular material, as calculated by the two programs, is shown to have a smaller modulus than that of the subgrade. This trend was observed for much of the data.

The table also shows that the subgrade modulus, as calculated by PADAL, increases with the layer depth (due to overburden pressure). It should be noted that WESDEF assumes the existence of a stiff layer at a depth of 6 m (20 ft) in the subgrade, whereas PADAL does not make this assumption. Hence, the subgrade modulus values obtained by PADAL tend to be higher than those obtained using WESDEF.

Some of the key summary data for GPS-1 and GPS-2 (with asphalt treated base) are shown in tables 7 and 8.

Table 6. PADAL versus WESDEF backcalculation results.

Program		Error	AC Layer	Granular Base	Subgrade (SG-1)	SG-2	SG-3	SG-4	SG-5	Rigid Layer
PADAL	t (in)	1	6.5	5.5	23.6	39.4	39.4	78.8	inf.	n/a
	E (ksi)		414	14	37	41	44	47	53	n/a
WESDEF	t (in)	1.5	6.5	5.5	240				inf.	
	E (ksi)		401	20	29				1000	

1 in = 25.4 mm
1 ksi = 6894 kPa

The layer moduli values given in tables 9 and 10 were obtained using the PADAL program. The AC layer moduli values reported were corrected for the mean annual pavement temperature, as discussed in the following sections.

The backcalculated moduli of GPS-2 sections with a base layer treatment other than asphaltic were found to have a larger basin fit error than that of GPS-1 and GPS-2 sections with an asphalt-treated base course. It was necessary to relax the acceptance criterion for the deflection fit basin to a 5-percent absolute error per sensor. As such, the analysis (backcalculation, forward calculation, and damage analysis) of these sections is reported separately in appendix C.

AC Layer Modulus Temperature Adjustment

The backcalculated modulus of the AC layer corresponds to the temperature at which deflection testing was conducted. To compare the modulus at different points and at different sections, the modulus values at each test location were adjusted to a pavement temperature of 20° C (68° F). The modulus values were also adjusted to the mean annual pavement temperature (MAPT), to arrive at an effective annual AC layer modulus. After adjustments to 20° C (68° F), modulus values greater than practical limits [8.6 GPa (1,250,000 psi)] were excluded from the analysis. The methods used to perform the temperature adjustments are discussed in the following paragraphs.

Mean Annual Pavement Temperature Calculation

To calculate the MAPT using the Asphalt Institute (AI) method [7], the mean monthly air temperature (MMAT) is required. The mean monthly pavement temperature (MMPT) is first calculated, and the MAPT is the mean value of the MMPT. The AI method, outlined here, was used to estimate the MAPT.

Table 7. Pavement layer thicknesses for GPS-1 sections.

State	Section	AC (in)	TB (in)	GB (in)	GS (in)	TS (in)	SG_1(in)	SG-2 (in)	SG-3 (in)	SG-4 (in)	SG-5 (in)
1	1019	8.5	0	0	5.5	0	23.6	39.4	39.4	78.8	INF
1	4128	13.1	0	18.4	0	0	23.6	39.4	39.4	78.8	INF
8	1029	4.2	0	5.8	11	0	23.6	39.4	39.4	78.8	INF
8	1047	3.6	0	6.3	12.9	0	23.6	39.4	39.4	78.8	INF
8	1057	3.9	0	3.9	13.8	0	23.6	39.4	39.4	78.8	INF
9	1803	7.2	0	12	0	0	23.6	39.4	39.4	78.8	INF
12	1030	3.3	0	9.8	17.1	0	23.6	39.4	39.4	78.8	INF
12	3996	1.5	0	8	14.2	0	23.6	39.4	39.4	78.8	INF
12	3997	3.1	0	11.6	15	0	23.6	39.4	39.4	78.8	INF
12	4099	3.6	0	10.5	11.2	0	23.6	39.4	39.4	78.8	INF
12	4106	8.2	0	10	14.5	0	23.6	39.4	39.4	78.8	INF
17	1002	13.2	0	0	0	0	23.6	39.4	39.4	78.8	INF
17	1003	12.1	0	0	0	12	23.6	39.4	39.4	78.8	INF
18	1028	15.3	0	0	0	0	23.6	39.4	39.4	78.8	INF
20	1005	13.2	0	0	0	0	23.6	39.4	39.4	78.8	INF
20	1010	8.8	0	0	0	0	23.6	39.4	39.4	78.8	INF
21	1010	6.7	0	9.2	0	0	23.6	39.4	39.4	78.8	INF
21	1034	14.6	0	0	0	0	23.6	39.4	39.4	78.8	INF
25	1002	7.8	0	4	8.4	0	23.6	39.4	39.4	78.8	INF
25	1003	6.6	0	12.7	0	0	23.6	39.4	39.4	78.8	INF
25	1004	9.6	0	25.6	0	0	23.6	39.4	39.4	78.8	INF
26	1004	4.2	0	5	0	0	23.6	39.4	39.4	78.8	INF
26	1012	6.1	0	4.8	21.6	0	23.6	39.4	39.4	78.8	INF
26	1013	6.7	0	4.8	18.6	0	23.6	39.4	39.4	78.8	INF
27	1016	3	0	6.5	0	0	23.6	39.4	39.4	78.8	INF
27	1019	5	0	6.4	0	0	23.6	39.4	39.4	78.8	INF
27	1023	10.5	0	4	6.8	0	23.6	39.4	39.4	78.8	INF
27	1028	9.6	0	0	0	0	23.6	39.4	39.4	78.8	INF
27	1029	8.4	0	0	0	0	23.6	39.4	39.4	78.8	INF
27	1085	11.3	0	0	0	0	23.6	39.4	39.4	78.8	INF
27	1087	15.7	0	0	0	0	23.6	39.4	39.4	78.8	INF
27	6251	7.1	0	10.2	0	0	23.6	39.4	39.4	78.8	INF
29	1002	6.8	0	6	0	0	23.6	39.4	39.4	78.8	INF
29	1008	11.4	0	4.4	0	0	23.6	39.4	39.4	78.8	INF
29	1010	13.9	0	4.2	0	0	23.6	39.4	39.4	78.8	INF
31	1030	7.2	0	0	0	0	23.6	39.4	39.4	78.8	INF
32	1021	7.8	0	2.8	3.2	0	23.6	39.4	39.4	78.8	INF
33	1001	8.4	0	19.3	14.4	0	23.6	39.4	39.4	78.8	INF
34	1003	7.5	0	7.4	24.9	0	23.6	39.4	39.4	78.8	INF
34	1011	9	0	6.9	24.2	0	23.6	39.4	39.4	78.8	INF
34	1030	6	0	6.8	23.4	0	23.6	39.4	39.4	78.8	INF
34	1031	7.3	0	11	0	0	23.6	39.4	39.4	78.8	INF
42	1597	6.4	0	16.4	0	0	23.6	39.4	39.4	78.8	INF
42	1599	12.3	0	12	0	0	23.6	39.4	39.4	78.8	INF
42	1605	8.1	0	16.2	0	0	23.6	39.4	39.4	78.8	INF
47	3075	5	0	9.2	0	0	23.6	39.4	39.4	78.8	INF
50	1002	8.5	0	25.8	0	0	23.6	39.4	39.4	78.8	INF
50	1004	8	0	24.3	22.8	0	23.6	39.4	39.4	78.8	INF
51	1002	5.7	0	7.7	0	0	23.6	39.4	39.4	78.8	INF
51	1023	10.1	0	5.6	0	8.4	23.6	39.4	39.4	78.8	INF
51	1484	8.4	0	5.1	0	5.4	23.6	39.4	39.4	78.8	INF
53	1006	3.4	0	3.3	3.6	0	23.6	39.4	39.4	78.8	INF
53	1008	3.4	0	3.1	9.8	0	23.6	39.4	39.4	78.8	INF
53	1801	9.2	0	3.7	0	0	23.6	39.4	39.4	78.8	INF
83	1801	4.4	0	5.6	13.2	0	23.6	39.4	39.4	78.8	INF
83	6450	4.4	0	4.5	4.2	0	23.6	39.4	39.4	78.8	INF
83	6451	4.1	0	7.2	3.7	0	23.6	39.4	39.4	78.8	INF
85	1801	3.2	0	9.9	11.2	0	23.6	39.4	39.4	78.8	INF
87	1620	5	0	5.7	23.9	0	23.6	39.4	39.4	78.8	INF
87	1622	5.6	0	6.6	26.3	0	23.6	39.4	39.4	78.8	INF
88	1645	6.4	0	3.5	0	11.7	23.6	39.4	39.4	78.8	INF
89	1127	4.9	0	16.4	23.4	0	23.6	39.4	39.4	78.8	INF

1 in = 25.4 mm

Table 8. Pavement layer thicknesses for GPS-2 sections.

State	Section	AC (in)	TB (in)	GB (in)	GS (in)	TS (in)	SG_1 (in)	SG-2 (in)	SG-3 (in)	SG-4 (in)	SG-5
1	1021	3.1	4.5	0	0	17.4	23.6	39.4	39.4	78.8	INF
1	4073	8.6	0	0	4.9	5.2	23.6	39.4	39.4	78.8	INF
5	3058	13.3	0	0	0	0	23.6	39.4	39.4	78.8	INF
5	3071	16.4	0	0	0	0	23.6	39.4	39.4	78.8	INF
8	7781	3.4	7.1	0	0	0	23.6	39.4	39.4	78.8	INF
12	4096	1.3	8.6	0	0	13.4	23.6	39.4	39.4	78.8	INF
12	4097	7.7	6.3	0	6.3	0	23.6	39.4	39.4	78.8	INF
12	4100	2.9	7.6	0	0	13.1	23.6	39.4	39.4	78.8	INF
12	4108	3.9	6	0	0	12.9	23.6	39.4	39.4	78.8	INF
28	3082	7.2	3.6	0	7.1	0	23.6	39.4	39.4	78.8	INF
32	1030	7.6	1.8	0	0	2.8	23.6	39.4	39.4	78.8	INF
32	7000	4.8	4.8	0	0	5.6	23.6	39.4	39.4	78.8	INF
34	1033	1.2	6.2	0	0	13.8	23.6	39.4	39.4	78.8	INF
34	1034	11.1	0	0	0	0	23.6	39.4	39.4	78.8	INF
36	1008	1.1	9.7	0	0	12	23.6	39.4	39.4	78.8	INF
36	1644	2.3	6.3	0	0	14.5	23.6	39.4	39.4	78.8	INF
40	4163	11.5	0	0	0	0	23.6	39.4	39.4	78.8	INF
40	4165	8.1	0	0	0	0	23.6	39.4	39.4	78.8	INF
47	1028	12.1	0	0	0	3.8	23.6	39.4	39.4	78.8	INF
47	3108	12.2	0	0	0	6.1	23.6	39.4	39.4	78.8	INF
47	3109	5.2	4.3	0	0	4.5	23.6	39.4	39.4	78.8	INF
47	3110	9.2	0	0	0	0	23.6	39.4	39.4	78.8	INF
47	9024	5.7	7.1	0	0	0	23.6	39.4	39.4	78.8	INF
47	9025	4.5	2.3	0	0	12	23.6	39.4	39.4	78.8	INF
50	1681	2.3	3.4	0	0	33.6	23.6	39.4	39.4	78.8	INF
50	1683	2.6	2.8	0	0	36	23.6	39.4	39.4	78.8	INF
51	1423	1.2	4.4	0	1	8.5	23.6	39.4	39.4	78.8	INF
51	2021	1.3	6.2	0	0	3.6	23.6	39.4	39.4	78.8	INF
88	1647	1.5	5.4	0	6.9	6.2	23.6	39.4	39.4	78.8	INF
89	2011	3	3.3	0	0	38.9	23.6	39.4	39.4	78.8	INF

1 in = 25.4 mm

Table 9. Layer moduli for GPS-1 sections.

State	Section	E(AC/TB)	E(BS/SB)	E(SG-1)	E(SG-2)	E(SG-3)	E(SG-4)	E(SG-5)
		E1_MPT	E2	E3	E4	E5	E6	E7
1	1019	526,927	13,856	37,080	40,794	44,189	47,899	53,223
1	4128	546,575	23,023	44,563	49,868	58,054	73,479	116,248
8	1029	794,334	16,633	15,329	15,373	15,418	15,451	15,529
8	1047	1,142,204	33,488	21,452	21,907	22,326	22,748	23,387
8	1057	1,263,462	23,454	18,156	18,204	18,220	18,228	18,245
9	1803	1,137,615	21,799	59,318	60,806	61,867	63,257	65,218
12	1030	775,995	74,725	40,358	40,822	41,227	41,653	42,281
12	3996	525,376	89,566	32,174	32,174	32,174	32,174	32,319
12	3997	521,828	21,024	28,860	30,380	31,849	33,568	36,232
12	4099	390,271	60,891	52,637	57,164	61,381	66,191	73,438
12	4106	670,550	39,193	32,105	32,457	32,795	33,202	33,796
17	1002	1,342,158	n/a	12,608	22,831	43,253	98,178	356,244
17	1003	648,966	21,322	15,205	20,810	30,003	49,409	117,869
18	1028	771,186	n/a	18,216	30,647	57,648	134,104	509,081
20	1005	780,465	n/a	8,414	17,160	35,265	84,776	320,618
20	1010	1,107,375	n/a	9,042	17,368	36,081	92,325	394,773
21	1010	800,613	13,222	24,063	36,664	58,129	104,030	261,977
21	1034	739,443	n/a	19,643	53,133	131,018	363,517	1,595,567
25	1002	1,101,015	14,973	27,529	30,303	33,374	37,480	44,719
25	1003	1,062,895	25,206	30,219	32,895	35,437	38,372	42,706
25	1004	726,585	19,507	40,116	42,957	46,377	51,392	61,131
26	1004	1,525,369	49,522	29,725	35,435	40,305	45,587	53,015
26	1012	1,302,063	32,242	17,774	24,415	34,255	52,235	102,378
26	1013	829,004	28,848	31,228	33,360	36,015	40,317	51,167
27	1016	1,527,991	38,632	32,103	32,838	33,393	33,973	34,712
27	1019	550,371	39,434	22,161	22,398	22,602	22,813	23,083
27	1023	993,010	29,927	35,338	40,580	46,160	53,438	66,136
27	1028	1,885,525	n/a	19,028	23,900	32,901	56,615	171,998
27	1029	938,212	n/a	16,038	21,932	35,797	80,098	330,923
27	1085	561,347	n/a	5,686	15,737	41,492	124,443	599,688
27	1087	1,317,266	n/a	9,762	20,817	42,082	95,956	329,254
27	6251	1,319,399	34,167	33,882	34,908	35,856	36,987	38,681
29	1002	1,070,979	47,499	20,895	24,178	27,659	32,404	41,267
29	1008	669,239	24,804	35,996	37,638	39,474	41,965	46,480
29	1010	522,295	34,347	33,665	40,725	53,189	81,398	196,701
31	1030	864,059	n/a	13,174	18,243	29,319	64,877	274,096
32	1021	910,676	17,448	15,744	20,408	26,482	36,634	65,534
33	1001	1,182,460	17,598	54,110	54,524	54,959	55,518	56,305
34	1003	494,996	20,380	56,939	59,983	63,280	67,501	74,475
34	1011	885,669	22,699	53,207	53,225	53,316	53,370	53,461
34	1030	911,777	15,845	52,573	65,991	87,223	131,173	285,367
34	1031	626,396	19,505	25,038	29,113	33,129	37,894	45,149
42	1597	1,303,033	13,897	58,394	66,828	77,763	94,591	130,734
42	1599	940,838	16,087	67,311	68,712	70,484	72,980	77,906
42	1805	1,180,691	19,010	59,735	60,774	61,788	62,947	64,814
47	3075	1,119,193	48,412	8,840	11,535	14,318	17,987	24,450
50	1002	1,469,430	19,865	27,490	28,473	29,871	32,153	37,861
50	1004	851,985	40,809	37,010	40,519	44,768	51,068	63,715
51	1002	639,167	19,553	21,326	26,861	33,093	41,540	57,000
51	1023	1,228,473	49,299	32,041	41,797	58,951	98,297	261,413
51	1464	596,023	69,876	40,106	40,995	41,799	42,701	44,012
53	1006	1,520,184	24,572	23,754	26,805	29,341	32,048	35,811
53	1008	1,709,669	25,694	23,844	29,489	34,969	41,463	51,553
53	1801	1,096,504	25,188	40,573	53,428	69,899	94,552	143,640
83	1801	963,427	28,602	22,222	23,157	24,068	25,207	27,076
83	6450	874,280	25,444	34,384	36,015	37,355	38,777	40,689
83	6451	1,125,872	28,891	26,522	29,457	31,913	34,496	37,920
85	1801	1,884,622	22,829	24,719	53,206	109,103	243,998	778,189
87	1820	1,437,538	19,488	9,926	13,194	17,664	25,150	43,568
87	1822	1,246,063	27,174	25,122	30,404	38,021	52,037	93,296
88	1845	928,869	21,164	34,385	38,490	42,932	48,761	58,911
89	1127	1,220,847	16,661	15,479	25,753	45,078	90,319	272,284

Table 10. Layer moduli for GPS-2 sections.

State	Section	E(AC/TB)	E(BS/SB)	E(SG-1)	E(SG-2)	E(SG-3)	E(SG-4)	E(SG-5)
		E1_MPT	E2	E3	E4	E5	E6	E7
1	1021	927,914	29,210	55,600	55,706	55,745	55,838	55,890
1	4073	740,395	27,977	77,388	79,961	82,505	85,439	89,802
5	3058	410,623	N/A	21,015	21,015	21,015	21,015	21,160
5	3071	791,852	N/A	17,841	45,798	110,408	301,527	1,272,007
8	7781	423,012	N/A	5,073	15,652	42,754	131,017	648,562
12	4096	691,455	11,907	21,829	22,263	22,709	23,334	24,382
12	4097	814,236	25,537	78,349	78,465	78,581	78,697	78,842
12	4100	846,805	17,952	21,430	21,498	21,537	21,595	21,662
12	4108	967,212	17,537	18,479	19,783	21,160	22,827	25,653
28	3082	862,677	299,504	55,631	65,620	77,259	94,572	131,017
32	1030	753,772	667,486	40,290	48,966	59,256	75,301	112,983
32	7000	545,391	24,707	38,940	43,792	48,414	53,845	62,129
34	1033	1,238,815	14,747	54,711	67,791	84,531	109,314	158,119
34	1034	841,128	N/A	16,232	22,151	32,823	59,788	184,870
36	1008	709,225	12,578	31,046	32,075	33,593	36,377	44,379
36	1644	637,480	35,347	23,778	30,202	39,842	59,765	132,730
40	4163	1,059,055	N/A	17,983	26,498	43,986	93,118	339,982
40	4165	1,057,564	N/A	22,935	25,979	28,841	32,319	37,863
47	1028	1,036,112	37,972	16,667	37,537	80,291	184,931	580,300
47	3108	1,195,673	339,142	41,831	53,576	70,659	103,063	197,346
47	3109	881,475	75,811	25,170	73,528	195,813	579,418	2,631,832
47	3110	585,750	N/A	34,682	36,522	38,015	39,624	41,928
47	9024	895,840	N/A	47,247	125,582	327,723	994,473	4,648,014
47	9025	735,498	31,049	34,694	69,856	132,834	276,984	839,981
50	1681	991,380	23,001	38,352	44,533	55,356	79,731	171,492
50	1683	672,518	20,100	21,081	28,911	40,642	62,643	127,153
51	1423	840,672	22,303	30,912	38,212	47,732	63,372	101,712
51	2021	540,233	633,569	13,959	14,390	14,787	15,241	15,912
88	1647	641,522	34,898	55,173	56,202	57,080	57,941	59,101
89	2011	280,810	19,512	33,107	36,126	39,503	44,001	52,083

$$(MMPT)_i = (MMAT)_i * \left[1 + \frac{1}{Z + 4} \right] - \frac{34}{Z + 4} + 6 \quad (3)$$

where: Z = Depth at which temperature is to be predicted. (The mid-depth of the AC layer was used for this analysis.)
 i = Index representing the month of the year.

$$MAPT = \frac{1}{12} \sum_{i=1}^{12} (MMPT)_i \quad (4)$$

Temperature Adjustment Algorithm

The following equation, developed by Braun Intertec [8] based on LTPP data, was used to adjust the AC modulus to 20° C (68° F) and to the MAPT:

$$\frac{E_1}{E_2} = 10^{0.01 * (T_2 - T_1)} \quad (5)$$

where: E_1 = Modulus at temperature T_1 °C (°F).
 E_2 = Modulus at temperature T_2 °C (°F).

This model is similar to other temperature correction models. See, for example, Ali et al. [9], Kim et al. [10], and Stubstad et al. [11].

CHAPTER 4. PAVEMENT STRUCTURAL ANALYSIS

Introduction

This chapter presents details on the analysis of the critical structural responses to traffic loading. Structural analysis is a pivotal component of M-E analysis, and the successful application of M-E distress prediction procedures depends on the selection of a reliable structural analysis technique.

For this study, the WESLEA [12] program was used to calculate the critical strains (i.e., the horizontal tensile strain at the bottom of the AC layer, and the vertical compressive strain at the top of the subgrade and other layers) due to traffic loading. Traffic loading is characterized by 140 axle-load/type combinations and the annual count of each combination. Test sections missing traffic data were excluded from the structural analysis. Also, for a competent structural analysis, pavement structural parameters should be representative of the entire performance life of the pavement. The seasonal, long-term, and spatial variations of pavement parameters were considered in the analysis, as appropriate and as the data permitted. The consideration of the seasonal and spatial variations is discussed in the following section.

Consideration of Spatial and Seasonal Variations in Pavement Layer Properties

The spatial variation of pavement layer moduli was determined by averaging the values at all testing points in the section, after adjusting the surface layer modulus to temperature. The seasonal variation of temperature was assumed to exert considerable influence on the elastic modulus of the AC layer. Therefore, the AC layer modulus was adjusted to the MAPT, as described in chapter 3.

A pavement section was assumed to freeze when the AC layer mid-depth temperature dropped below 0°C (32°F). It was further assumed that traffic load repetition would cause negligible damage during freezing. The number of load (axle) counts was reduced by a factor equal to the ratio between the number of months with an MMPT of less than 0°C (32°F) to the total number of months. For instance, if a section had 3 months a year of an MMPT of less than 0°C (32°F), then it was assumed that the pavement was frozen 25 percent of the time; hence, 25 percent of traffic had a negligible damage effect, and 75 percent of the axle counts were used in the damage analysis. In so doing, it was also assumed that traffic was uniformly distributed throughout the year. This assumption was made because there were no reliable data available to characterize the seasonal variation in traffic.

Some approximate models (simulation-based) are available to adjust the modulus of the unbound layers to moisture and precipitation conditions, or to the degree of saturation of the subgrade (e.g., infiltration and drainage, and climate/material/structure models of the FHWA integrated model). However, these models require parameters that were not available, especially for nonseasonal sites. Moreover, the above models are still in the process of validation and are viewed as only research tools. For instance, the CMS model may be used to predict changes in the AC layer stiffness, the resilient modulus, and Poisson's ratio of the base, subbase, and subgrade with time, given the sunshine percentage, wind speed, air temperature, solar radiation,

physical and thermal material properties, initial soil suction profile, initial soil temperature profile, heat transfer coefficients, rainfall intensity coefficients, pavement infiltration parameters, and pavement geometry. Obviously, a large number of the required variables are not available in the LTPP data.

An approximate method to adjust the modulus of the unbound layers to moisture and other seasonal climatic variations involves applying a seasonal factor to the backcalculated moduli, to relate the stiffness of the pavement at a given time to that of the average, year-round conditions. Pavement sections within the same LTPP experimental cells are subject to similar environmental conditions and have similar design characteristics. Hence, it may be reasonable to assume that their seasonal patterns are also similar. With this assumption in mind, the seasonal adjustment factors derived from a seasonal section may be used to characterize the seasonality of other nonseasonal sections falling in the same experimental cell. The seasonal adjustment factors may be calculated as follows:

- For each seasonal site for which backcalculated monthly layer moduli are available, the average modulus is calculated by:

$$E_{AV} = \frac{1}{12} \sum_{i=1}^{12} E_i \quad (6)$$

where: E_i = Backcalculated base (or subgrade) layer modulus of month i .

- For every month, a seasonal factor (F_i) is calculated as the ratio of the modulus for that month to that of the average for the year (E_{AV}), that is:

$$F_i = \frac{E_i}{E_{AV}} \quad (7)$$

- The adjusted modulus for the nonseasonal GPS sites is then calculated as follows:

$$E_{AV} = \frac{E_i}{F_i} \quad (8)$$

This approach may also be used to adjust the AC layer modulus to seasonal variations. However, since the experimental cell design of the SMP program does not classify sites based on temperature, the approach described earlier for the AC layer modulus seasonal adjustment may be more accurate than the approach outlined here, especially when the nonseasonal site in question is far enough away from the seasonal site that the temperature patterns at the two sites are significantly different.

The initial analysis plan was intended to follow this approach. However, at the time of the analysis, it was found that fewer than expected seasonal sections were available. The

seasonal sections that had traffic, deflection, and temperature data were not well-distributed across the experimental cells (about 3 of 16 flexible pavement cells were available). It was then decided that the best available estimate of the effective unbound layer modulus would be the mean of the values taken in different seasons. Many of the nonseasonal sites had deflection measurements taken in more than one month (in different years). Obviously, the reliability of the modulus of the few seasonal sections is greater than that of the nonseasonal sections, since deflection testing was conducted more frequently and covered more seasons.

Chapter 8 uses a case study to compare three different approaches to considering the seasonal variations of the pavement moduli, and the effects of using such methods on pavement damage. The first method uses individual modulus values, corresponding to individual seasons, assuming that the moduli values of each season are representative of the year-round pavement moduli. This is often the case when FWD testing is performed once a year, and the analyst does not have a way to estimate the seasonal variability. The second method uses the average moduli values of all seasons. The third sums the damages from all seasons, resulting from the corresponding moduli values, the most theoretically appealing method.

Consideration of Traffic Loading

In mechanistic evaluation, traffic is characterized as the number of passages of each axle-load/type combination. There are 140 axle-load/type combinations in the database for single, tandem, and tridem axles. The critical responses are calculated for a single application of each axle-load/type combination.

A debate in the literature concerns how to calculate the maximum strain under multiple loads, and whether a passage of one tandem axle should be considered as one or two passages of a single axle. If the passage of each set of multiple axles is assumed to be one repetition, the damage caused by an 80-kN (18-kip) single axle is nearly the same as that caused by 160-kN (36-kip) tandem axles or 240-kN (54-kip) tridem axles. On the other hand, if one passage of a tandem axle is assumed to be two repetitions of a single axle and that of tridem axles to be three repetitions, the damages caused by 160-kN (36-kip) tandem and 240-kN (54-kip) tridem axles are two and three times greater, respectively, than that caused by an 80-kN (18-kip) single axle. Both assumptions are apparently incorrect. The equivalent factors suggested by the Asphalt Institute are 1.38 and 1.66 for tandem and tridem axles, respectively.

As recommended by Huang [13], a detailed process was used to calculate the critical responses due to multiple axles. It was assumed that the passage of a tandem axle caused primary damage corresponding to the strain magnitude under the first axle, and secondary damage corresponding to the difference between the strain under the first axle and the strain midway between the two axles. The total damage was the summation of the primary and secondary damages. The ratio between the total tandem- or tridem-axle damage and the total single-axle damage is the equivalent axle load factor (EALF). The process is described here:

- *For single axles, single wheel:* Calculate the tensile strain at the bottom of the AC layer (e_t) and the compressive strain at the subgrade surface (e_c) at point 1, as shown in figure 4.

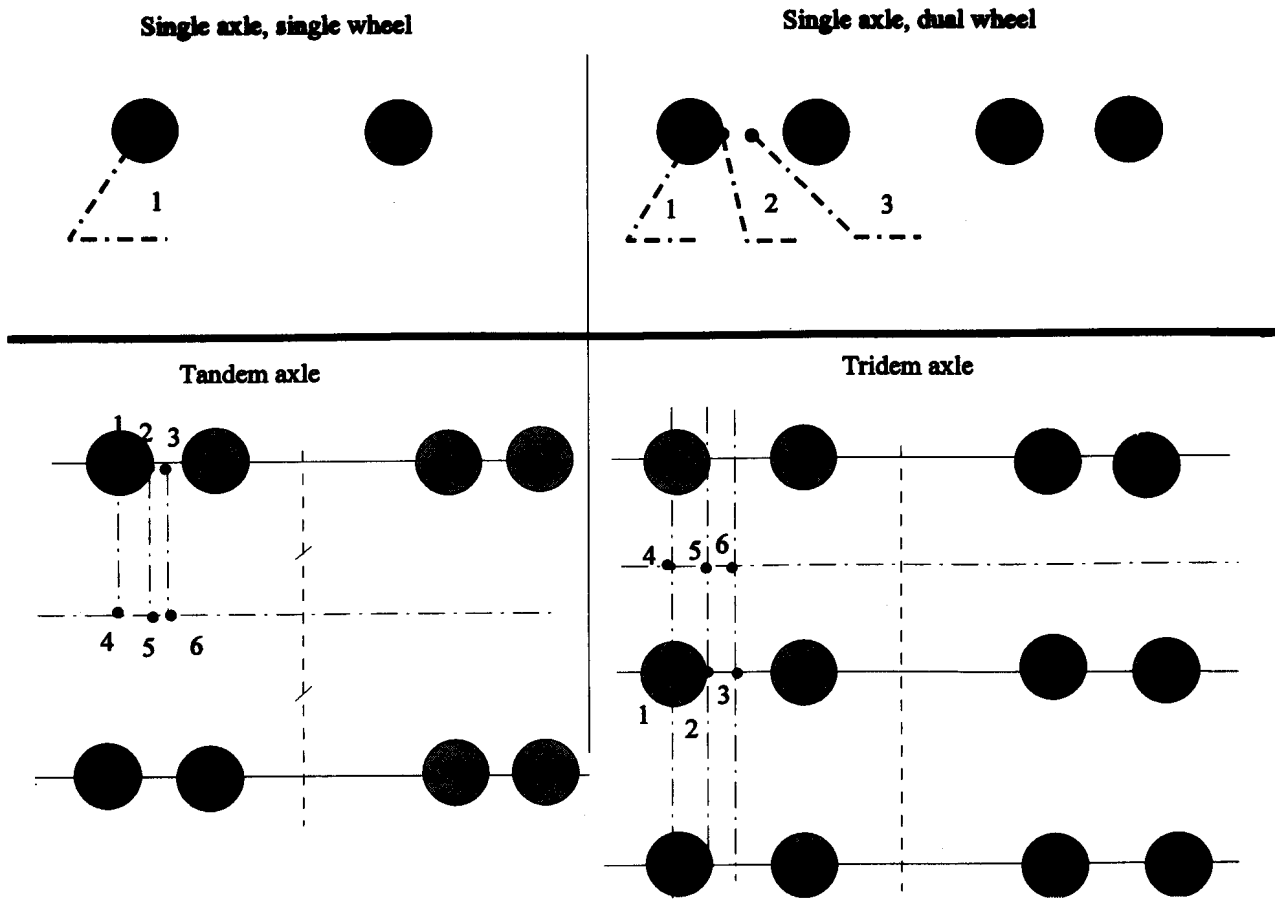


Figure 4. Response points.

Use these values to calculate the number of repetitions to failure associated with this type of loading, based on fatigue (N_f) and permanent deformation (N_p). No data are available in the LTPP database to identify this type of loading. Therefore, this case was not considered in the analysis.

- *For single axle, dual wheel:* Calculate the tensile strain at the bottom of the AC layer (e_t) and the compressive strain at the subgrade surface (e_c) at points 1, 2, and 3, as shown in figure 4. Use the maximum of the three values in the calculation of N_f and N_p . It was assumed that all axles consisted of dual wheels.
- *For tandem axles:*
 - (a) Calculate e_t and e_c at points 1, 2, and 3, as shown in figure 4. Use the maximum value of each response to calculate the required N_f and N_p for the first of the two axles.
 - (b) Calculate e_t and e_c midway between the two axles at the point located along the path of the point of maximum response in step (a). For example, if the maximum response in step (a) was at point 2, then point 5 should be used to calculate the response in step (b). Calculate the N_f and N_p of the second axle based on the difference in the strain values between (a) and (b), i.e., $N_{f \text{ for the second axle}} = f_f(e_{t \text{ of A}} - e_{t \text{ of B}})$ and $N_{p \text{ of the second axle}} = f_p(e_{c \text{ of A}} - e_{c \text{ of B}})$, where f_f and f_p are the Asphalt Institute functions for fatigue and permanent deformation, respectively. If the response in step (b) is in a different sign from that of (a) (i.e., one is compressive and the other is tensile), we considered the value of the strain at (b) to equal zero. This was done to prevent the tandem-axle damage from being more than twice that of the single axle.
- *For tridem axles:* Follow the same process as for tandem axles:
 - (a) Calculate e_t and e_c at points 1, 2, and 3, as shown in figure 4. Use the maximum value of each response to calculate the required N_f and N_p for the first of the two axles.
 - (b) Follow the same procedure outlined previously in (b).
 - (c) Assume that the damage associated with the third axle equals that of the second axle. (Use the same values obtained in (b).)

Calculation of Cumulative Traffic Application

The annual number of axle-load/type passages is given for each axle-load/type category. For some sections, traffic counts were available for more than one year. The year with the maximum number of WIM days was selected as the best estimate of the annual traffic counts. The total number of load applications (cumulative up to the date of the last distress survey) for each axle-load/type combination was calculated as follows:

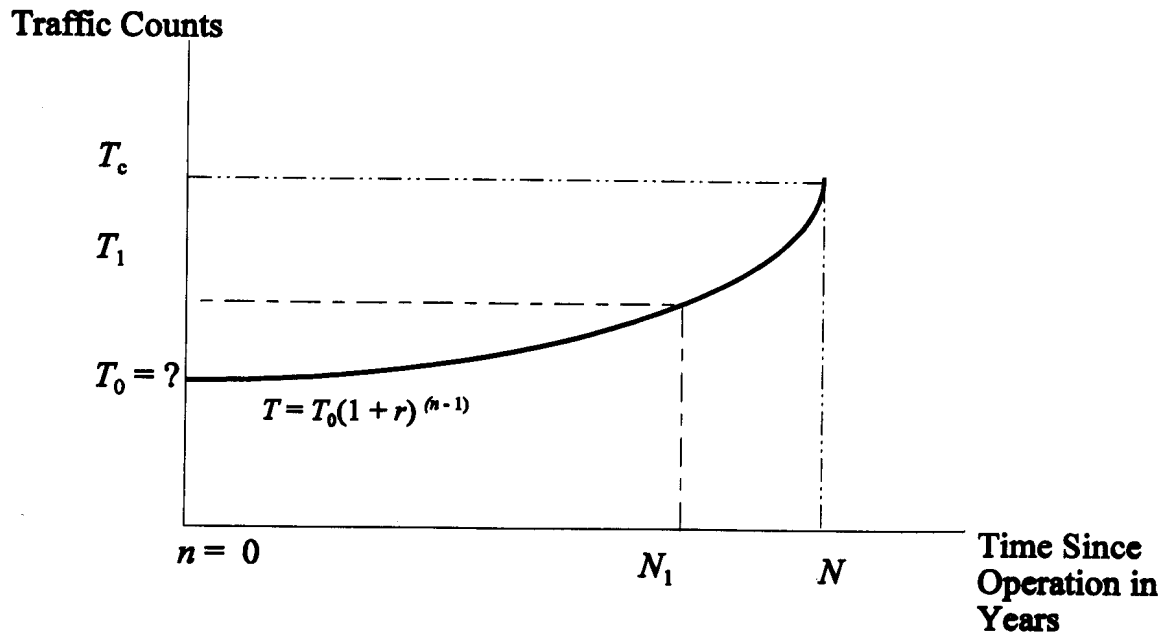


Figure 5. Cumulative traffic consideration.

Figure 5 is a schematic showing the traffic growth function, where traffic (in load applications) in the first year of operation is T_0 . The traffic T , at any given year, is given by:

$$T = T_0 (1 + r)^{(n-1)} \quad (9)$$

where: r = Annual traffic growth rate, in percent (estimated by each state).
 n = Number of years since the first year of operation.

The cumulative traffic to year N is then computed as follows:

$$\text{Cumulative } T = \int_0^N T_0 (1 + r)^{(n-1)} dn \quad (10)$$

The initial number of load application (T_0) is unknown, but may be calculated from

$$T_1 = T_0 (1 + r)^{(N_1-1)} \quad \text{or} \quad T_0 = \frac{T_1}{(1 + r)^{(N_1-1)}} \quad (11)$$

where: T_1 = Annual traffic at year N_1 .

The term $(1 + r)$ is constant and may be called B . Cumulative T may be computed as follows:

$$\text{Cumulative } T = T_0 \int_0^N B^{(n-1)} dn \quad (12)$$

Simplifying and integrating yields:

$$\text{Cumulative } T = \frac{T_0 (B^N - 1)}{B \ln B} \quad (13)$$

where: $B = (1 + r)$, and \ln is the natural logarithm.

Example: A GPS section was opened to traffic in January 1970, and the last distress survey was conducted in May 1994. In 1990, LTPP traffic data indicated that a 111-kN (25-kip) single axle was counted 1000 times in that year. Calculate the cumulative counts of this axle/load category for the period since the section was opened to traffic until the date of the last distress survey. Assume that the annual traffic growth rate is 3 percent.

Solution: First calculate the initial traffic $T_0 = 1000/(1.03)^{(20-1)} = 570$ load applications in 1970. The cumulative count is calculated from the equation:

$$\text{Cumulative } T = \frac{570 (1.03^{24.5} - 1)}{(1.03 \ln 1.03)} = 19,902 \text{ applications} \quad (14)$$

The solution may be expressed in one equation for programming purposes:

$$\text{Cumulative } T = \frac{T_1 (B^N - 1)}{B^N \ln B} \quad (15)$$

Based on the estimated historical annual ESAL values, the annual growth rate was calculated for each section. The rate was found to be highly variable from one year to the next within the same section, and from one section to another. The growth rate ranged from -13 percent to +30 percent, and averaged 2.4 percent. It should also be noted that individual load groups had different growth rates. However, it was not feasible to calculate the traffic growth rate, because many sections only had monitoring traffic data for one year. Also, other sections had an unrealistic variability in the counts of specific load groups from one year to the next. In the calculation of the cumulative traffic applications, a simplifying assumption was made that the annual traffic growth rate was 2 percent for all loading groups. The last survey dates (for rutting and fatigue cracking) were used to project the axle counts up to that date.

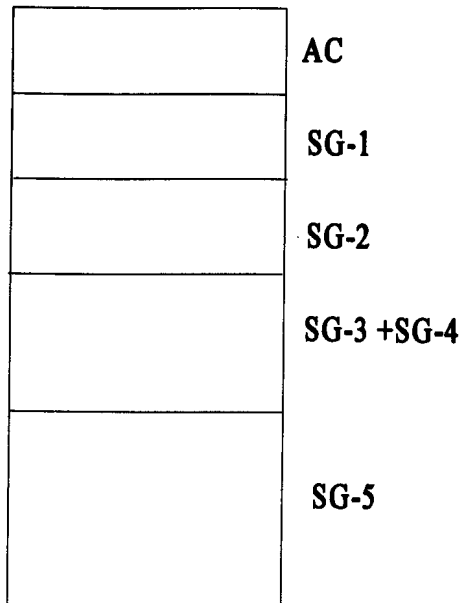
The effect of traffic wander was accounted for by reducing the number of traffic load counts by a factor of 10 percent. This adjustment factor was suggested by Brown et al. [14]. The rationale behind this adjustment is that if we assume that each load application will result in a maximum strain at a given point, the result will be an overestimation of the damage, because the wheels do not always pass over the exact same path. The damage is therefore distributed over a range of points.

A more accurate estimate of the effect of traffic wander may be obtained by developing frequency charts (histograms) of the lateral wheel positions across the traffic lane. The histograms could then be used to estimate the number of occurrences of the maximum strain value. The development of such charts requires more data on the lateral locations of the traffic loads.

Calculation of Critical Strains

Using the backcalculated elastic moduli of pavement layers (adjusted for temperature, seasonal, and spatial variations) and traffic, characterized by the axle loads and configuration, the WESLEA program calculated the critical pavement responses. The program output was the maximum vertical compressive strain at the top of the subgrade and the maximum horizontal tensile strain at the bottom of the AC layer, all resulting from one load application of each

Case 1: No base layer



Case 2: Base layer

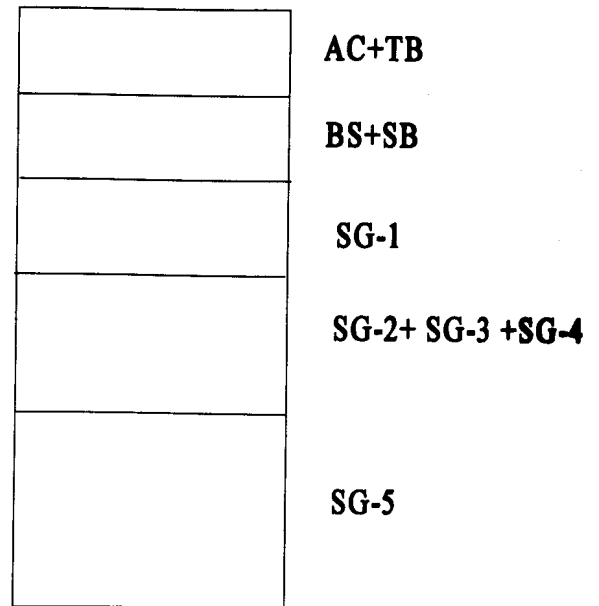


Figure 6. Layer model used in the structural analysis.

axle-load/type category. These values were then used to perform damage analysis. Appendix E shows a sample of WESLEA output.

To account for the nonlinearity of the subgrade layer, in the backcalculation, the subgrade was modeled as a 5-layer system with thicknesses of 0.6, 1.0, 1.0, and 2.0 m, and infinity. Additional backcalculation trials were run without dividing the subgrade layer. In general, the backcalculation error was much larger than that of the divided subgrade. Thus, in subsequent analyses, the 5-layer subgrade was retained as the better pavement model. Since WESLEA is a 5-layer program, the layers were combined to form a total of 5 layers. Figure 6 is a schematic showing the manner in which the layers were combined.

It should be noted that there are two cases, depending on the existence of a base layer. In the first case, no base layer exists and the first layer is the AC layer. The second layer is the first subgrade layer. The third is the second subgrade layer. The fourth is the third and fourth subgrade layers together, combined using Odemark's transformation equation. The fifth is the fifth subgrade layer. Odemark's transformation combines the layers as follows:

$$E_e = \left[\frac{\sum_{i=1}^n h_i \sqrt[3]{E_i}}{\sum_{i=1}^n h_i} \right]^3 \quad (16)$$

where: E_e = Equivalent modulus.
 i = Layer index.
 n = Total number of layers to be combined.
 h_i = Thickness of layer i .
 E_i = Modulus of layer i .

In the second case, a base layer does exist and the first layer is the AC layer combined with the asphalt-treated base (if present). The second layer is the granular base and subbase layers together, combined using Odemark's transformation equation. The third layer is the first subgrade layer. The fourth is the second, third, and fourth subgrade layers together, again combined using the Odemark transformation. Finally, the fifth layer is the fifth subgrade layer.

Since the tire pressure magnitude and distribution were not available in the database, the tire pressure was assumed to be 689 kPa (100 psi). Also, Poisson's ratio was assumed to be 0.35 for the AC and asphalt-treated layers and 0.4 for the granular base and subgrade layers.

Additional WESLEA runs were performed later to calculate the vertical compressive strain in the middle of each pavement layer, in conjunction with a new rutting model that considered the deformation within each pavement layer. The new model development, calibration, and validation is presented in chapter 9.

CHAPTER 5. FATIGUE DAMAGE ANALYSIS

Introduction

Fatigue cracking, one of the most common distresses in AC pavements, is a series of interconnecting cracks caused by fatigue failure of the AC layer or a stabilized base, under repeated traffic loading. The initiation and propagation of fatigue cracking has long been correlated with horizontal tensile strain at the bottom of the surface layer. Fatigue cracking may also be correlated with shear strain at the bottom of the AC layer. The objective of this study was to evaluate how well existing fatigue damage models would predict the development of fatigue cracks. Another important objective was to develop a continuous function relating the fatigue damage ratio to the extent of fatigue cracking. It should be noted that many pavement engineers believe that some of the fatigue cracking may be due to high tensile strains occurring at the top of the surface layer. However, not much work has been done in the United States to validate this hypothesis, and the phenomenon was not considered in the analysis of the LTPP fatigue cracking data.

The horizontal tensile strain at the bottom of the AC layer, corresponding to each load group, was calculated using the structural analysis procedure described in chapter 4. The calculation of the fatigue damage was performed according to two well-established sets of models, the Asphalt Institute (AI) model and the Shell models. Fatigue damage analysis using the AI model is presented in this chapter. Chapter 7 presents fatigue damage and rutting analyses using the Shell models.

Observed Fatigue Cracking

As mentioned earlier, many of the analysis sections have only been surveyed a few times under the LTPP data collection efforts. Fatigue cracking data reported in the last survey (at the time this analysis was conducted) were used in the analysis. The areas of low-, moderate-, and high-severity cracking were added to produce one measure of fatigue cracking.

The total area of fatigue cracking is divided by the total area surveyed [over 152.4-m (500-ft) length], to produce the percentage cracked area. Tables 11 and 12 show the percentage fatigue cracking in the GPS-1 and GPS-2 sections used in the analysis. The tables show that the GPS-2 sections exhibited very little fatigue cracking compared to those of GPS-1.

Asphalt Institute Fatigue Cracking Model

The approach for developing M-E-based fatigue cracking models was based on fatigue cracking models developed through laboratory beam-type testing. Laboratory fatigue test data are typically expressed as follows:

$$N_f = K_1(e)^{-K_2} (E_{ac})^{-K_3} \quad (17)$$

Table 11. Observed fatigue cracking in GPS-1 sections.

Number	State	Section	Observed Fatigue Cracking	Number	State	Section	Observed Fatigue Cracking
1	1	4126	0.000	25	29	1002	0.005
2	8	1029	0.007	26	29	1008	0.000
3	8	1047	0.000	27	29	1010	0.000
4	8	1057	0.000	28	31	1030	0.000
5	9	1803	0.000	29	32	1021	0.028
6	12	1030	0.008	30	33	1001	0.000
7	12	3996	0.011	31	34	1030	0.409
8	12	3997	0.780	32	42	1597	0.000
9	12	4099	0.000	33	42	1599	0.000
10	12	4106	0.000	34	42	1605	0.000
11	18	1028	0.002	35	47	3075	0.000
12	20	1005	0.000	36	50	1002	0.000
13	21	1034	0.000	37	50	1004	0.000
14	25	1002	0.008	38	51	1002	0.037
15	25	1003	0.000	39	51	1023	0.000
16	25	1004	0.000	40	51	1464	0.000
17	26	1012	0.069	41	53	1006	0.006
18	26	1013	0.000	42	53	1008	0.006
19	27	1019	0.544	43	53	1801	0.000
20	27	1023	0.000	44	85	1801	0.000
21	27	1028	0.000	45	87	1620	0.000
22	27	1029	0.000	46	87	1622	0.000
23	27	1085	0.000	47	89	1127	0.000
24	27	1087	0.000				

Note: Observed fatigue cracking value is the total area exhibiting fatigue cracking divided by the test section area.

Table 12. Observed fatigue cracking in GPS-2 sections.

Number	State	Section	Observed Fatigue Cracking
1	1	1021	0.010
2	1	4073	0.102
3	5	3058	0.000
4	5	3071	0.000
5	8	7781	0.000
6	12	4096	0.000
7	12	4097	0.000
8	12	4100	0.000
9	12	4108	0.000
10	32	1030	0.000
11	32	7000	0.000
12	34	1033	0.000
13	34	1034	0.000
14	36	1008	0.000
15	36	1644	0.000
16	40	4163	0.000
17	40	4165	0.000
18	47	1028	0.000
19	47	3108	0.000
20	47	3109	0.000
21	47	3110	0.000
22	47	9024	0.000
23	47	9025	0.000
24	50	1681	0.000
25	50	1683	0.013
26	51	1423	0.000
27	51	2021	0.005
28	88	1647	0.000
29	89	2011	0.000

Note: Observed fatigue cracking value is the total area exhibiting fatigue cracking divided by the test section area.

where: N_f = Number of load repetitions to failure.
 e = Repetitive tensile strain.
 E_{ac} = Dynamic modulus of elasticity of asphalt concrete.
 K_1, K_2, K_3 = Constant depending on material properties.

Based on the results of extensive laboratory testing and on correlations with field observations, the Asphalt Institute established the following model for AC pavements. The model relates the number of load repetitions to failure, N_f , to the horizontal tensile strain, e_t , at the bottom of the AC layer:

$$N_f = 18.4 * (10^M) * 0.004325 * (e_t)^{-3.291} * (E_{ac})^{-0.854} \quad (18)$$

$$M = 4.84 * \left(\frac{V_b}{V_v + V_b} - 0.69 \right) \quad (19)$$

where: N_f = Number of load repetitions to failure.
 E_{ac} = Dynamic modulus of elasticity of asphalt concrete, in psi.
 V_v = Percent volume of air voids.
 V_b = Percent volume of asphalt.
 e_t = Magnitude of tensile strain at the bottom of the AC layer.

Typically, $V_v = 5$ percent and $V_b = 11$ percent; then $M = 0$, and the equation for N_f may be reduced to:

$$N_f = 0.0796 * (e_t)^{-3.291} * (E_{ac})^{-0.854} \quad (20)$$

Failure is defined as 45 percent fatigue cracking in the wheelpath, which is equivalent to about 20 percent fatigue cracking of the total lane area. This equation was used to calculate the number of load repetitions to failure associated with each axle-load/type combination. As mentioned earlier, tandem axles were considered as two axles. The N_f value for the first axle is that associated with the maximum tensile strain under the first axle (maximum of three points); for the second axle, N_f is associated with the difference between the horizontal tensile strain under the first axle and that midway between the two axles. The third axle in tridem axles is assumed to have a similar effect as the second axle.

Fatigue transfer functions indicate that the allowable number of applications of any axle-load/combination is a function of the strain (horizontal tensile strain at the bottom of the AC layer) caused by that load application. The pavement damage caused by a load combination is expressed as the ratio of the actual to the allowable number of load applications of the load combination. This is referred to as the damage ratio, D_f . To accumulate the damages caused by various axle-load/type combinations, Miner's cumulative damage hypothesis [1] was used.

Failure is expected when the cumulative damage ratio, D_f , equals or exceeds 100 percent, according to the following expression:

$$D_f = \sum_{i=1}^k \frac{n_i}{N_{fi}} \leq 1.0 \quad (21)$$

where: k = Number of loading groups (axle-load/type combinations).
 n_i = Cumulative number of passages of load group i .
 N_{fi} = Allowable number of passages to failure of load group i .

Appendix E contains a summary of the calculated cumulative fatigue damage ratios for each GPS-1 section.

Comparison: Predicted Versus Observed Performance, GPS-1 Sections

According to the AI fatigue cracking transfer function, it is expected that less than 20 percent of the total pavement area will exhibit fatigue cracking when the damage ratio is less than 100 percent. Figure 7 shows a plot of the fatigue damage ratio versus the percent of fatigue cracking. It should be noted that fatigue cracking is given as the ratio of the total area of fatigue cracking (of all severity levels) to the total area surveyed.

Figure 7 shows that there were four sections with a damage ratio greater than 100 percent. Two of these sections demonstrated a negligible amount of fatigue cracking, and the other two showed fatigue cracking of greater than 20 percent. The section with the largest fatigue damage ratio ($D_f=17$) showed the largest amount of fatigue cracking (78 percent of the area).

Although the AI fatigue model does well at predicting the formation of fatigue cracking at a damage ratio greater than 100 percent (based on the limited amount of data), it does not really define or quantify the amount of cracking to be expected at each damage ratio level. The only defined point on the curve is 100 percent damage, corresponding to 20 percent fatigue cracking. A continuous function is needed to correlate the two variables and to predict one in terms of the other more accurately. The development and calibration of such a function is presented next.

New Fatigue Cracking Model

Theoretically, fatigue cracking should be minor until the damage ratio approaches 100 percent. At this point, the reduction in the AC-layer effective modulus and the subsequent increase in tensile strain leads to accelerated crack propagation. The cracking propagates until it reaches a level that prompts the highway agency to take remedial action. However, the percent of fatigue cracking as it forms in the wheelpaths only may not exceed a practical value, say 80 percent of the total area, assuming that the wheelpaths constitute 80 percent of the lane area. It should be noted that the maximum observed value was 78 percent. Therefore, the shape of the model should allow for stabilization at 80 percent fatigue cracking. The best form of model that represents this behavior is the constrained growth model, which takes the following form:

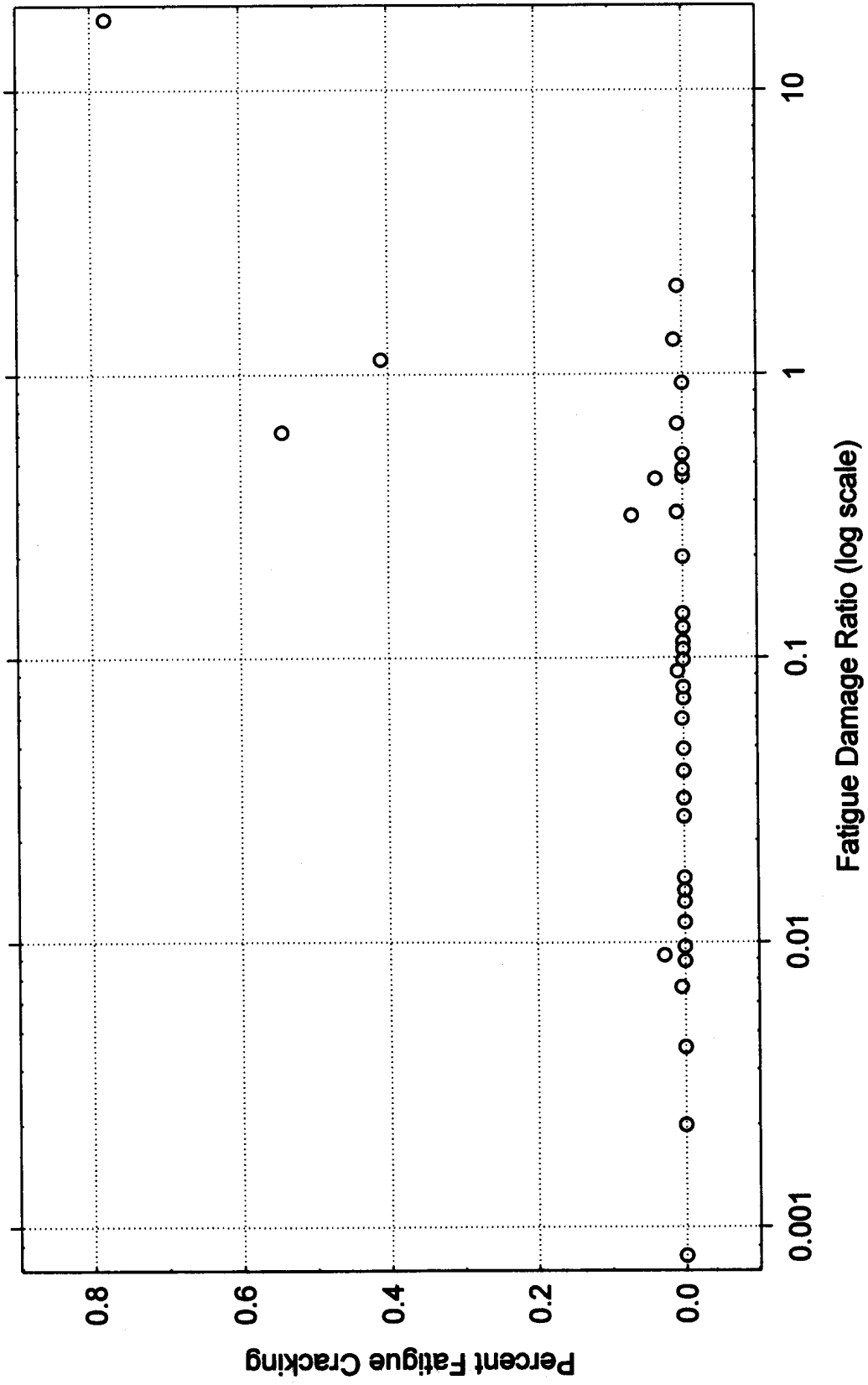


Figure 7. Plot of fatigue cracking versus damage ratio for GPS-1.

$$Y = \frac{a}{c + e^{(b \cdot X)}} \quad (22)$$

where: X = Explanatory variable (damage ratio).
 Y = Criterion variable (percent of cracked area).
 a, b and c = Regression coefficients.

Model Calibration

The model was calibrated using GPS-1 data. Figure 8 is a graphical presentation of the model as it fits the data points. The calibrated model is:

$$\% \text{ Fatigue Cracking} = \frac{0.021}{0.027 + e^{(-0.85 \cdot D_f)}} \quad (23)$$

The goodness of fit statistics are: percent of variance accounted for, $R^2 = 57$ percent; and the standard error of estimate, $Se = 9.5$ percent. The standard deviation of the observed fatigue cracking is 15 percent. Hence the relative error of the model is 0.63, indicating that the model's prediction is better than that obtained by using the average value in this data set. The model indicates that when the damage ratio is 100 percent, the expected fatigue cracking is 4.6 percent. This is considerably less than what would have been predicted by the AI model. The following is a modified model to force fatigue cracking at zero, when the damage ratio is zero:

$$\% \text{ Fatigue Cracking} = \frac{0.0026 * D_f}{e^{(0.00147 \cdot D_f)} - 0.967} \quad (24)$$

This model, illustrated in figure 9, has a slightly better fit; the explained variance (R^2) is 60 percent, and the standard error of estimate is 9.4 percent. The model predicts 7.5 percent fatigue cracking at a damage ratio of 100 percent.

Linear Model

A linear model was fitted to the data, as shown in figure 10. It should be noted that the model appears to be nonlinear, because the scale of the horizontal axis is logarithmic. The model is expressed as:

$$\% \text{ Fatigue Cracking} = 0.045 * D_f \quad (25)$$

Model: Fatigue = $a/(c + \text{euler}^{(b*df_r_)})$
 $y = (0.02111034)/((0.02708555) + \text{euler}^{((-0.8501576)*x)})$

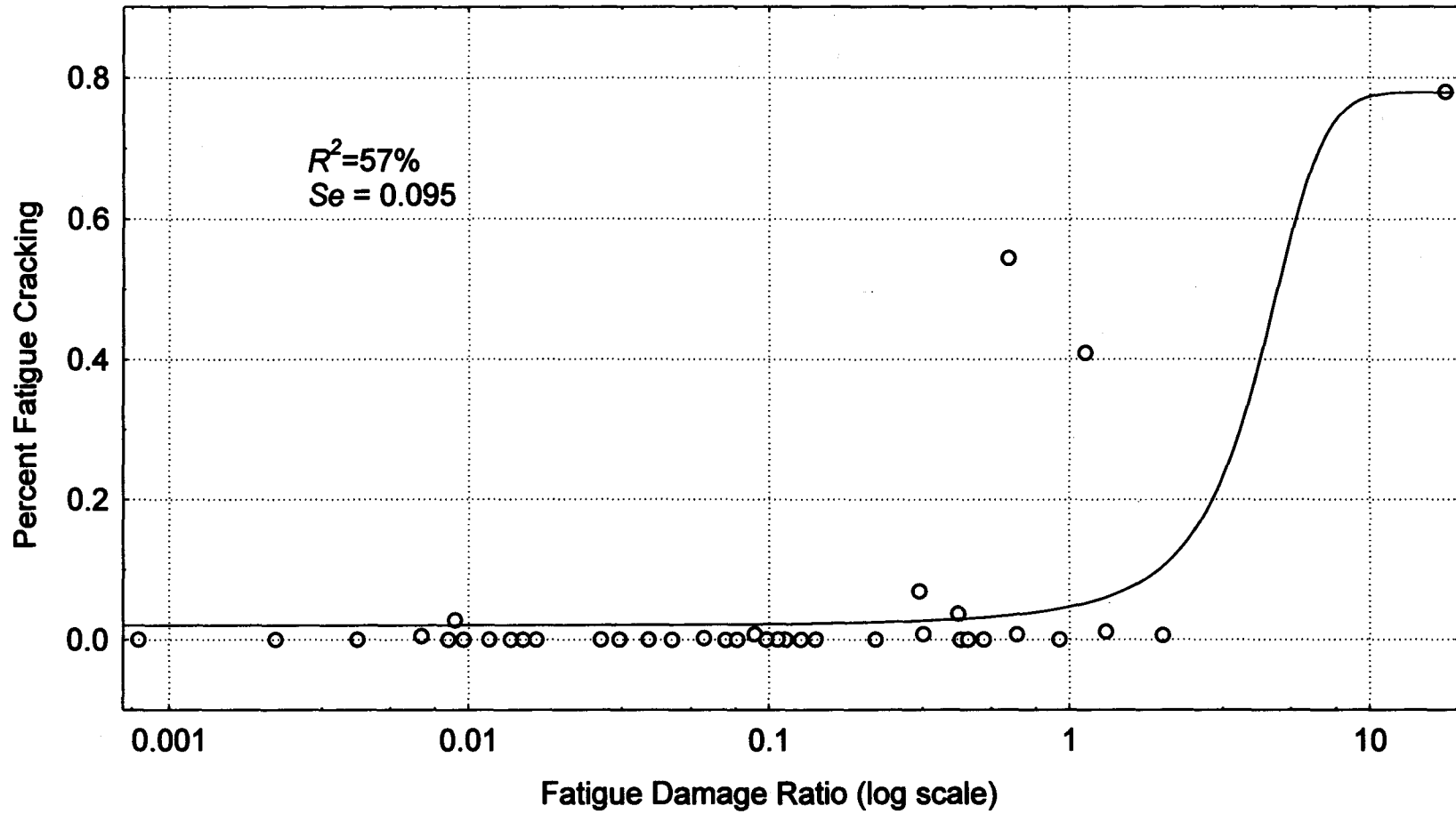


Figure 8. Constrained growth model.

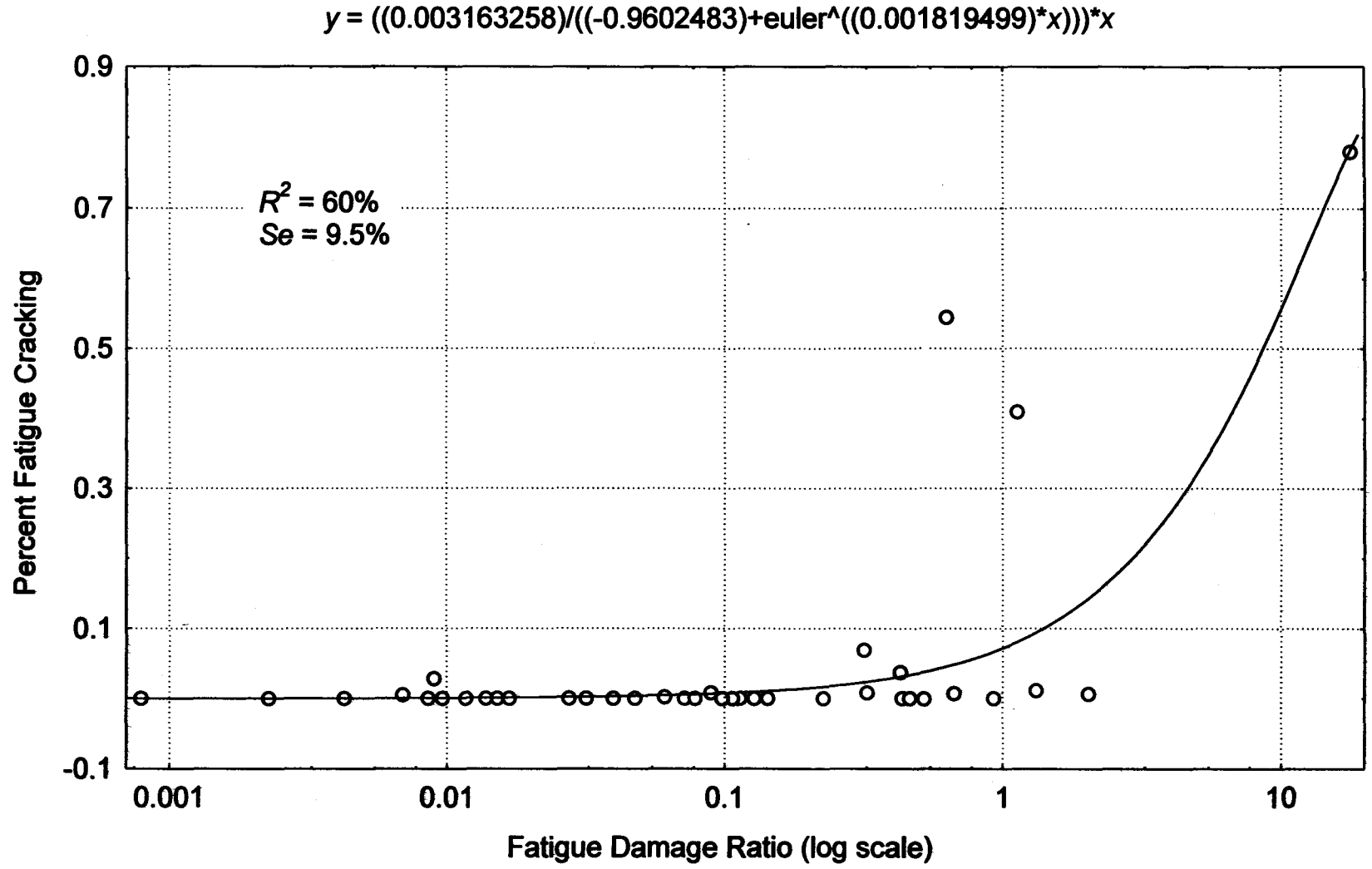


Figure 9. Modified constrained growth model.

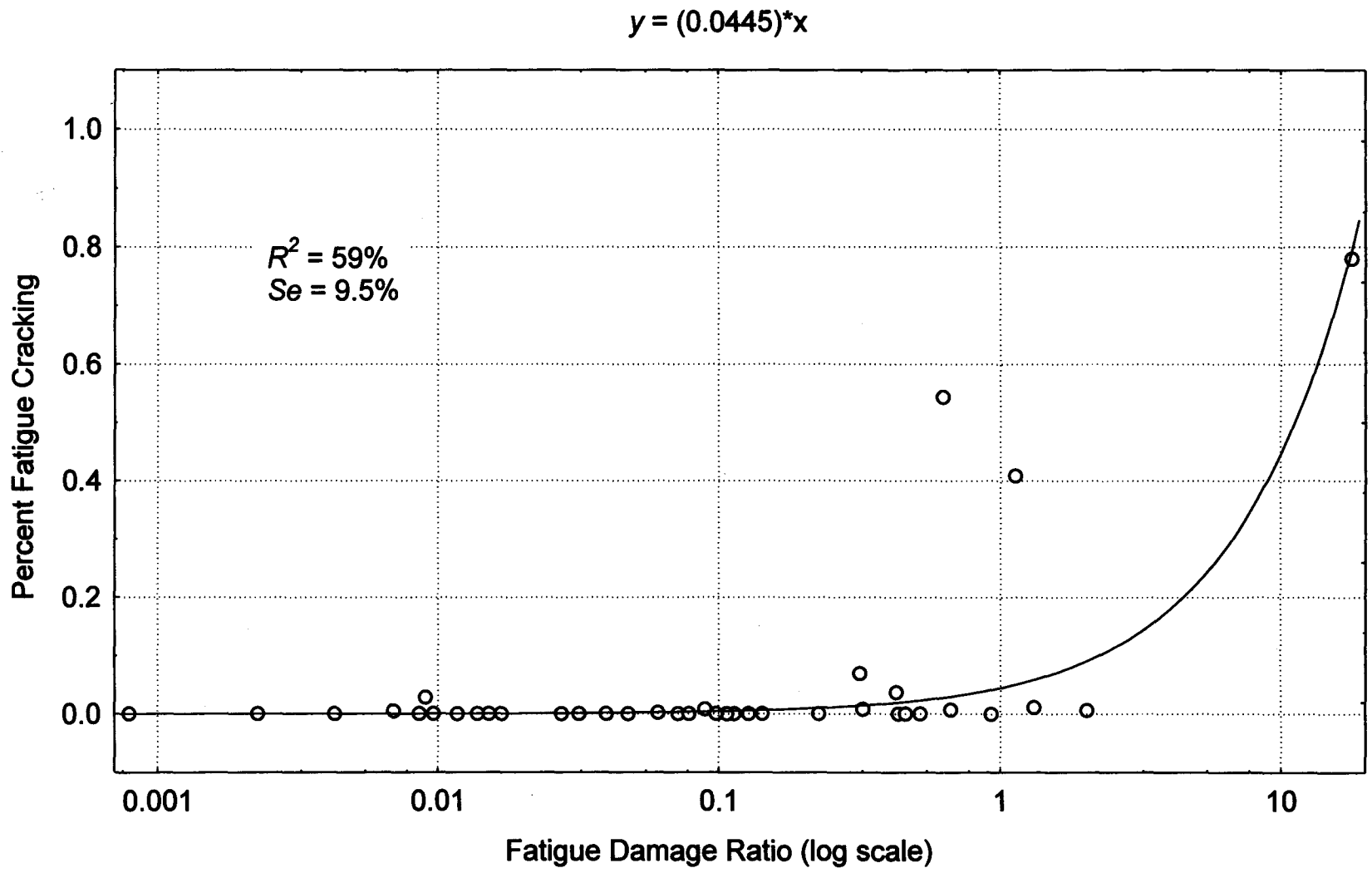


Figure 10. Linear model.

The goodness of fit statistics are similar to those of the previous models: $R^2 = 61$ percent, and $Se = 9.5$ percent. The shape of this model indicates that a fatigue cracking of higher than 100 percent is possible, which is not correct. However, the model is simpler and similar in its fit to the previous models. It should be noted that at a damage ratio of 100 percent, the expected fatigue cracking is less than 5 percent of the area.

Exponential Growth Model

An exponential growth model was also fitted to the data. The following is the model after calibration:

$$\% \text{ Fatigue Cracking} = e^{(3.57 + 0.0012 \cdot D_p)} - 35.5 \quad (26)$$

The model, presented in figure 11, is similar to the previous ones, with $R^2 = 59$ percent and $Se = 9.3$ percent. The model predicts 7.5 percent fatigue cracking at a damage ratio of 100 percent.

Fatigue Modeling Discussion

It should be noted that there are only a few points with a damage ratio greater than 100 percent. Consequently, the part of the model that describes failure is not well defined; four different models were fitted to the data and resulted in a comparable fit. This stresses the need for analyzing additional failing sections, so that pavement deterioration may be modeled accurately.

Based on the limited amount of data, a group of models was fitted to the data to construct a continuous function between fatigue damage ratio and fatigue cracking. The linear constrained growth and exponential growth models are comparable in terms of their goodness of fit. However, the linear model is the simplest of all. It indicates that fatigue cracking, as a percentage of the total pavement area, is about 4.5 percent of the fatigue damage ratio. All models predicted less than 10 percent fatigue cracking at a damage ratio of 100 percent. This leads to the conclusion that although the AI model can predict the general pattern, it overestimates the amount of fatigue cracking.

Fatigue Cracking Analysis, GPS-2 Sections

Most of the pavement sections in the GPS-2 experiment had a stabilized base layer. In the analysis reported in this chapter, only sections with an asphalt-stabilized base are considered. The analysis results of those GPS-2 sections with other base treatments are presented in appendix C.

It is expected that the GPS-2 sections resist fatigue cracking better because of the stabilized base. Figure 12 shows that the GPS-2 sections had much less fatigue cracking than the GPS-1 sections. All sections in the analysis, both those with less fatigue damage than 100

Model: Exponential growth ($y = c + \exp(b_0 + b_1 \cdot x_1 + b_2 \cdot x_2 \dots)$)
 $y = -35.50381 + \exp(3.569979 + (0.001216587) \cdot x)$

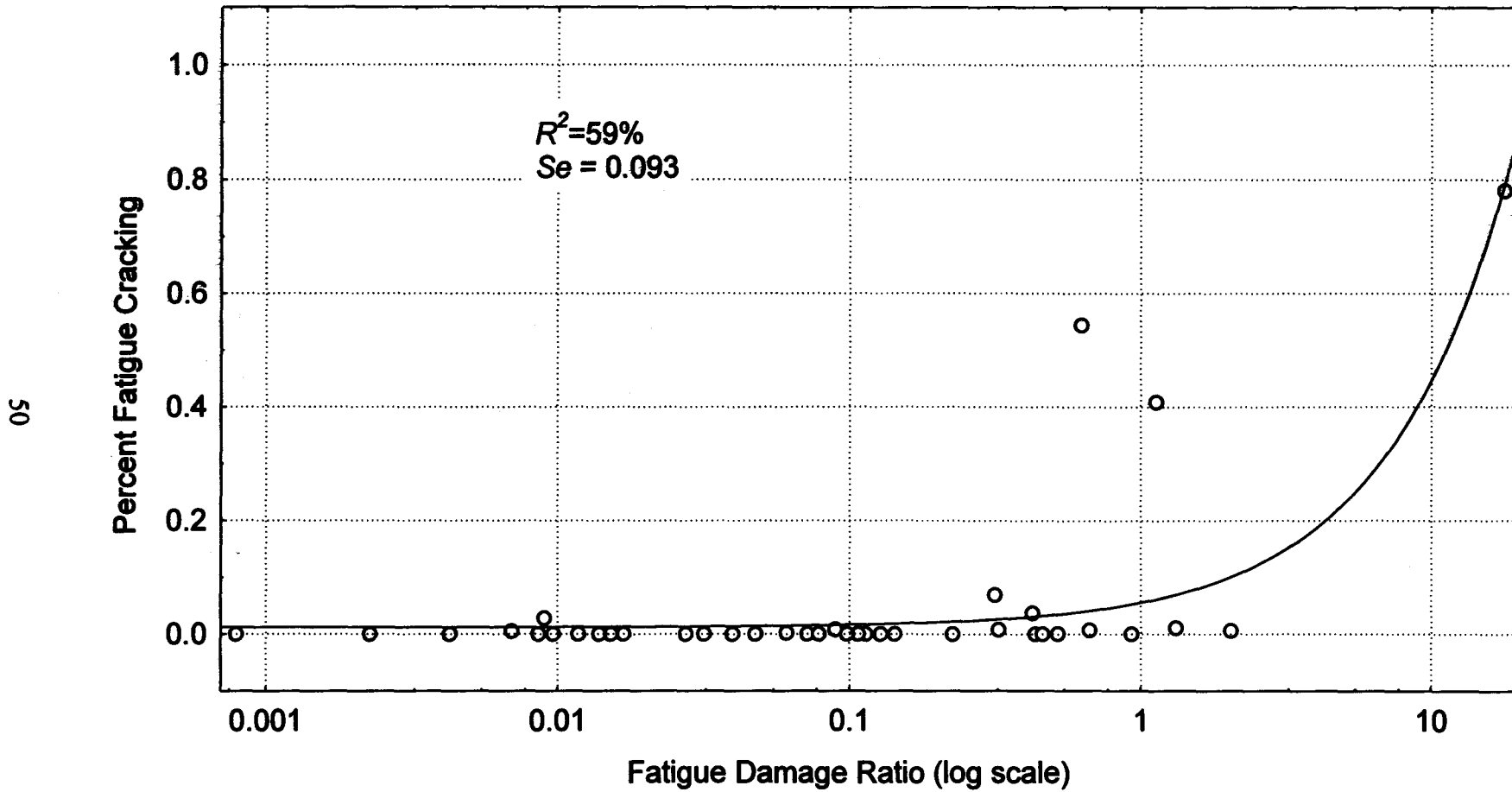


Figure 11. Exponential growth model.

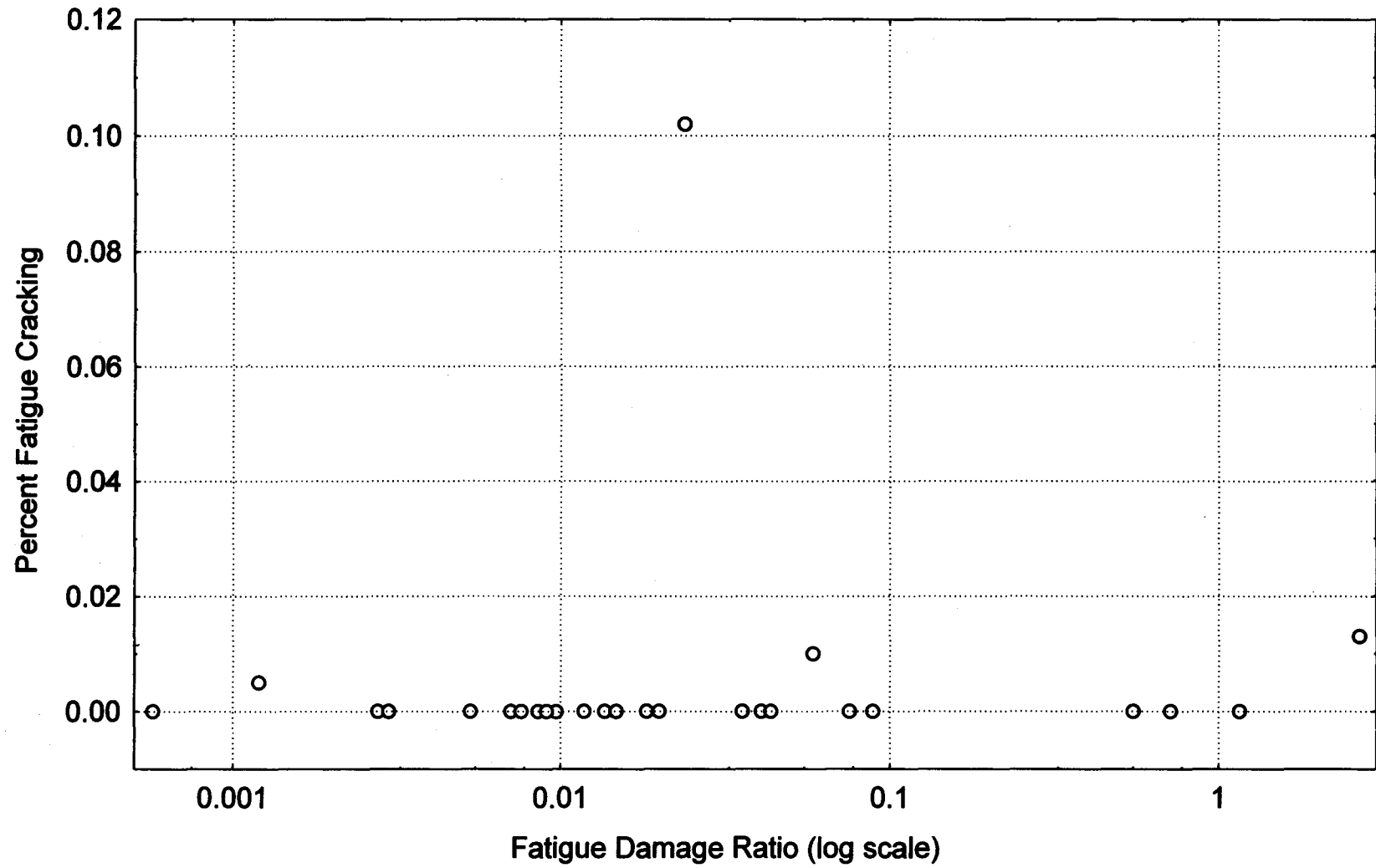


Figure 12. Fatigue damage versus fatigue cracking for GPS-2.

percent and those with more, had less than 10 percent fatigue cracking. Only two sections had a fatigue damage ratio of more than 100 percent. It is obvious that there were not enough failing sections to model fatigue cracking for these test sections. Therefore, unless more data are available from pavements exhibiting large amounts of fatigue cracking, very little can be done to develop or validate fatigue cracking models using data from the GPS-2 sections.

To compare the performance of the GPS-1 and GPS-2 sections, the fatigue cracking versus fatigue damage ratio plot was generated for both experiments on the same graph. Figure 13 shows that the GPS-1 sections exhibited considerably more cracking than the GPS-2 sections, especially at higher damage ratios. This is surprising, since the mechanistic analysis should have accounted for the structural differences between the two pavement types and factored that into the damage analysis. A number of reasons may explain this observation. One is that the pavement models used to represent the pavement structure in the backcalculation process may not be accurate. For instance, combining the AC layer and the asphalt-treated base may affect the damage analysis. Another reason might be that the assumptions of linear elasticity, material homogeneity, and the stress mode under which the transfer functions were derived may not necessarily be applicable for in-service pavements. It is conceivable that one type of pavement may be more sensitive to the underlying assumptions than the other.

Summary

The GPS-1 sections exhibited more fatigue cracking than the GPS-2 sections, for the same damage ratio. The existence of a treated base in the GPS-2 sections may be responsible for their superior performance. Theoretically, the structural analysis should account for the differences between the two types of pavements, through the use of appropriate base-layer moduli. However, the underlying assumptions under which the transfer functions were derived may not apply to in-service pavements. One type of pavement may be more sensitive to those assumptions than the other. Thus, there is a need to investigate the correctness of modeling AC pavements with stabilized bases.

The Asphalt Institute fatigue cracking transfer function appears to model adequately the fatigue behavior of GPS-1 type pavements (AC on granular base). A lack of failing pavements (with observed fatigue cracking in excess of 10 percent of the total area) made it difficult to model more accurately the rate of pavement deterioration. It is recommended that this type of analysis be performed again, after more of the pavement sections have started exhibiting higher levels of fatigue cracking.

A group of models was fitted to the data, to construct a continuous function between fatigue cracking damage ratio and observed fatigue cracking. The linear constrained growth and exponential growth models were comparable in fit. However, the linear model is simpler. It indicates that fatigue cracking is about 5 percent of the computed fatigue damage ratio. All models predicted less than 10 percent fatigue cracking at a damage ratio of 100 percent. The conclusion is that although the AI model can predict the general fatigue pattern, it overestimates the amount of fatigue cracking.

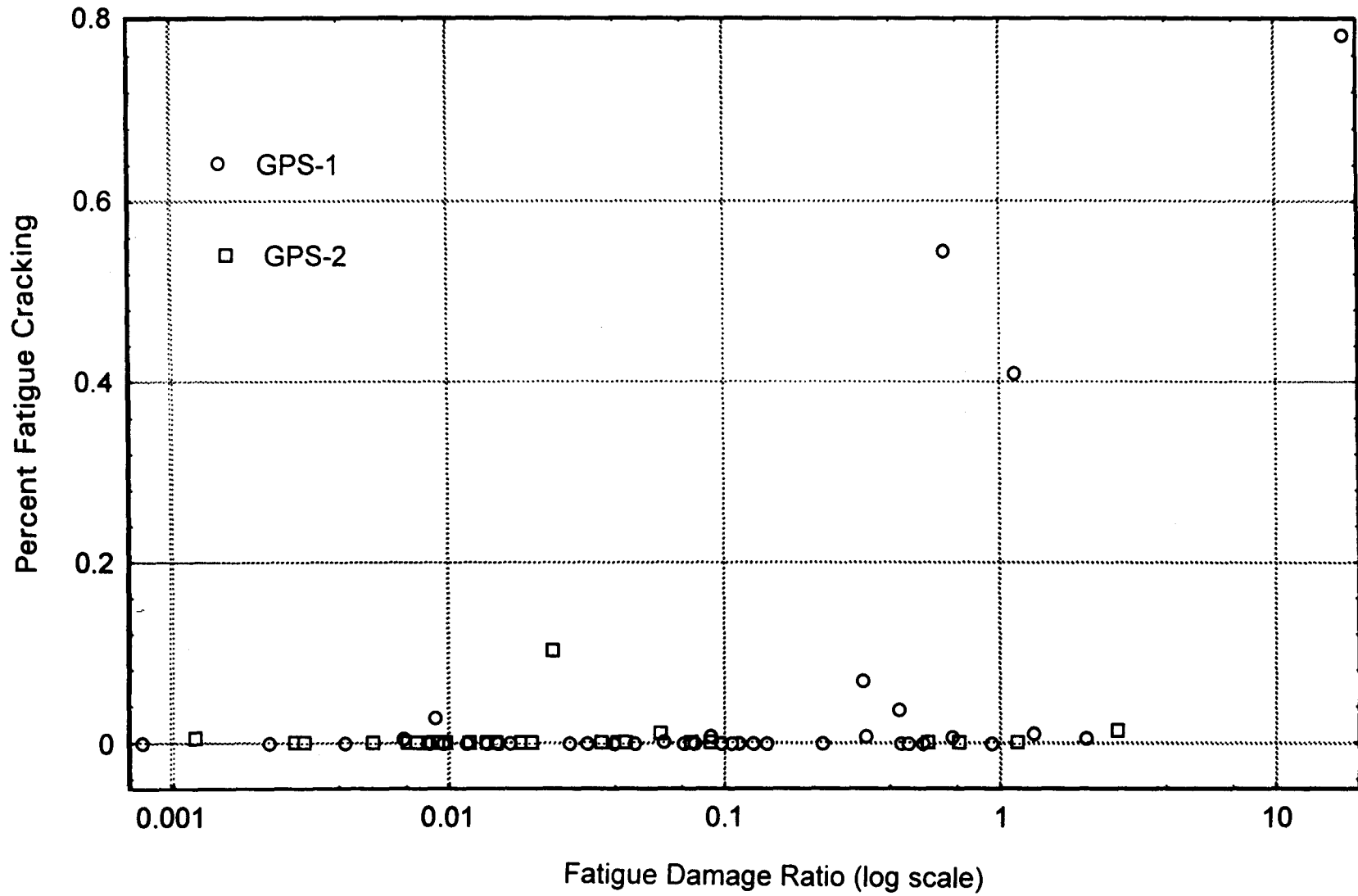


Figure 13. Fatigue cracking, GPS-1 versus GPS-2.



CHAPTER 6. RUTTING ANALYSIS

Introduction

Rutting is another major failure mode for flexible pavements. Pavement engineers have been trying for years to control and arrest the development of ruts. Many models are available to relate pavement rutting to design features, load, and climatic conditions. These models range from purely empirical to mechanistic. In this chapter, the AI model is used to predict the development of rutting. In chapter 7, the Shell model is used to predict rutting, and the results are compared with those obtained using the AI model.

Two approaches have been considered for the mechanistic modeling of rutting. The first approach, typically referred to as the subgrade strain model approach, assumes that most of the rutting is due to permanent deformation within the subgrade layer, and that the deformation within the AC and base/subbase layers is negligible, as the quality of these layers is controlled through mix design and construction specifications. The second approach considers permanent deformation within each layer of the pavement. Although several techniques have been proposed for the second approach, it has not been widely used because of the difficulty in obtaining elasto-plastic or visco-plastic characterizations for the various paving materials.

Observed Rutting

Many of the sections used in the analysis have been surveyed several times under the LTPP data collection efforts. Rut depths reported in the last survey (at the time this analysis was conducted) were used in the analysis. The rut depth was calculated using the 1.8-m (6-ft) straightedge method. The rut depth was averaged over 11 cross-profile measurements taken along each section. Tables 13 and 14 summarize the observed average rut depths for the GPS-1 and GPS-2 sections, respectively.

Asphalt Institute Rutting Model

The Asphalt Institute's permanent deformation model assumes that rutting takes place in the subgrade and that rutting in other pavement layers is negligible. Hence, the model relates the vertical compressive strain at the subgrade surface, ϵ_c , to the number of load repetitions to failure due to permanent deformation, N_p , according to the following expression:

$$N_p = 1.365 * 10^{-9} * \epsilon_c^{-4.477} \quad (27)$$

Failure is defined as the development of 13 to 19 mm (0.5 to 0.75 in) of rutting. Hence, it is expected that a permanent deformation damage ratio of 100 percent would correspond to rutting of 13 to 19 mm (0.5 to 0.75 in).

Table 13. Observed rutting in GPS-1 sections.

Number	State	Section	Observed Rutting, in	Number	State	Section	Observed Rutting, in
1	1	1019	0.539	32	27	6251	0.111
2	1	4126	0.183	33	29	1002	0.128
3	8	1029	0.239	34	29	1008	0.277
4	8	1047	0.156	35	29	1010	0.142
5	8	1057	0.151	36	31	1030	0.424
6	9	1803	0.169	37	32	1021	0.248
7	12	1030	0.180	38	33	1001	0.304
8	12	3996	0.224	39	34	1003	0.582
9	12	3997	0.723	40	34	1011	0.331
10	12	4099	0.306	41	34	1030	0.693
11	12	4106	0.154	42	34	1031	0.433
12	17	1002	0.200	43	42	1597	0.185
13	17	1003	0.143	44	42	1599	0.266
14	18	1028	0.594	45	42	1605	0.740
15	20	1005	0.218	46	47	3075	0.267
16	20	1010	0.415	47	50	1002	0.348
17	21	1010	0.224	48	50	1004	0.250
18	21	1034	0.178	49	51	1002	0.127
19	25	1002	0.216	50	51	1023	0.526
20	25	1003	0.162	51	51	1464	0.329
21	25	1004	0.329	52	53	1006	0.141
22	26	1004	0.106	53	53	1008	0.820
23	26	1012	0.314	54	53	1801	0.118
24	26	1013	0.287	55	83	1801	0.168
25	27	1016	0.239	56	83	6450	0.121
26	27	1019	0.252	57	83	6451	0.094
27	27	1023	0.211	58	87	1620	0.522
28	27	1028	0.277	59	87	1622	0.341
29	27	1029	0.193	60	88	1645	0.131
30	27	1085	0.220	61	89	1127	0.814
31	27	1087	0.118				

1 in = 25.4 mm

Table 14. Observed rutting in GPS-2 sections.

Number	State	Section	Observed Rutting, in
1	1	1021	0.261
2	1	4073	0.159
3	5	3058	0.147
4	5	3071	0.202
5	8	7781	0.219
6	12	4096	0.159
7	12	4097	0.204
8	12	4100	0.330
9	12	4108	0.436
10	28	3082	0.207
11	32	1030	0.176
12	32	7000	0.126
13	34	1033	0.311
14	34	1034	0.228
15	36	1008	0.121
16	36	1644	0.092
17	40	4163	0.263
18	40	4165	0.237
19	47	1028	0.320
20	47	3108	0.213
21	47	3109	0.161
22	47	3110	0.062
23	47	9024	0.186
24	47	9025	0.208
25	50	1681	0.106
26	50	1683	0.134
27	51	1423	0.146
28	51	2021	0.391
29	88	1647	0.297
30	89	2011	0.266

1 in = 25.4 mm

Theoretically, the pavement rutting rate should decrease with time as the subgrade reaches compaction and the AC layer hardens. The accumulated damage was calculated using Miner's hypothesis, as described earlier for fatigue cracking. The allowable load repetitions were computed for each strain level imposed by the axle-load/type combination, and the damage ratio was computed for each axle-load/type combination. Appendix E contains a summary of the calculated cumulative permanent-deformation damage ratios, for both the GPS-1 and GPS-2 sections.

The relationship between observed rutting and rutting damage ratio is expected to take an S shape. The rate of pavement rutting starts at a high level and decreases with time. Therefore, the point of 100 percent damage ratio does not have the same implication as that of fatigue. In fatigue analysis, the 100 percent damage ratio, corresponding to about 20 percent cracking, is the point at which the cracking starts to propagate progressively and the pavement starts to deteriorate more quickly. Conversely, the 100 percent damage ratio for rutting is an arbitrary one that corresponds to about 13 mm (0.5 in) of rutting. The rate of rutting development after this point does not increase significantly. The 13-mm (0.5-in) rutting criterion is a functional, rather than a structural, criterion.

Comparison: Predicted Versus Observed Rutting

Figures 14 and 15 show the relationship between observed rutting and the calculated rutting damage ratio for the GPS-1 and GPS-2 sections, respectively. Figures 14 and 15 show that, overall, the AI model appears to perform well. Most of the data points meet the one-point AI model criterion; that is, the observed rutting is less than about 13 to 19 mm (0.5 to 0.75 in) if the computed damage is less than 1.0, or 100 percent. Only 2 out of 61 GPS-1 sections did not meet the AI criterion. Rutting in the GPS-2 sections did not exceed 13 mm (0.5 in), and the maximum computed damage ratio was less than 1.0. However, there was a large scatter of the data points in Figures 14 and 15. The AI model presumes that the pavement layers above the subgrade do not contribute much to rutting. Consequently, the plastic characteristics of the upper pavement layers are excluded from the analysis. In the absence of other predictor variables, this may have resulted in the scatter of the data points.

Figures 14 and 15 show no consistent trend in the observed rutting versus the computed damage ratio. Many sections with a small rutting damage ratio exhibited a large rut depth; conversely, many sections with a large rutting damage ratio exhibited a small rut depth. It is apparent that the AI damage ratio is not a good predictor of rut depth. In general, the data did not exhibit the expected S-shaped curve that represents the hardening of the AC layer and rutting stabilization with time.

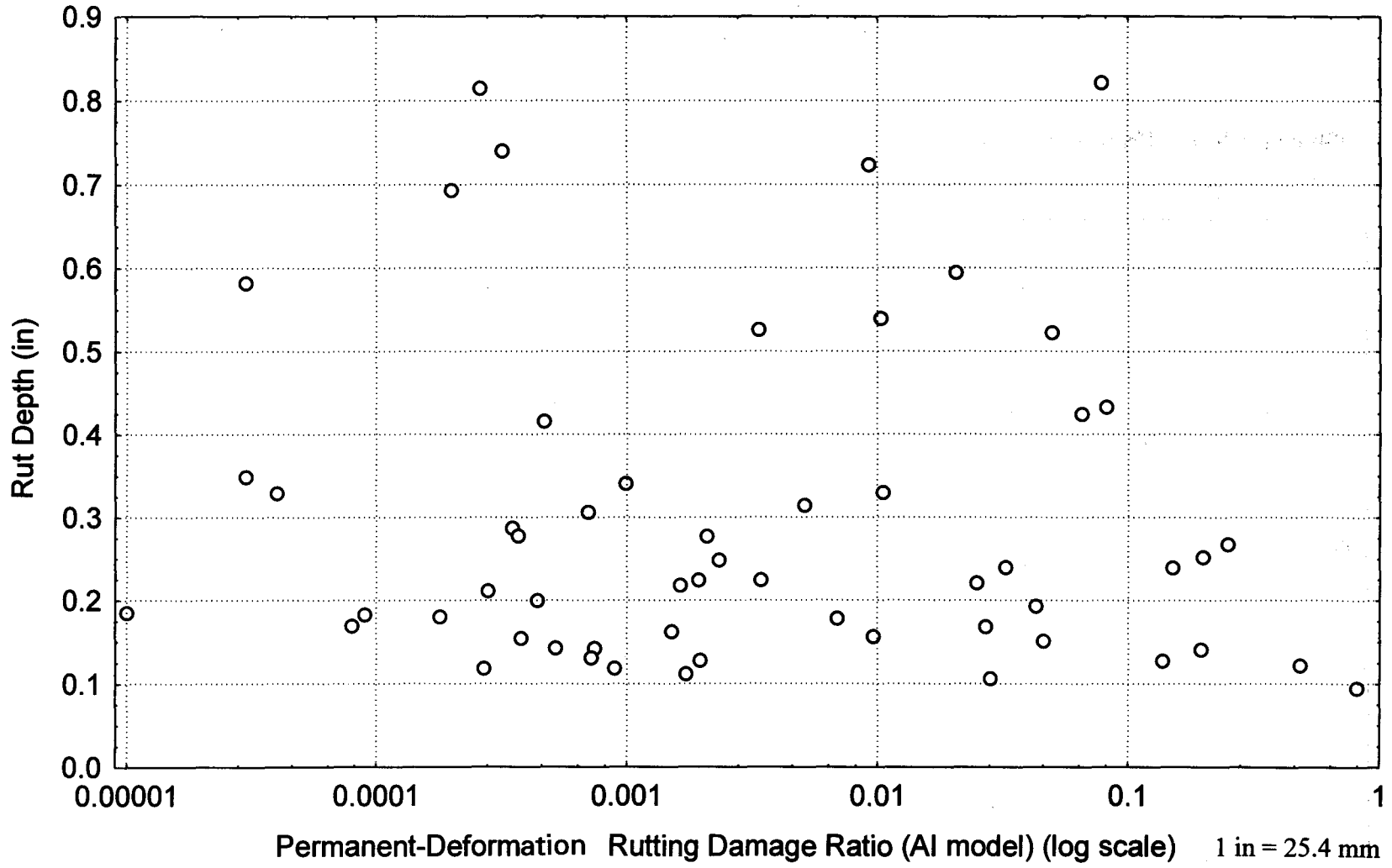


Figure 14. Rutting for GPS-1.

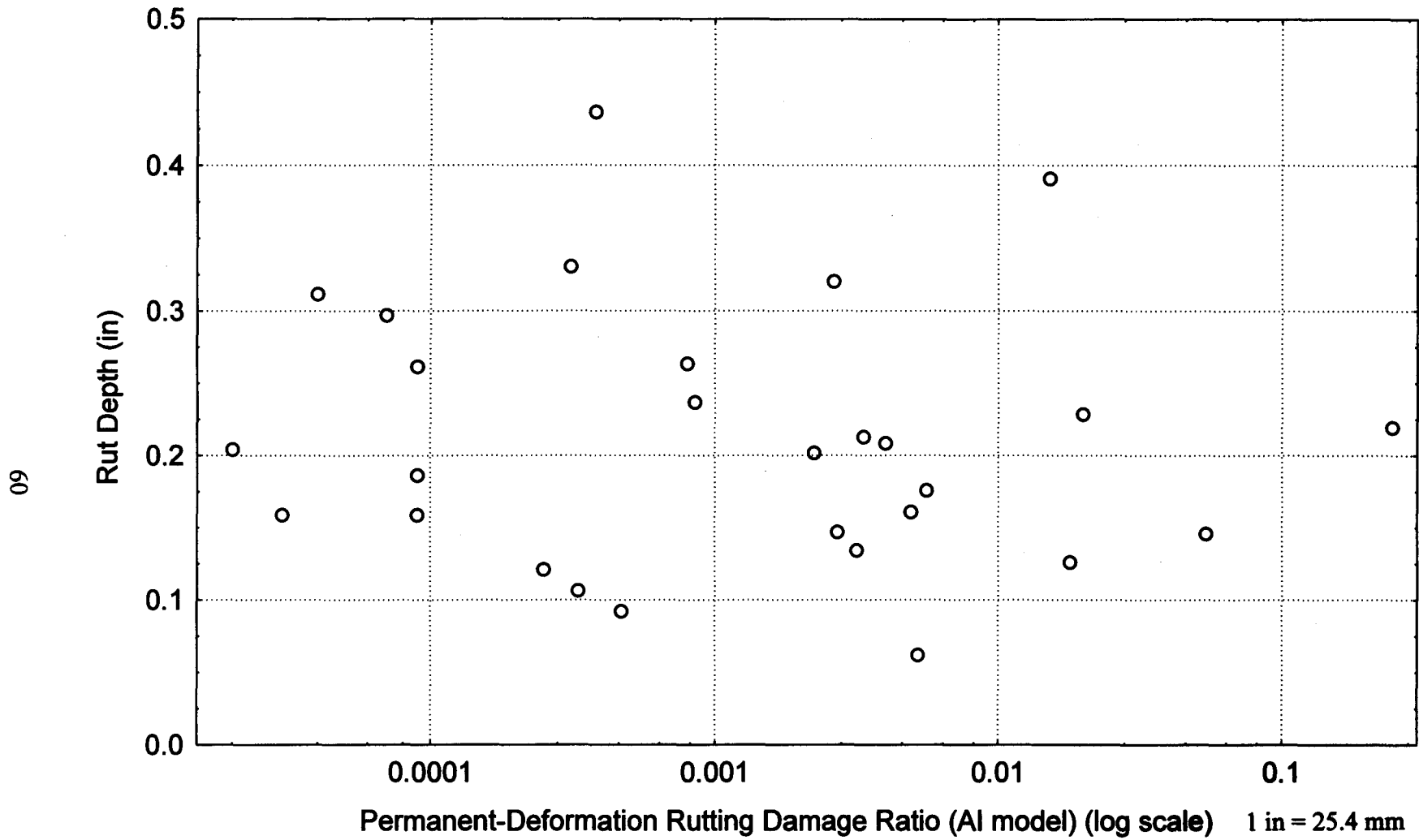


Figure 15. Rutting for GPS-2.

Summary

It is well known that rutting increases at an increasing rate during the initial years of operation and then stabilizes with time. The AI model is limited in that while it appears to be reliable in predicting a one-point event, it provides no indication of the behavior of rutting over time or with the application of traffic loading. It also does not provide any indication of rate-hardening, nor does it consider the contribution of the nonsubgrade layers to rutting. In order to account for the rate-hardening and the contribution of all layers to rutting, a new rutting model was formulated. The development of this new model is discussed in chapter 9.

CHAPTER 7. THE SHELL MODELS

Introduction

In the forgoing analysis, the AI models were used to predict fatigue and permanent deformation damage. In this section, the Shell transfer functions are used to predict both fatigue cracking and rutting for the GPS-1 sections.

Shell Fatigue Cracking Model Evaluation

The Shell transfer function (model) is very similar in form to the AI model. It relates the fatigue damage to the horizontal tensile strain at the bottom of the AC layer, as follows:

$$N_f = 0.0685 * (e_t)^{-5.671} * (E_{ac})^{-2.363} \quad (28)$$

where: N_f = Number of load repetitions to failure.
 E_{ac} = Modulus of asphalt concrete in psi.
 e_t = Magnitude of tensile strain at the bottom of the AC layer.

Compared to the AI model, the Shell model places more emphasis (higher exponent) on the tensile strain at the bottom of the AC layer and less emphasis on the elastic modulus of the layer.

Figure 16 is a plot of the observed fatigue cracking versus fatigue damage ratio, based on the Shell model. The plot is similar to that of the AI model in its shape and in predicting the development of fatigue cracking for damage ratios higher than 100 percent. The Shell model produced a higher damage ratio, especially at the higher end of the scale. As with the AI model evaluation discussed in chapter 5, the lack of sections exhibiting significant amounts of fatigue cracking did not allow for a detailed evaluation of the accuracy of the Shell models. Table 15 presents the results of a comparative t-test for the difference between the predictions of the AI model and the Shell model. The test showed that for a 95-percent confidence level, the mean value of the difference between the two predictions was not different from zero. In other words, the two models did not produce significantly different results. The significance level (probability of error) at which the two models produce different results is 22 percent. This is shown in the rightmost column of table 15.

Figure 17 is a combined scatter plot of the damage ratio versus the observed fatigue damage for both models. The figure shows that the two models produced a similar trend. For some sections, the AI model produced higher damage ratios than the Shell model, and the situation was reversed for other sections.

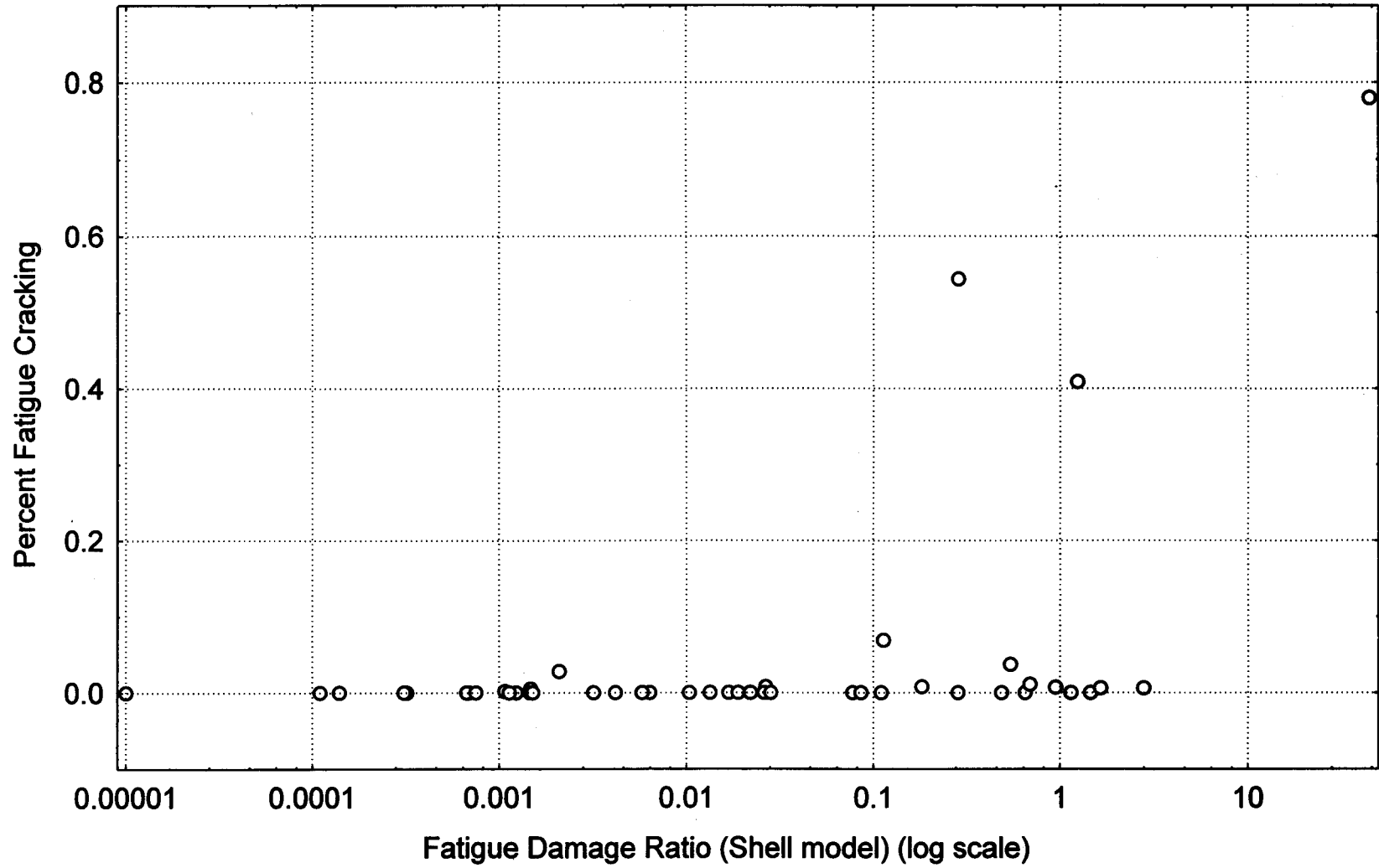


Figure 16. The Shell fatigue model, GPS-1 sections.

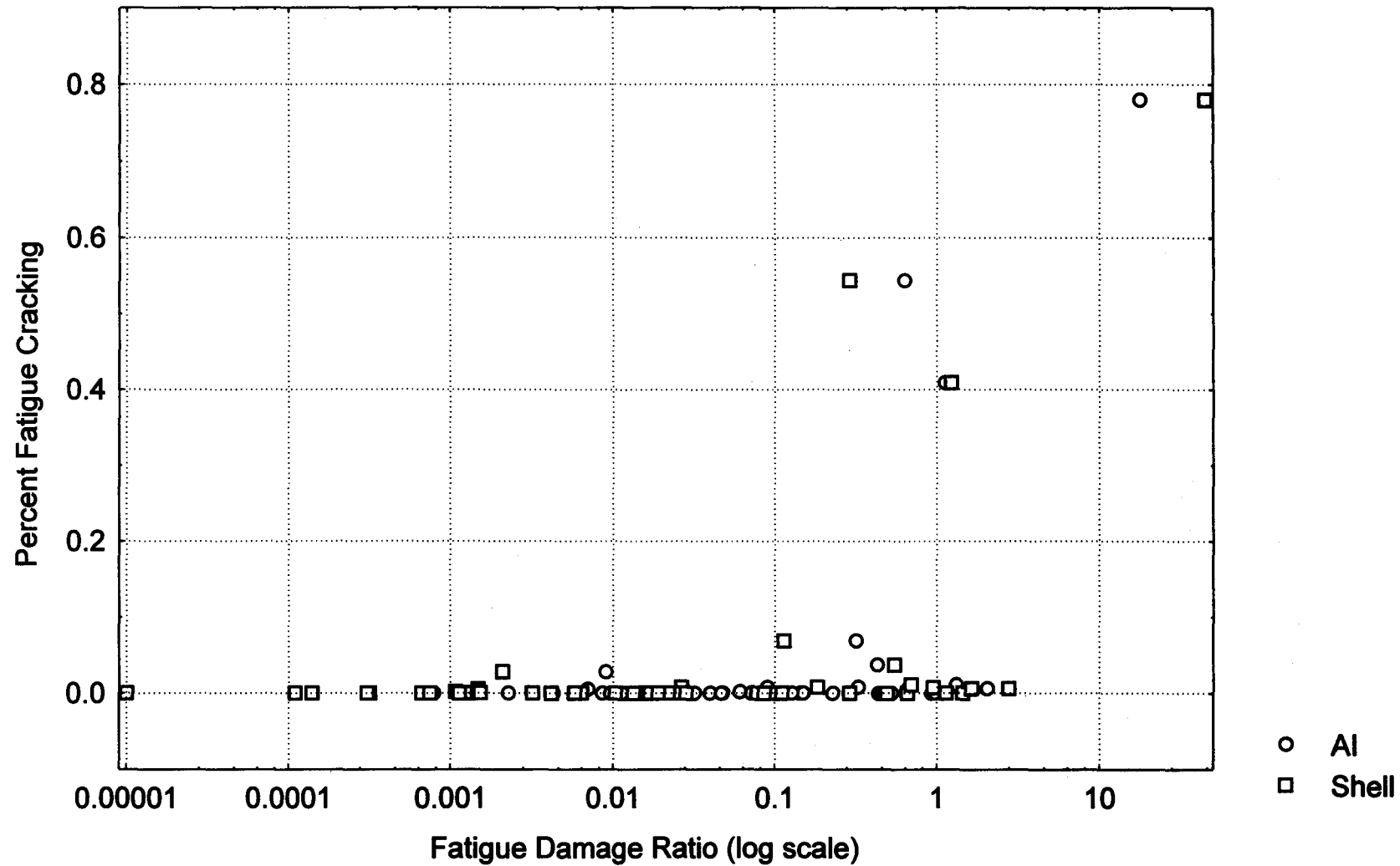


Figure 17. The AI versus the Shell fatigue models, GPS-1 sections.

Table 15. T-test for the difference between the AI and the Shell fatigue models.

Model	Mean	Std. Dev.	Number of Readings	Diff.	Std. Difference	t	D _f	p
AI	0.8175	2.53	62	-0.552	3.51	-1.235	61	0.221
Shell	1.3694	5.97	62					

Shell Rutting Model Evaluation

The revised (1985) Shell transfer function for rutting relates the rutting damage to the vertical compressive strain at the top of the subgrade, as follows:

$$N_d = 6.15 * 10^{-7} * (e_c)^{-4} \tag{29}$$

where: N_d = Number of load repetitions to failure (rutting equal to 13 mm [0.50 in]), corresponding to 50-percent reliability.
 e_c = Vertical compressive strain at the top of the subgrade.

A permanent-deformation damage analysis was performed using this model. Figure 18 is a plot of the rut depth versus the total damage ratio. Similar to the AI rutting model, the Shell model met the one-point criterion of less than 13 mm (0.5 in) rutting if the damage ratio is less than 1.0. The expected S-shape trend in data points was not observed. The wide vertical scatter of the data points suggests that other nonsubgrade layers may contribute significantly to rutting.

Figure 19 compares the AI and Shell models. It is clear that the AI model produced larger damage ratios than those of the Shell model. Table 16 shows the results of a t-test to compare the difference between the predictions of the two models. The test indicated that at 95-percent confidence, the two models produce significantly different results (p-level is less than 0.05). The AI model is more conservative in evaluating the damage than the 50-percent-reliability Shell model.

Table 16. T-test for the difference between the AI and the Shell rutting models.

Model	Mean	Std. Dev.	Number of Readings	Diff.	Std. Difference	t	D _f	p
AI	0.0453	0.127	62	0.04	0.113	2.8	61	0.0067
Shell	0.0049	0.013	62					

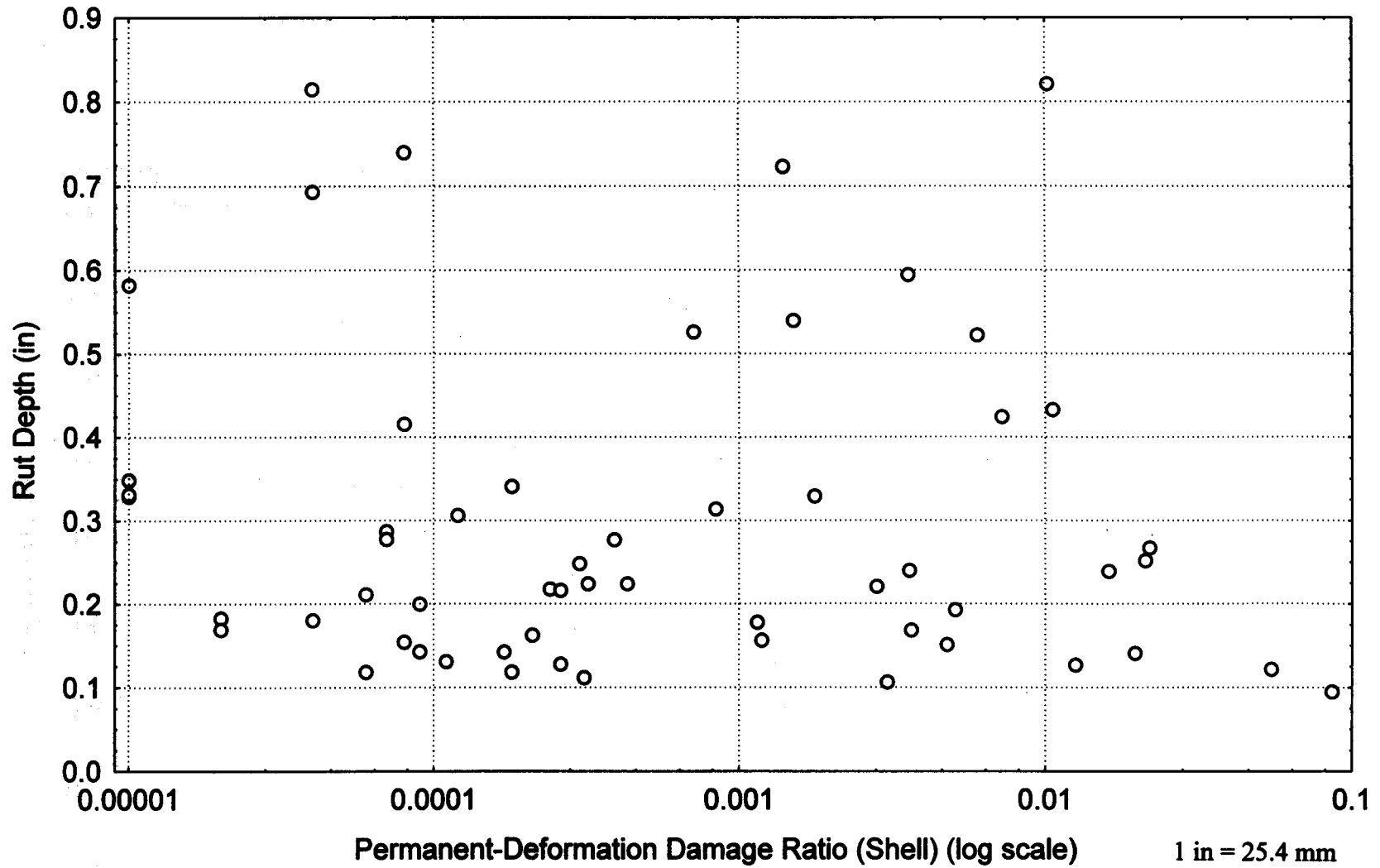


Figure 18. Shell rutting model, GPS-1 sections.

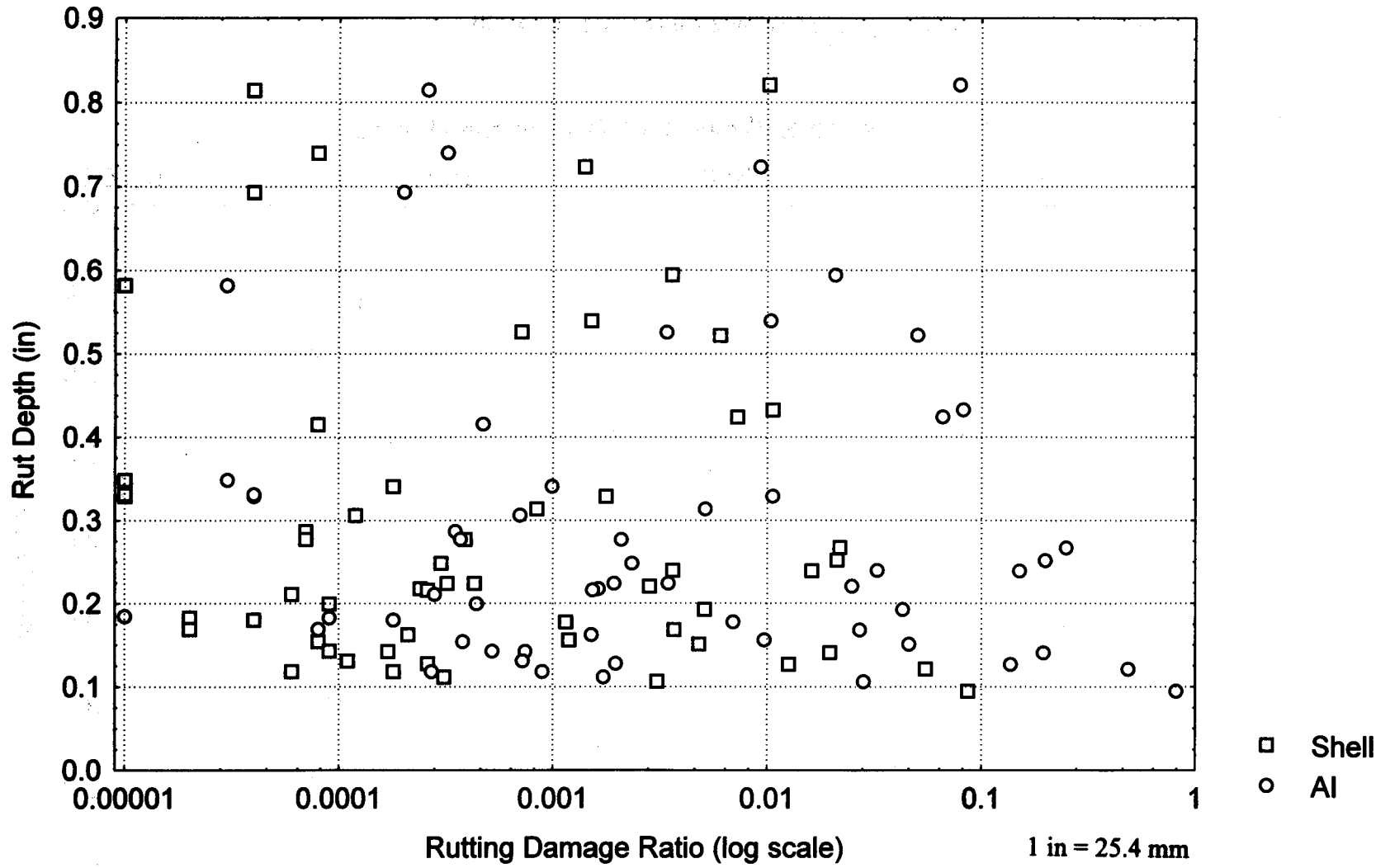


Figure 19. Comparison between the AI and the Shell rutting models.

Summary

The Shell fatigue cracking model is comparable to the AI fatigue cracking model in predicting the fatigue behavior of pavements. Although the Shell model produced slightly higher damage ratios than the AI model, the t-test showed that the two models did not produce significantly different results.

The Shell 50-percent-reliability permanent-deformation transfer function appears to perform as well as the AI model in predicting the rut depth within the limitation of the one-point criteria. Both models neglect the contributions to rutting by the upper pavement layers. The t-test showed that the two models produce significantly different damage results, with the Shell model producing lower damage values.

The large scatter in the plots of observed versus computed rutting damage for both the AI and the Shell rutting models indicates that the damage ratio calculated by these models is not a good predictor of rut depth. It was hypothesized that if the models considered the contribution of the nonsubgrade layers to the measured rutting, a better match would result.

CHAPTER 8. CASE STUDY: COMPARING METHODS OF ASSESSING THE EFFECTS OF SEASONAL VARIATIONS ON DAMAGE ANALYSIS

One of the assumptions made in the damage analysis is that the average pavement layer moduli values may be used as an estimate of the effective year-round values. If pavement moduli are available at only one random point of time, then this value would be used as a representative of the effective (true) values. If several values, representing different seasons, are available (as in the case of the seasonal sections), two approaches may be used in the damage analysis:

- The first involves dividing the analysis period into seasons. In each season, the moduli values are used to calculate the damage ratio. The damage ratios are then summed over all seasons. If seasonal traffic variation is known, then traffic volume in each season is associated with the moduli values in that season; otherwise, a uniform traffic distribution is assumed.
- The second involves calculating the best estimate of the effective year-round moduli and then using these values in the damage analysis. A good estimate of the effective moduli is the weighted average of the seasonal values, with the weights proportional to the traffic volume in each season. For the purpose of this analysis, the weights are considered equal, since the seasonal variation of traffic volume is not known (only annual traffic counts are available in the LTPP database).

Although the first method is more appealing than the second, it is more calculation-intensive. For example, for a seasonal section with 12 seasonal pavement moduli values and 100 axle/load categories (there are actually a total of 140 axle/load categories in the LTPP database), it would be necessary to perform the structural analysis 1200 times. However, using the second approach, it would only be necessary to perform the structural analysis 100 times. Two important questions addressed in the following case are: How significant is the difference between the results of the two methods? Also, what if only one set of values of the pavement moduli, taken at a random point in time, was used in the analysis?

Case Study: LTPP Section 311030

Section 311030 is a seasonal section located in Nebraska. For this section, nine sets of pavement layer moduli, taken in different years and seasons, are available.

Damage analysis was conducted using three scenarios, outlined in Table 17. Figures 20 and 21 graphically show the results of the fatigue cracking damage analysis and the permanent-deformation damage analysis, respectively. The first and second analysis approaches listed in the table are as previously outlined. The third scenario listed in the table uses the individual value taken at one given day. This analysis approach is used when the section is not a seasonal section and is visited only once every few years.

As the table shows, depending on the day at which FWD testing was done, the results differ. The fatigue damage ratio ranged between 0.035 and 0.15. The permanent-deformation

Table 17. Effects of seasonal variations on damage analyses.

Approach Used in Structural and Damage Analyses	Fatigue Damage Ratio	Permanent-Deformation Damage Ratio
1. Using all seasonal moduli.	0.096	0.118
2. Using the average moduli.	0.078	0.065
3. Using a single reading taken on:		
8/8/89	0.125	0.280
11/29/90	0.035	0.017
11/20/91	0.101	0.098
12/11/91	0.080	0.072
1/16/92	0.043	0.019
2/26/92	0.106	0.107
3/23/92	0.151	0.207
4/16/92	0.149	0.193
4/20/93	0.075	0.072

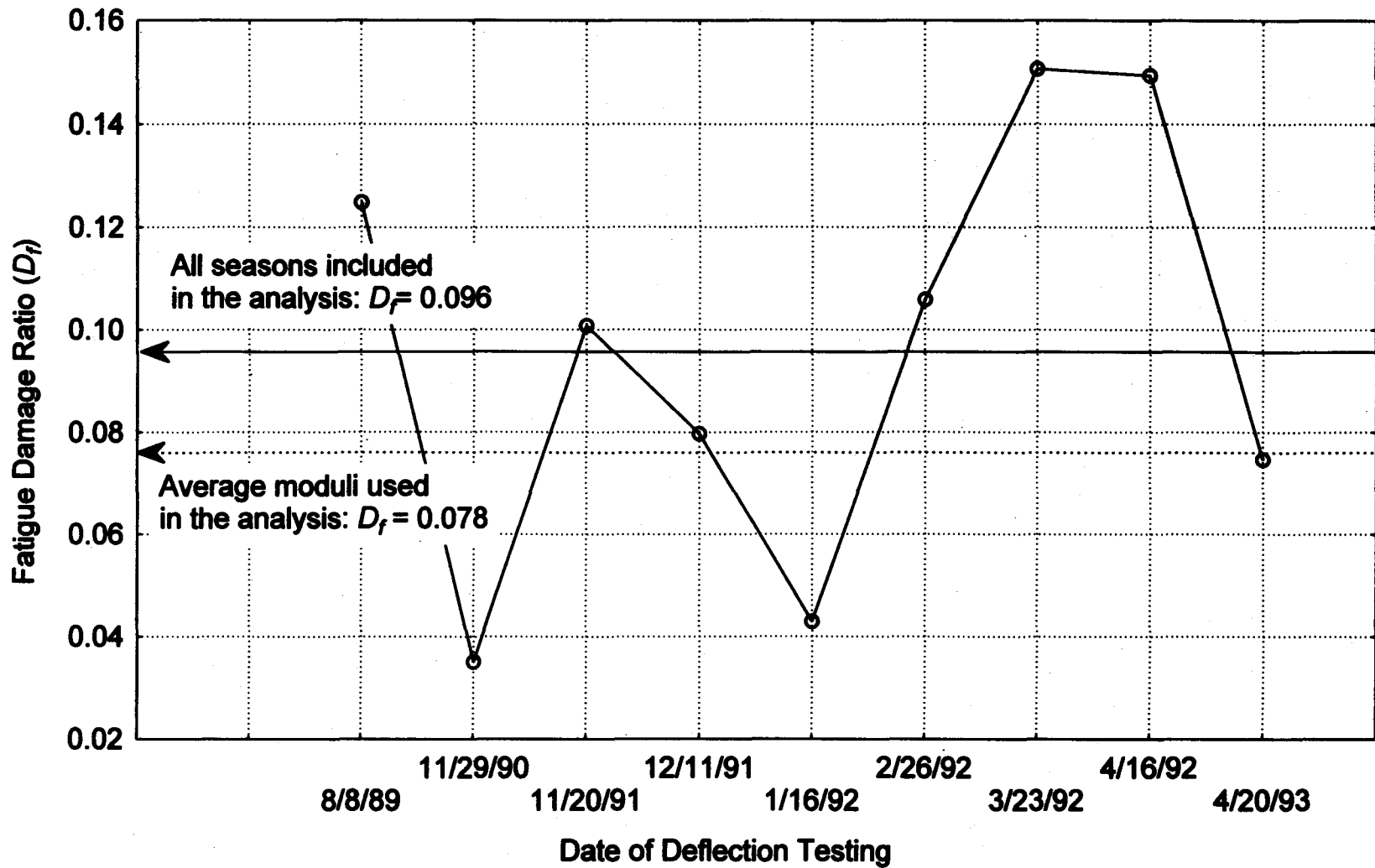


Figure 20. Seasonal variation effects on fatigue damage ratio.

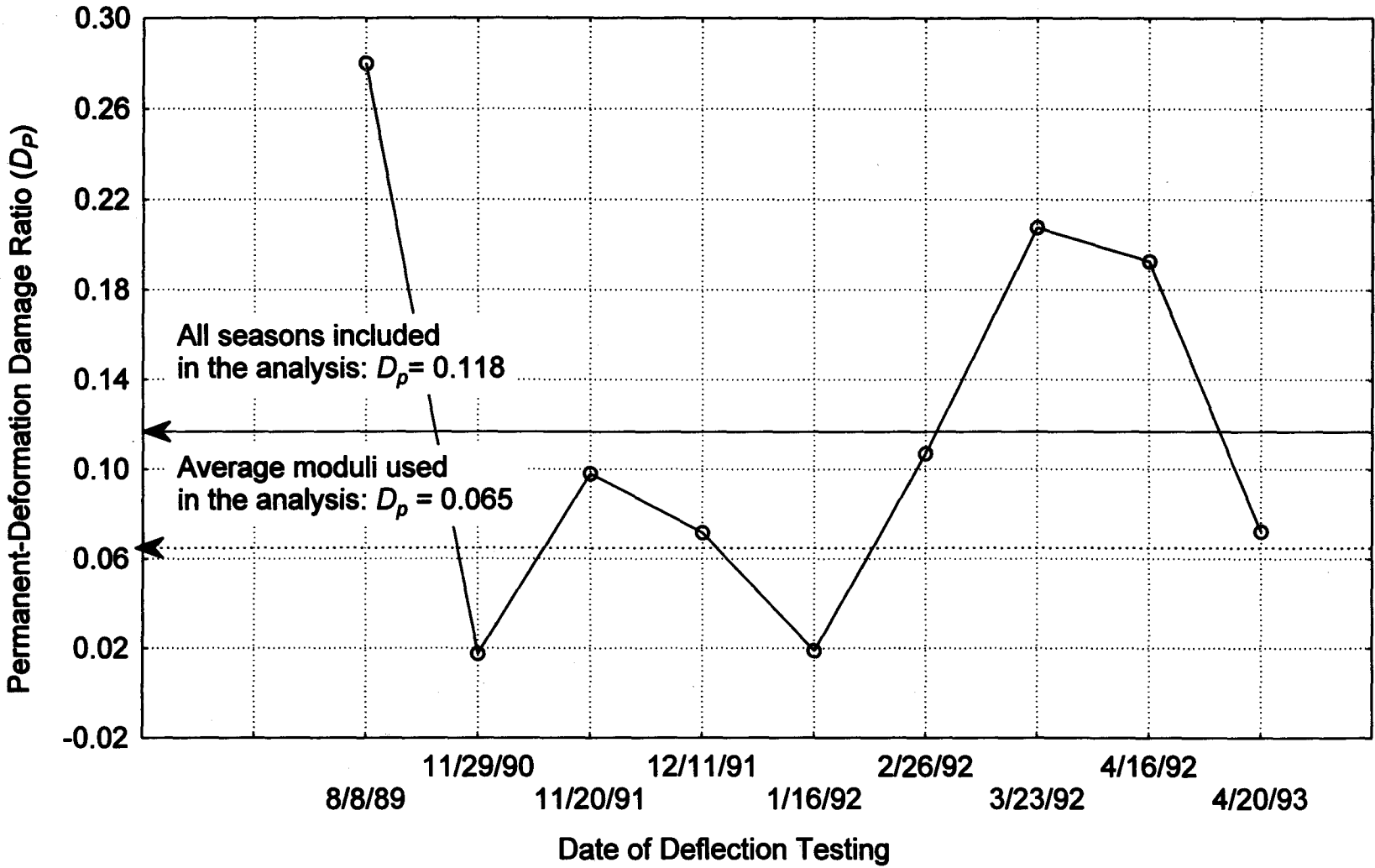


Figure 21. Seasonal variation effects on rutting damage ratio.

damage ratio ranged from 0.017 to 0.28. The implication of such variation is that pavement life expectancy may be greatly under- or over-estimated, depending on the time at which pavement testing is conducted. This stresses the need for quantifying the seasonal effects and considering them in damage analysis.

Comparison: Approach 1 Versus Approach 2

Table 17 shows that for the same traffic magnitude, the fatigue damage ratio equals 0.096 if all the seasonal values are used, and equals 0.078 if the average pavement moduli are used. A single t-test was used to compare a single value of 0.078 to a population with a mean value of 0.096 and a variation expressed by the 9 points (given in approach 3). However, more data points would be required to arrive at a definitive conclusion. Based on the limited data available, the test fails to show that the two values are significantly different compared to the seasonal variation of the damage ratio.

The same test was conducted to compare the permanent deformation damages using approaches 1 and 2 versus the seasonal variation of the damage ratios. Similar results were obtained. That is, the two values (0.118 and 0.065) were not significantly different. It should be noted, however, that assumptions of normality and sample independence were made. The comparison also indicates that the second approach yielded lower damage values than the first approach. This indicates that, in this case, the first approach is more conservative.

In conclusion, the results of the case study indicate that, for section 311030:

- A lack of seasonal data (layer moduli) may lead to a too-large or too-low estimate of pavement damage. A difference of up to 16 times the magnitude was observed when different sets of pavement layer moduli, taken at different points in time, were used individually in the analysis.
- The damage ratio obtained using all seasonal moduli values did not appear to be significantly different from that obtained using the average moduli values. However, the former approach tended to yield more conservative results.

These conclusions are based on the assumption that traffic volume is uniform throughout the year. It is expected that if the seasonal fluctuations in traffic volume are considered in the damage analysis, the methods described for considering the seasonal variation effect on pavements may produce even more different results.

CHAPTER 9. NEW RUTTING MODEL

Introduction

As discussed in chapters 6 and 7, the subgrade-strain-based rutting models developed by the Asphalt Institute and Shell have serious limitations. These models neglect the contributions of the AC layer, the base, and the subbase layers to rutting, and they do not account for rate-hardening in the progression of rutting over time. Data from the AASHO road test experiments showed that the subgrade contributed only about 9 percent of the total measured rutting. The AC layer, the base, and the subbase layers contributed about 34 percent, 14 percent, and 45 percent, respectively [15]. In general, the contribution of each layer to rutting will depend on such factors as the layer compaction, modulus, shear strength, shear and normal stresses and strains, the layer position in the pavement and the corresponding stress levels, permanent deformation parameters, etc. Therefore, it is important to consider the contribution of all pavement layers to rutting.

A number of models are available for considering the additive permanent deformation from all pavement layers. The direct method [13], the VESYS model [16], and the Ohio State [17] model are examples. However, none of the available model forms directly allows for using axle-load/type combinations to characterize traffic. In addition, they require material parameters that are not available in the LTPP database. The following section describes the development and calibration of a mechanistic-based rutting model that can consider the actual axle load spectrum.

Model Formulation

Assume that we have k loading groups (axle/load combinations) and that each load group i is associated with a vertical elastic compressive strain $\epsilon e_{i,j}$ in pavement layer j (there are L pavement layers). Each load group i has n_i axles. The plastic strain is assumed to be a linear function of the plastic deformation; and it is related to the number of load applications by a negative power model. The negative power relationship reflects the pavement hardening effect due to repetitive loading. The following model relates: (a) the vertical compressive plastic strain $\epsilon p_{i,j}$ in a given layer resulting from one load increment of axle group i , to (b) the elastic compressive strain $\epsilon e_{i,j}$ in layer j resulting from the load passage and the number of load applications N .

$$\epsilon p_{x,j} = \mu_j * \epsilon e_{i,j} * N^{-\alpha_j} \quad (30)$$

where: μ_j = Slope of the elastic-strain/plastic-strain line for layer j .
 $-\alpha_j$ = Negative exponent reflecting hardening of layer j with repetitive loading.

Figure 22 represents the three-dimensional plastic strain model. In each loading group i , the amount of plastic strain differs from one axle to the next, while the elastic strain is constant for the group. That is, the first axle causes more permanent deformation than the second,

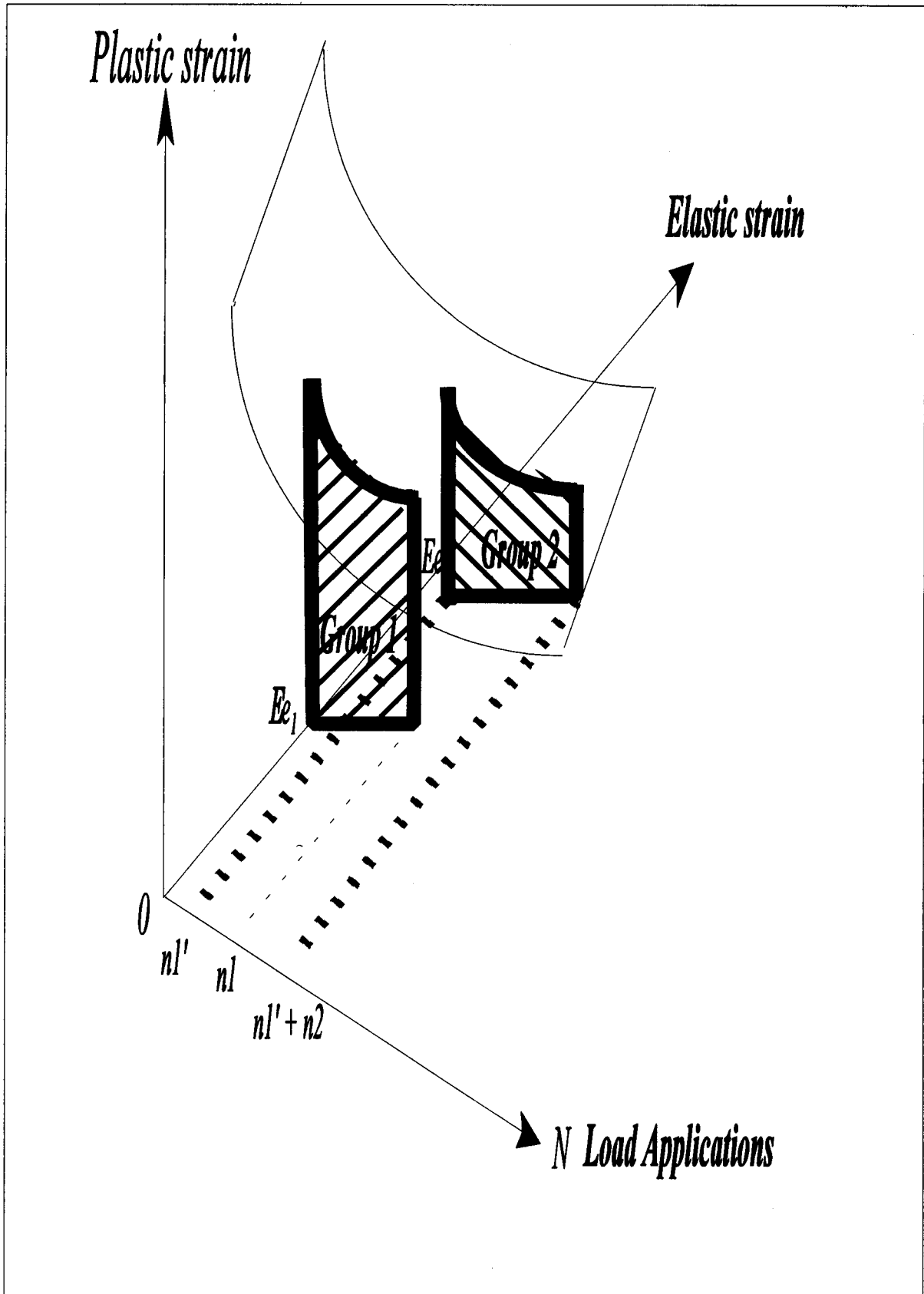


Figure 22. Three-dimensional strain model.

because of the hardening effect. The total plastic strain in layer j due to the first load group is calculated by:

$$\begin{aligned}\epsilon p_{i=1,j} &= \int_0^{n_1} \mu_j \epsilon e_{1j} N^{\alpha_j} dN \\ &= \frac{\mu_j \epsilon e_{1j}}{1 - \alpha_j} n_1^{1-\alpha_j}\end{aligned}\quad (31)$$

where: n_i = Number of applications of load group i .

We calculate the cumulative plastic strain for the second load group as follows:

$$\begin{aligned}\epsilon p_{i=2,j} &= \int_{n_{1j}'}^{n_{1j}'+n_{2j}} \mu_j \epsilon e_{2j} N^{\alpha_j} dN \\ &= \frac{\mu_j \epsilon e_{2j}}{1 - \alpha_j} [(n_{1j}' + n_{2j})^{1-\alpha_j} - (n_{1j}')^{1-\alpha_j}]\end{aligned}\quad (32)$$

where: n_{1j}' = Equivalent number of applications of the first load group in the second group's space (scale) for layer j .

Then, n_{1j}' may be calculated from the following assumption:

$$\frac{n_{1j}}{n_{1j}'} = \frac{N_{f1j}}{N_{f2j}}\quad (33)$$

That is, the ratio between two load counts equals the ratio between the number of repetitions of each needed to cause critical damage. The critical plastic strain $\epsilon p_{c,j}$ at layer j is calculated by:

$$\epsilon p_{c,j} = \frac{\mu_j \epsilon e_{1j}}{1 - \alpha_j} N_{f1j}^{1-\alpha_j}\quad (34)$$

$$N_{flj} = \left(\frac{\epsilon p_{c_j}(1 - \alpha_j)}{\mu_j \epsilon e_{1j}} \right)^{\frac{1}{1-\alpha_j}} \quad (35)$$

$$N_{f2j} = \left(\frac{\epsilon p_{c_j}(1 - \alpha_j)}{\mu_2 \epsilon e_{2j}} \right)^{\frac{1}{1-\alpha_j}} \quad (36)$$

$$\frac{N_{flj}}{N_{f2j}} = \left(\frac{\epsilon e_{2j}}{\epsilon e_{1j}} \right)^{\frac{1}{1-\alpha_j}} \quad (37)$$

$$\frac{n'_{1j}}{n_{1j}} = \frac{N_{f2j}}{N_{flj}} = \left(\frac{\epsilon e_{1j}}{\epsilon e_{2j}} \right)^{\frac{1}{1-\alpha_j}} \quad (38)$$

$$n'_{1j} = n_{1j} \left(\frac{\epsilon e_{1j}}{\epsilon e_{2j}} \right)^{\frac{1}{1-\alpha_j}}$$

Substituting equation 38 in equation 32, we get:

$$\epsilon p_{2j} = \frac{\mu_j \epsilon e_{2j}}{1 - \alpha_j} \left[\left(n_{1j} \left(\frac{\epsilon e_{1j}}{\epsilon e_{2j}} \right)^{\frac{1}{1-\alpha_j}} + n_{2j} \right)^{1-\alpha_j} - \left(n_{1j} \left(\frac{\epsilon e_{1j}}{\epsilon e_{2j}} \right)^{\frac{1}{1-\alpha_j}} \right)^{1-\alpha_j} \right] \quad (39)$$

Similarly, the cumulative plastic strain in layer j resulting from n_k axle applications of load group k is:

$$\epsilon p_{kj} = \frac{\mu_j \epsilon e_{kj}}{1 - \alpha_j} \left[\left(n'_{kj} + n_{kj} \right)^{1-\alpha_j} - \left(n'_{kj} \right)^{1-\alpha_j} \right] \quad (40)$$

where:

$$n'_{kj} = \sum_{i=1}^k n_i \left(\frac{\epsilon e_{ij}}{\epsilon e_{kj}} \right)^{\frac{1}{1-\alpha_j}} \quad (41)$$

This equation is the equivalent number of load applications of all previous load groups in the k group scale.

The cumulative plastic strain for all load groups in layer j is:

$$\epsilon p_j = \sum_{i=1}^k \frac{\mu_j \epsilon e_j}{1 - \alpha_j} \left[(n'_{ij} + n_{ij})^{1-\alpha_j} - (n'_{ij})^{1-\alpha_j} \right] \quad (42)$$

The parameters μ_j and α_j are constant for each layer. If we have L layers, each having h_j thickness, then the total plastic deformation ρ_p is obtained by:

$$\rho_p = \sum_{j=1}^L h_j \frac{\mu_j}{1 - \alpha_j} \sum_{i=1}^k \epsilon e_{ij} \left[(n'_{ij} + n_{ij})^{1-\alpha_j} - (n'_{ij})^{1-\alpha_j} \right] \quad (43)$$

The coefficients μ and α for each layer may be evaluated by laboratory testing, or by using numerical optimization techniques, given rutting and traffic data.

To simplify this equation, it may be prudent to convert the number of applications of all load groups to a single load level, using equation 30. The concept was applied here to convert the counts of a previous load group to an equivalent count in terms of the group in question. Equation 38 may be used for this purpose. For example, we may convert the counts of all load groups into an equivalent count of the first load group, as follows:

$$Ne_{1j} = n_{1j} \left(\frac{\epsilon e_{1j}}{\epsilon e_{1j}} \right)^{\frac{1}{1-\alpha_j}} + n_{2j} \left(\frac{\epsilon e_{2j}}{\epsilon e_{1j}} \right)^{\frac{1}{1-\alpha_j}} + \dots + n_{kj} \left(\frac{\epsilon e_{kj}}{\epsilon e_{1j}} \right)^{\frac{1}{1-\alpha_j}} \quad (44)$$

$$Ne_{1j} = \sum_{i=1}^k n_{ij} \left(\frac{\epsilon e_{ij}}{\epsilon e_j} \right)^{\frac{1}{1-\alpha_j}} \quad (45)$$

where: $Ne_{1,j}$ = The equivalent number of applications of all groups, in terms of the first group.

In this case, we convert the number of load applications into Ne (corresponding to ϵe). If $\epsilon e_j = \epsilon e_{1,j}$, i.e., converting any load group to the first load group, then the first term in equation 44 equates to $n_{1,j}$. The cumulative plastic strain corresponding to $Ne_{1,j}$ applications may be calculated by:

$$\epsilon p_j = \frac{\mu_j \epsilon e_{1,j}}{1 - \alpha_j} (Ne_{1,j})^{1-\alpha_j} \quad (46)$$

and the cumulative strain in all layers may be calculated by:

$$\epsilon p = \sum_{j=1}^L \frac{\mu_j}{1 - \alpha_j} \epsilon e_{1,j} (Ne_{1,j})^{1-\alpha_j} \quad (47)$$

Multiplying the plastic strain of each layer by the layer thickness to obtain the plastic deformation and substituting $Ne_{1,j}$ from equation 45 gives:

$$\rho_p = \sum_{j=1}^L h_j \frac{\mu_j}{1 - \alpha_j} \left(\sum_{i=1}^k n_i (\epsilon e_{i,j})^{\frac{1}{1-\alpha_j}} \right)^{1-\alpha_j} \quad (48)$$

where: ρ_p = Cumulative permanent deformation in all layers from all load groups (i.e., rut depth).
 $\epsilon e_{i,j}$ = Vertical compressive strain in the middle of layer j due to the passage of an axle of group i .
 h_j = Thickness of layer j .

The subgrade may be divided into several layers and the calculations performed until the vertical elastic strain = 0, the subgrade thickness is then determined accordingly.

It should be noted that this model does not account for the lateral flow resulting from the horizontal shearing strain in the layers. The model may be modified to use the shearing strain as another predictor of rutting. However, the regression coefficients of the model will partially compensate for the absence of this second predictor. It is also possible to formulate a model in terms of the elastic deflection within each layer.

Model Calibration

The parameters μ_j and α_j may be determined for each layer using numerical optimization. To perform this task, a forward elastic layer analysis program, such as the WESLEA program, must be used to calculate the vertical compressive strain at the mid-depth of each layer.

Finding the set of parameters μ and α for each layer involves solving the following optimization problem:

$$\text{Minimize: } F = \sum_{i=1}^S (\rho_i - RD_i)^2 \quad (49)$$

where: ρ_i = Calculated cumulative rut depth from the rutting model, for section i .
 RD_i = Observed rut depth in section i .
 S = Total number of sections.

The result of this calibration is a set of μ_j and α_j values (average values) for each layer of the pavement. If such values yield an accurate rutting prediction (small standard error of estimate), then the model and the coefficients may be used to produce an estimate of rutting.

It should be noted that, ideally, α_j and μ_j are site-specific. That is, each section or project should have its own unique parameters. However, there are not enough data points to support the calibration of the model for each section individually. For example, a section with 5 layers has 10 unknowns, 2 for each layer, but only one rutting value. The availability of time-series traffic and distress survey data is necessary to perform site-specific calibration.

If the average plastic parameters (μ_i and α_i), rather than the actual site-specific values, are used to predict rutting, a rutting estimation error is expected. The standard error of estimate Se may be used to assess the magnitude of error expected from the model. Such magnitude encompasses: the error due to using the average, rather than the actual, parameters; the modeling error; and the measurement error. Hence, Se is calculated in both the calibration and validation of the model.

Model Calibration Results

A total of 61 GPS-1 sections were used to calibrate the model. Vertical elastic compressive strains were calculated at the mid-depth of each layer, assuming that the mid-depth strain represents the layer's average strain. The subgrade was divided into a number of layers until the strain value approached zero for the lowest layer. Given that WESLEA is a five-layer program, the subgrade was divided into three or four layers, depending on the existence of a base layer, and the upper subgrade layers were considered to have finite thickness. The thickness of such layers was large enough that the strain values approached zero at the lowest layer.

An error minimization algorithm was implemented to find the parameters α and μ for each pavement layer such that the squared deviation between observed and calculated rutting was minimal. The following are the calibration results.

	AC	Combined Granular Base and Subbase	Subgrade
α	0.10	0.95	0.644
μ	$1.03 \cdot 10^{-4}$	1.163	$8.0 \cdot 10^{-3}$

The model may be rewritten in the following form:

$$\begin{aligned}
 \rho_p = & h_{AC} \frac{\mu_{AC}}{1 - \alpha_{AC}} \left(\sum_{i=1}^k n_i (\epsilon e_{i,AC})^{\frac{1}{1-\alpha_{AC}}} \right)^{1 - \alpha_{AC}} \\
 & + h_{Base} \frac{\mu_{Base}}{1 - \alpha_{Base}} \left(\sum_{i=1}^k n_i (\epsilon e_{i,Base})^{\frac{1}{1-\alpha_{Base}}} \right)^{1 - \alpha_{Base}} \\
 & + h_{Subgrade} \frac{\mu_{Subgrade}}{1 - \alpha_{Subgrade}} \left(\sum_{i=1}^k n_i (\epsilon e_{i,Subgrade})^{\frac{1}{1-\alpha_{Subgrade}}} \right)^{1 - \alpha_{Subgrade}}
 \end{aligned} \tag{50}$$

- where: ρ_p = Total cumulative rut depth (in the same units as the layer thickness h).
 i = Subscript denoting load groups (e.g., single axle with 44.5 kN).
 k = Number of load groups.
 h = Layer thickness.
 $AC, Base, Subgrade$ = Subscripts denoting the AC layer, the combined base/subbase layer, and the subgrade, respectively.
 μ_j = Layer parameter representing the slope of the elastic/plastic strain line.
 α_j = Layer parameter reflecting the hardening of layer j with repetitive loading.
 $\epsilon e_{i,j}$ = Vertical compressive elastic strain in the middle of layer j , corresponding to load group i .

Substituting the applicable coefficients in this equation gives:

$$\begin{aligned}
 \rho_p = & 0.00011 * h_{AC} \left(\sum_{i=1}^k n_i (\epsilon e_{i,AC})^{1.111} \right)^{0.9} + 23.26 * h_{Base} \left(\sum_{i=1}^k n_i (\epsilon e_{i,Base})^{20} \right)^{0.05} \\
 & + 0.022 * h_{Subgrade} \left(\sum_{i=1}^k n_i (\epsilon e_{i,Subgrade})^{2.81} \right)^{0.356}
 \end{aligned} \tag{51}$$

Goodness of Fit

The sum of the squared error is 961 mm squared (1.49 in squared). The standard error of estimate is 4.14 mm (0.164 in). This is not much larger than the error in measuring the rut depth [about 2 mm (0.08 in)]. The relative error (i.e., the ratio between the standard error of estimate of the model and the standard deviation of observed rutting) is 0.87; hence, the model provides improved prediction, compared to the mean rut depth.

Figure 23 shows that the residuals are normally distributed. The bias (mean residual) is 0.7 mm (0.027 in). Fifty-five percent of the observations were within an error of 2.5 mm (0.1 in). Eighty percent of the observations were within 5 mm (0.2 in) error.

Figure 24 is a plot of the predicted versus observed rutting values. The observations are distributed with a constant variance around the 45-percent degree line, an indication of a good fit between the model and the data. The plot indicates that the model underpredicted rut depth values in excess of 20 mm (0.8 in).

The Wilcoxon Matched Pair test, a nonparametric alternative to the t-test, was performed to test the hypothesis that the observed and predicted rutting values are drawn from the same distribution. The test is significant at the 0.01 level. The test shows that the p-level (significance level) is 0.316. Hence, the distributions of the observed and predicted values are not different at this level of significance.

The model parameters indicate that the AC layer contribution to surface rutting is marginal for the sections considered in the analysis. The combined base/subbase layer contributed the most to the measured rutting. In addition, the contribution of the subgrade to the measured rutting was greater than that of the AC layer, but much less than that of the base/subbase layer. However, the vertical elastic strain values may not be the same in all layers, and this comparison was based on the value of the constant multiplied by the strain value of each layer. It should also be noted that the model is very sensitive to the layer moduli used. For example, the apparent higher contribution of the base/subbase layer to rutting may be due to the fact that the backcalculated moduli for the base/subbase were generally low; in many cases, they were lower than the subgrade moduli values.

Model Validation

The rutting model described here was calibrated using the rut depth, as measured in the last rutting survey, and the traffic loading counts projected up to the date of the last survey. To evaluate the model's accuracy in predicting the rut depth, the model was used to predict the rut depth at the first rutting survey date, given the traffic loading counts projected up to that date. The predicted versus observed values are plotted in Figure 25. The standard error of estimate of the rut depth was 3.55 mm (0.14 in), which is lower than that of the calibration set.

Section 091047 was selected randomly to compare its actual measured rutting values to rutting development as a function of time, as predicted by the model. Figure 26 is a graphical presentation of the comparison. The figure shows the expected rutting of the pavement at ages

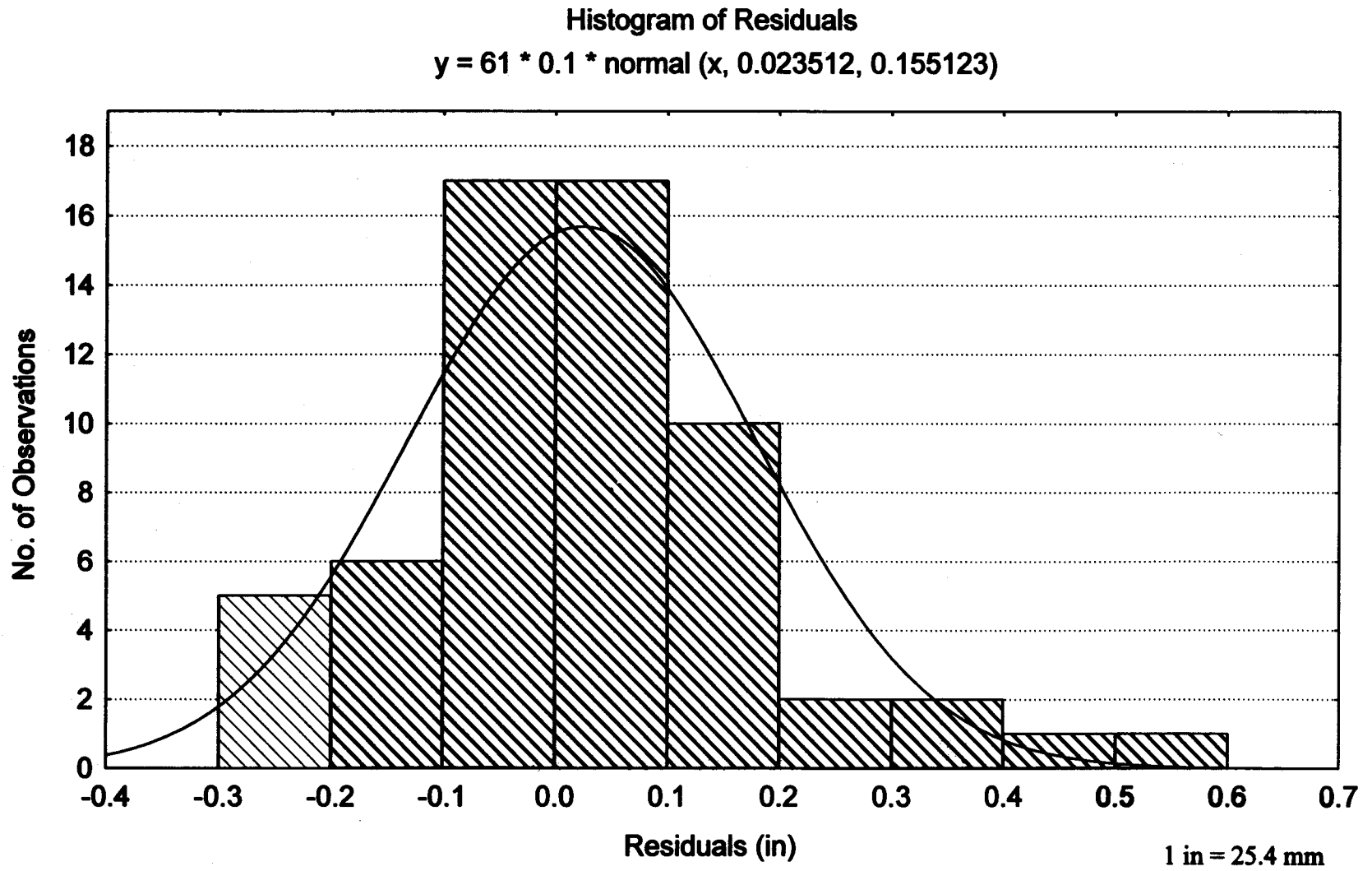


Figure 23. Histogram of residuals.

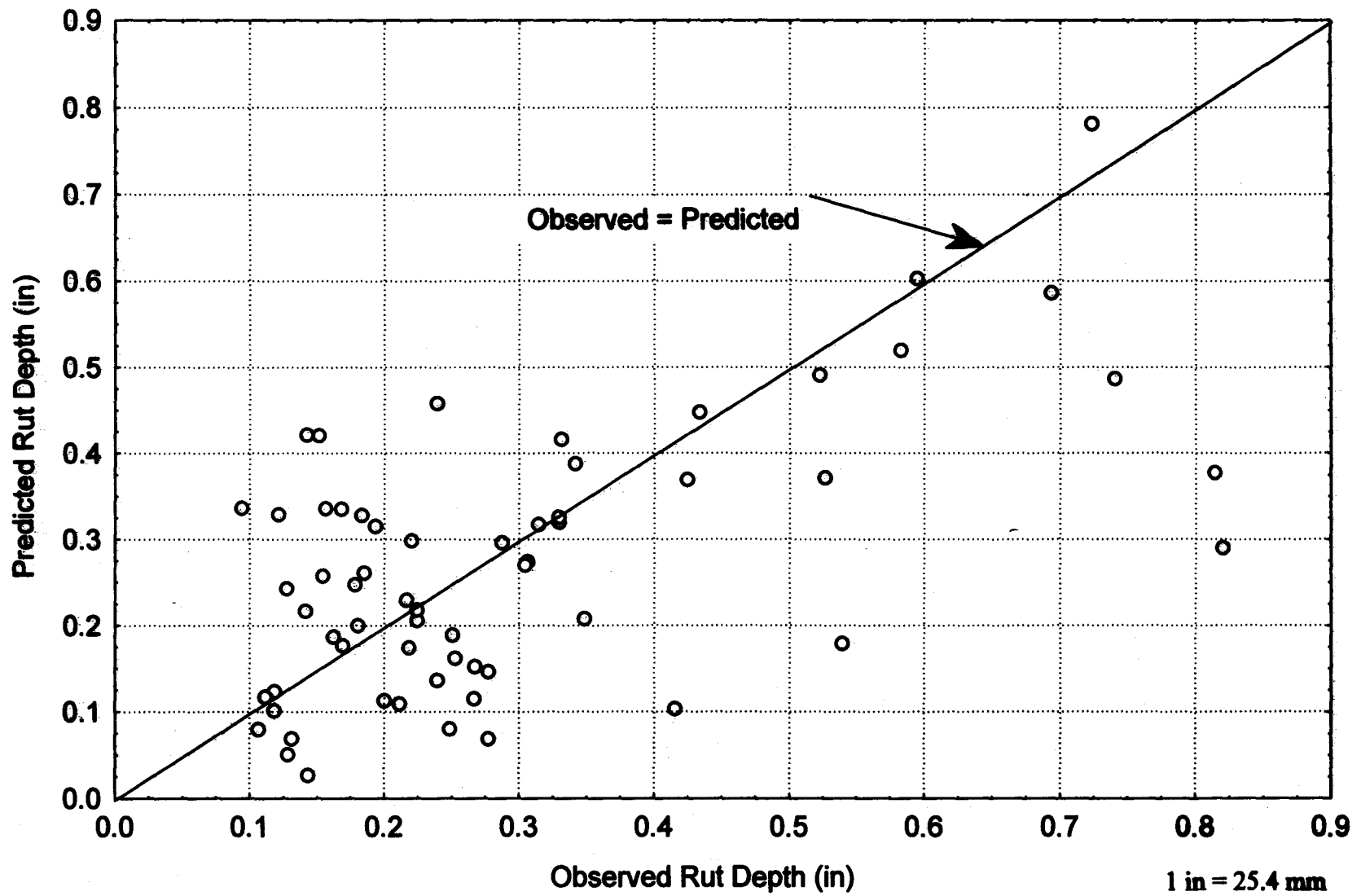


Figure 24. Observed versus predicted rut depth.

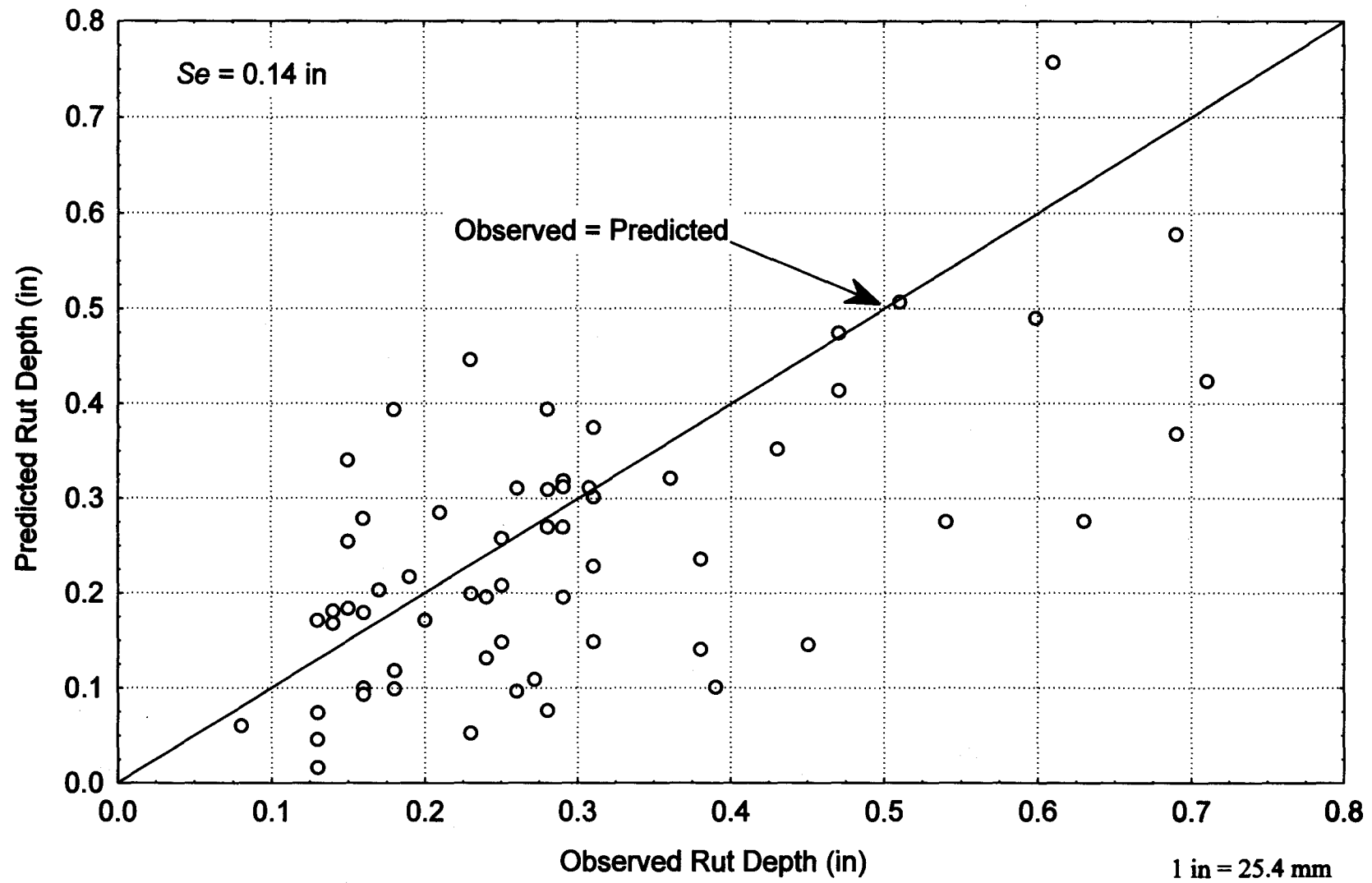


Figure 25. Observed versus predicted rut depth, based on validation data set.

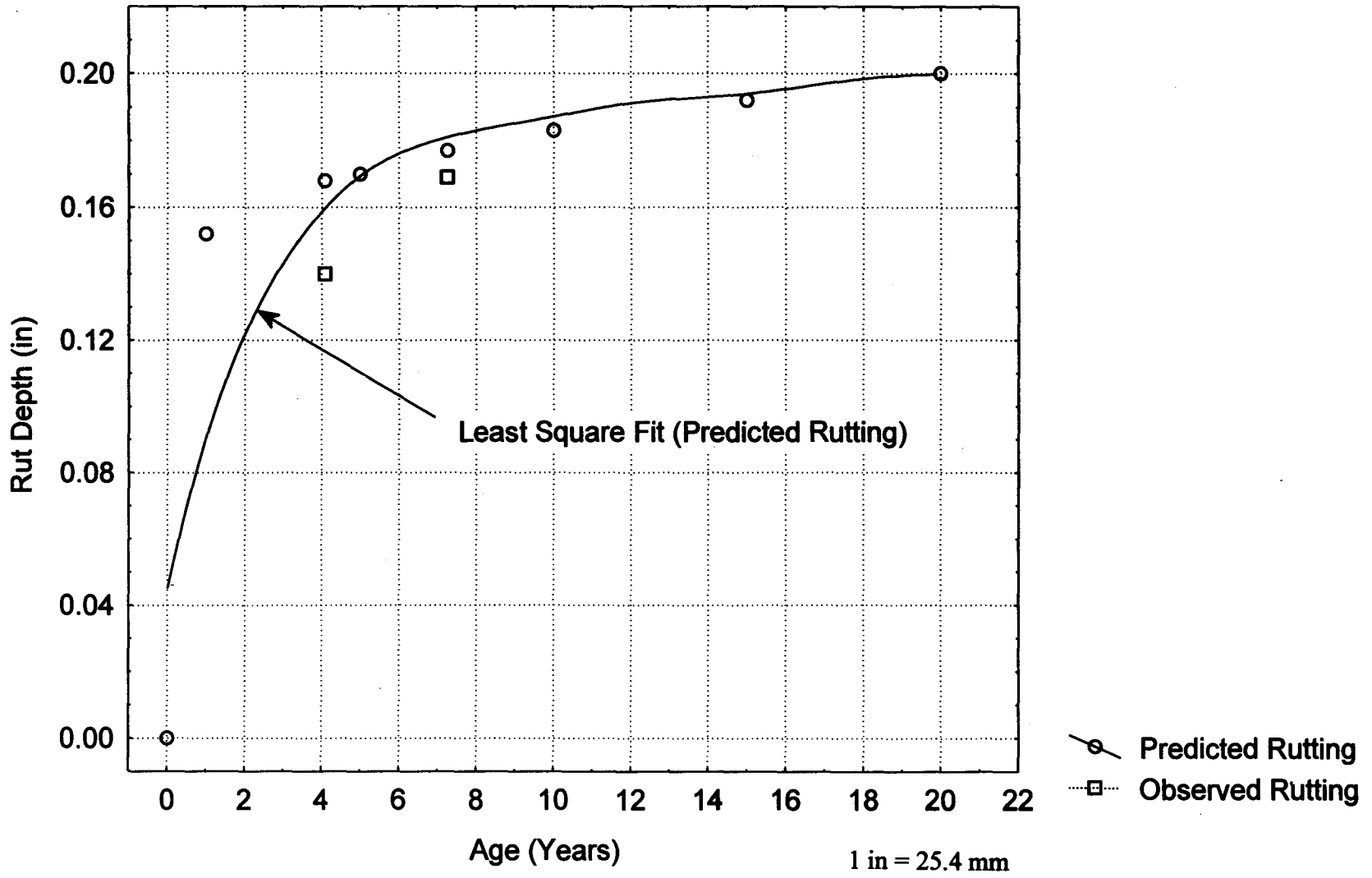


Figure 26. Rutting development for section 091047 (GPS-1).

between 0 and 20 years. Two points are plotted on the graph to represent the actual rutting values, corresponding to the first and last rutting surveys. As the figure shows, the observed and predicted rut depths match closely.

Summary

In summary, the proposed rutting model was developed based on the assumption that the relationship between the plastic and elastic strains is linear for all pavement layers. It further assumes that this relationship is nonlinearly related to the number of load applications. Two parameters are required to characterize the permanent deformation in each layer. These parameters were not available in the LTPP database, nor were there enough data to estimate the site-specific layer parameters. However, there were enough data to calibrate the model for the entire data set. The result was a set of rough estimates, or average values, of these parameters for the surface, base, and subgrade layers. The calibrated model fits reasonably well with the data points, with a standard error of estimate not much larger than the measurement error of the rut depth.

CHAPTER 10. SUMMARY AND RECOMMENDATIONS

General Observations

The primary objective of the study reported here was to evaluate the accuracy of some well-known, mechanistic-empirical models for predicting the performance of in-service AC pavements. Two distress types were considered in this study: fatigue cracking, and rutting. Another objective was to develop and calibrate new performance prediction models, as deemed necessary.

In this analysis, when data were not available, assumptions were made to estimate the missing data. For instance, annual traffic growth rate, long-term variations in the pavement layer moduli, seasonal variations of the unbound pavement layers, aging of the AC layers, lateral distribution of traffic, and vehicle tire pressure are examples of key factors for which there were not enough data; yet, these factors significantly influence the results. To evaluate the sensitivity of the output to each assumption, it would be necessary to repeat the analysis, changing only one assumption at a time, and examine the output. Although such a sensitivity analysis requires more time and resources, it would be useful in establishing the level of accuracy required for the key design parameters. Table 18 summarizes the uncertainty factors, and their expected effects on fatigue cracking and rutting damage computations.

Fatigue Cracking: Mechanistic Prediction Procedures

The following are some of the important observations, based on the analysis of fatigue cracking:

- The GPS-1 sections exhibited more fatigue and rutting than the GPS-2 sections, for the same level of computed damage ratio. The existence of a treated base in the GPS-2 sections may have been responsible for their superior performance. Theoretically, the structural analysis accounts for the difference between the two types of pavements by means of the base layer modulus. However, the assumptions of linear elasticity, material homogeneity, and the stress mode (constant stress versus constant strain) under which the transfer functions were derived may not necessarily hold in real pavements. It is conceivable that one type of pavement may be more sensitive to the underlying assumptions than the other. The structural differences that may contribute to differences in performance between the two pavement types need further investigation.
- The Asphalt Institute fatigue model appeared adequately to model the fatigue behavior of GPS-1 type pavements. The lack of failing pavements (i.e., pavements with an observed fatigue cracking in excess of 10 percent of the total area) made it difficult to model the rate of pavement deterioration. It is recommended that this analysis be performed again at a later date, after more pavement sections have started exhibiting higher levels of fatigue cracking.

Table 18. Uncertainty factors and their expected effects on pavement performance.

Factor	Effect on Damage
Seasonal variation in traffic.	Depends on the magnitude and timing of the seasonality relative to the seasonality of the layer moduli.
Effect of traffic wander.	Reduction in computed damage.
Seasonal variation in the modulus of unbound layers.	Depends on the magnitude and timing of the seasonality relative to the seasonality of traffic.
Long-term variation in elastic modulus of the surface layer (including aging effects).	Depends on the direction of change. Age-hardening of the surface layer may decrease or increase fatigue damage. The development of cracks, on the other hand, may accelerate the damage.
Pavement layers backcalculated moduli may be sensitive to the modeling assumptions, the program used, the specified closure error, and the layer thickness variation. There is concern that there is no unique solution to a given deflection basin, within a given tolerance of the closure error.	Could have a significant effect on damage, since the elastic moduli of the pavement layers are major inputs to structural and damage analyses. The direction of the effect is not predictable, due to compensating errors.
Tire pressure.	Increases with tire pressure.

- A group of models was fitted to the data to construct a continuous function relating the fatigue damage ratio to the amount of fatigue cracking. The linear constrained growth and exponential growth models were comparable in terms of goodness of fit. However, the linear model is the simplest; it indicates that fatigue cracking, as a percentage of the total pavement area, is about 5 percent of the fatigue damage ratio.
- The Shell fatigue model is comparable to the AI fatigue model in its adequacy in predicting the fatigue behavior of pavements. Although the model produced slightly higher damage ratios than the AI model, the t-test showed that the two models did not produce significantly different results.

Rutting: Mechanistic Prediction Procedures

The following are some of the important observations, based on the analysis of rutting.

- The Asphalt Institute permanent-deformation transfer function appears to satisfy the Asphalt Institute one-point criterion for rutting in both GPS-1 and GPS-2 pavement sections. However, there was a large scatter of the data points in the plot showing the permanent-deformation damage ratio versus observed rut depth plot. The models are not capable of estimating rutting in the early stages. The AI model presumes that all pavement layers above the subgrade do not contribute much to rutting. Consequently, the plastic characteristics of the upper pavement layers are excluded from the analysis.
- The 50-percent-reliability Shell permanent-deformation transfer function also appears to satisfy the one-point criterion for rutting in GPS-1 sections. This model is also not capable of estimating rutting in the early stages. It is similar to the AI model in neglecting the rutting in the upper pavement layers. The t-test shows that the two models produce significantly different damage results, with the Shell model producing lower damage values.
- The large scatter in the results from the AI and Shell rutting models may indicate that these models do not correctly estimate rutting. Also, they are only applicable to pavement sections that do not exhibit permanent deformation in any of the layers above the subgrade. Hence, they need to be used cautiously.
- A new mechanistic model was developed to predict rut depth as a function of the vertical compressive elastic strain in all pavement layers. The model was derived from a well-established plastic deformation functional form. To be compatible with mechanistic analysis, the model allows the characterization of traffic in terms of loading groups, rather than ESALs. The proposed model was developed based on the assumption that the relationship between the plastic and elastic strains is linear for all pavement layers. It further assumes that this relationship is nonlinearly related to the number of load applications. Two parameters are required to characterize the permanent-deformation behavior of each layer. These

parameters were not available in the LTPP database, nor were there enough data to estimate the site-specific layer parameters. However, there were enough data to calibrate the model for the entire data set (61 GPS-1 sections); the result was a set of rough estimates, or average values, of these parameters for the surface, base, and subgrade layers.

- The calibrated model reasonably fits the data points, with a standard error of estimate not much larger than the measurement error of rut depth. The model parameters indicate that the AC-layer contribution to surface rutting is marginal. The combined base/subbase layer contributes the most to the measured rutting. The contribution of the subgrade to the measured rutting is greater than that of the AC layer, but less than that of the base layer.
- The model was validated using a different set of data from the same sites, but obtained at different times. The results showed a reasonable agreement between predicted and observed rut depths. Future enhancement to the model may be realized by calibrating it to specific material types. For instance, the parameters α and μ could be calibrated separately for fine-grained and coarse-grained subgrades. Treated bases also need a separate calibration. It is also recommended that the laboratory permanent-deformation parameters be compared to those derived from the mechanistic analysis.

LTPP Data Issues

In the following paragraphs, issues relating to specific data elements are discussed. The purpose of this discussion is to provide feedback to the LTPP data collection efforts, identify areas of improvement, discuss the rationale behind selecting specific sources of data when options were available, and identify future research needs to fill the gaps.

Materials Data

Only a limited amount of laboratory-derived resilient modulus data was available; therefore, these data were not used in the analysis. As discussed, the moduli data used were based on backcalculation analyses of the deflection data. It is well known that pavement structural properties may exhibit significant seasonal and spatial variations. Deflection testing is performed at different times and at many testing points along a section. The pavement layer moduli backcalculated from deflection testing were used in this study, since they were derived using a larger sample size that covered wider ranges of time and space.

Future research should be directed towards relating the material properties derived from laboratory testing to those obtained by field testing at different seasons. A study of the spatial variability of pavement structural properties is needed, to help construct confidence bands on the values measured at any point along the test section.

Traffic Data

In this analysis, traffic was characterized as annual counts of an array of specific loading groups. The analysis was thus complicated, since there were up to 140 loading groups. The annual growth rate was calculated for each section based on the estimated, historical annual ESAL values. The rate was found to be highly variable within the same section, from one year to the next and from one section to another. The growth rate ranged from -13 percent to +30 percent, and it averaged 2.4 percent. It should also be noted that individual load groups had different growth rates. However, it was not feasible to calculate the traffic growth rate because many sections only had monitoring traffic data for 1 year. Other sections had an unrealistic variability in the counts of specific load groups from 1 year to the next. In the calculation of the cumulative traffic applications, a simplifying assumption was made that the annual traffic growth rate was 2 percent for all loading groups.

Future improvement to traffic data would include providing traffic counts for each season. This would help in matching the seasonal variation in the structural properties of pavements with the seasonal variation in traffic applications, to calculate more accurate damage values.

Traffic wander is another factor that needs to be studied. In this study, a 10-percent reduction in traffic counts was used to account for the lateral distribution of the wheels. This adjustment coefficient was suggested by Brown et al. [14]. The rationale behind this adjustment is that if we assume that each load application will result in a maximum strain at a given point, that will result in overestimating the damage, because the wheels will not always pass over the same exact path; therefore, the damage will be distributed over a range of points. A more accurate estimate of the effect of traffic wander may be obtained by developing frequency charts (histograms) of the lateral wheel positions across the traffic lane. The histograms could then be used to estimate the number of occurrences of the maximum strain value. The development of such charts requires that more data be collected on the lateral locations of the traffic loads.

Deflection Test Data

Deflection data were used to backcalculate the elastic layer moduli of pavement sections. One limitation of the analysis reported here was that there was no basis for adjusting the modulus of the unbound layers for the seasonal variations, since deflection data were only available for one or two seasons of the year. In a case study reported in chapter 8, it was shown that the seasonal variations in the layer moduli could have significantly affected the expected pavement damage and performance.

Future research efforts should be directed toward evaluating and possibly modeling the seasonal variations in the pavement layers moduli, and relating those variations to readily available environmental variables. Moreover, the long-term variations in pavement moduli need to be investigated.

Distress Data

There were some concerns about the quality of the distress data. It was observed that some sections had less distresses at a later time. This inconsistency may be explained by measurement errors, incorrect distress identifications (e.g., longitudinal, block, and fatigue cracks), and environmental effects.

A study is needed to quantify the magnitudes of errors in distress data, investigate the seasonality of distress data, and in the case of significant seasonality, provide guidelines as to when and how to measure distresses. A study is underway to compare manual and photographic distress surveys and address the variability and reliability of distress data.

Sensitivity Data

In an attempt to evaluate the sensitivity of the damage analysis results to the method used for including the seasonal variation of pavement moduli, a seasonal section was studied using three different methods (chapter 8). Two lessons were learned from this case study. First, the lack of seasonal data (FWD data) may lead to a too-large or too-low estimate of pavement damage. A difference of up to 16 times the magnitude of damage was observed when different sets of pavement layer moduli, obtained from FWD testing at different points in time, were used individually as being representative of the year-round layer moduli. Second, the damage ratio obtained using all seasonal moduli value did not appear to be significantly different from that obtained using the average moduli values. However, the former approach tended to yield more conservative results. These conclusions were based on the assumption that traffic volume was uniform throughout the year. It is expected that if the seasonal fluctuations in traffic volume are considered in damage analyses, the methods used here for considering the seasonal variation effect on pavements may produce even more different results.

Summary

In an ideal M-E procedure, damage in relation to a specific distress should be determined as follows:

$$\begin{aligned} \text{Damage}_{ijk\ell} &= f(e_{ijk\ell}) \\ \text{and} \\ e_{ijk\ell} &= f(E_{jk\ell}) \end{aligned} \tag{52}$$

- where: $e_{ijk\ell}$ = Critical pavement structural response is considered to be a predictor of the distress under consideration for the i th axle group at the j th time period of the k th month of the ℓ th year.
- $E_{jk\ell}$ = Modulus of elasticity of each layer of the pavement system at the j th time period of the k th month of the ℓ th year.

Thus, a major consideration in developing and using M-E procedures is the appropriate characterization of E_{jkl} for each pavement layer. Our capability for realistically modeling pavement behavior has seen much progress in the last few decades. However, the capability to consider the material characterization (e.g., E_{jkl}) realistically for the pavement layers remains less than desired because of the lack of knowledge on realistically accounting for seasonality effects, spatial variability, and deterioration effects due to traffic loading and environment.

In this study, distress-specific damage was estimated for a segment of LTPP test sections. However, as discussed in the report, the damage estimation was seriously handicapped by two primary factors: lack of adequate traffic data, in terms of reliability and completeness, and the many approximations that had to be made to develop an appropriate characterization of the pavement layer properties in terms of E_{jkl} . Future endeavors in the LTPP and other pavement research programs should attempt to minimize these serious inadequacies.

The LTPP database is one of the most important advances made in improving pavement technologies. This study has shown that, even given the many limitations, the LTPP data can be used successfully to develop a better insight into pavement behavior and ultimately to improve pavement performance.

REFERENCES

1. M.A. Miner, "Cumulative Damage in Fatigue," *Transactions of ASME*, Vol. 67, 1945, pp. A159-A164.
2. H.V. Quintus, and B. Killingsworth, "Analysis Relating to Pavement Material Characterization and Their Effects on Pavement Performance," Report Number FHWA-RD-97-85, Federal Highway Administration, August 1996.
3. F.S. Brown, S.W. Tam, and J.M. Brunton, "Structural Evaluation and Overlay Design: Analysis and Implementation," Paper presented at the 6th International Conference on Structural Design, Ann Arbor, MI, 1986.
4. F.J. Van Cauweleaert, D.R. Alexander, T.D. White, and W.R. Baker, "Multilayer Elastic Program for Backcalculation Layer Moduli in Pavement Evaluation," STP 1026, *American Society for Testing and Materials*, 1989, pp. 171-188.
5. J. Uzan, T. Scullion, C. Michalek, M. Paredes, and R. Lytton, "General Procedure for Backcalculating Layer Moduli," STP 1026, *American Society for Testing and Materials*, 1989, pp. 217-228.
6. *Deflection Testing and Backcalculation Expert Task Group Meeting*, Washington, DC, June 29, 1994.
7. Asphalt Institute, *Research and Development of the Asphalt Institute's Thickness Design Manual (MS-1)*, Ninth Edition, Research Report No. 82-2, August 1982.
8. Erland Lukanen, "Temperature Adjustment for Backcalculated Asphalt Moduli," Facsimile Memorandum received from Braun Intertec Corporation, July 1996.
9. Hesham Ali and Aramis Lopez, "Statistical Analyses of Temperature and Moisture Effect on Pavement Structural Properties," Paper presented at the Annual Meeting of the Transportation Research Board, Washington, DC, January 1996.
10. Y. Richard Kim et al., "Temperature Correction of Deflection and Backcalculated Moduli," Paper presented at the Annual Meeting of the Transportation Research Board, Washington, DC, January 1995.
11. R.N. Stubstad, S. Baltzer, E.O. Lukanen, and H.J. Ertman-Larsen, "Prediction of AC Mat Temperatures for Routine Load/Deflection Measurements," *Proceedings of the Fourth International Conference of Bearing Capacity*, Minneapolis, MN, July 1994.
12. *WESLEA Structural Analysis Program*, U.S. Army Engineer Waterways Experimental Station, Vicksburg, MS, 1989.

13. Yang H. Huang, *Pavement Analysis and Design*, Prentice Hall, Englewood Cliffs, NJ, 1993.
14. S.F. Brown, J.M. Brunton, and A.F. Stock, "The Analytical Design of Bituminous Pavement," Paper 8834, Transportation Engineering Group, May 1985.
15. Per Ullidtz, "Pavement Analysis," *Developments in Civil Engineering Series*, #19, Elsevier, 1987.
16. William J. Kenis, "Predictive Design Procedures, A Design Method for Flexible Pavements Using the VESYS Structural Subsystem," *Proceedings, Fourth International Conference on the Structural Design of Asphalt Pavements*, Ann Arbor, MI, 1977.
17. K. Majidzadeh et al., *Implementation of a Pavement Design System*, Final Report, Volumes 1 and 2, Research Project Number EES 579, Ohio State University, Columbus, OH, 1981.